

Fast Algorithms and Theory for High-Dimensional Bayesian Varying Coefficient Models *

Ray Bai^{†‡}, Mary R. Boland[§], Yong Chen[§]

December 30, 2022

Abstract

Nonparametric varying coefficient (NVC) models are widely used for modeling time-varying effects on responses that are measured repeatedly. In this paper, we introduce the *nonparametric varying coefficient spike-and-slab lasso* (NVC-SSL) for Bayesian estimation and variable selection in NVC models. The NVC-SSL simultaneously selects and estimates the functionals of the significant time-varying covariates, while also accounting for temporal correlations. Our model can be implemented using an efficient expectation-maximization (EM) algorithm, thus avoiding the computational intensiveness of Markov chain Monte Carlo (MCMC) in high dimensions. We also introduce a simple method to make our model robust to misspecification of the temporal correlation structure. In contrast to frequentist NVC models, hardly anything is known about the large-sample properties for Bayesian NVC models. In this paper, we take a step towards addressing this longstanding gap between methodology and theory by deriving posterior contraction rates for the NVC-SSL model under both correct specification and misspecification of the temporal correlation structure. Finally, we illustrate our methodology through simulation studies and data analysis. Our proposed method is implemented in the publicly available R package *NVCSSL*.

*Keywords and phrases: spike-and-slab, spike-and-slab group lasso, posterior contraction, variable selection, varying coefficient model

[†]Department of Statistics, University of South Carolina, Columbia, SC 29208.

[‡]Email: RBAI@mailbox.sc.edu

[§]Department of Biostatistics, Epidemiology, and Informatics, University of Pennsylvania, Philadelphia, PA 19104.

1 Introduction

Consider the nonparametric varying coefficient (NVC) model with p covariates,

$$y_i(t_{ij}) = \sum_{k=1}^p x_{ik}(t_{ij})\beta_k(t_{ij}) + \varepsilon_i(t_{ij}), i = 1, \dots, n, j = 1, \dots, n_i, \quad (1.1)$$

where $y_i(t)$ is the response for the i th subject at time point $t \in \mathcal{T}$, \mathcal{T} is the time interval on which the n_i different measurements are taken, $x_{ik}(t)$ is a possibly time-dependent covariate with corresponding smooth coefficient function $\beta_k(t)$, and $\varepsilon_i(t)$ is random error. Throughout this paper, we denote $N = \sum_{i=1}^n n_i$ as the total number of observations. We also assume that the $N \times 1$ vector $\mathbf{Y} = (y_1(t_{11}), \dots, y_1(t_{1n_1}), \dots, y_n(t_{n1}), \dots, y_n(t_{nn_n}))'$ is centered to avoid the need for an intercept, and we assume that the error terms $\varepsilon_i(t)$'s are independent, zero-mean Gaussian processes. That is, $\boldsymbol{\varepsilon}_i = (\varepsilon_i(t_{i1}), \dots, \varepsilon_i(t_{in_i}))' \sim \mathcal{N}_{n_i}(\mathbf{0}, \boldsymbol{\Sigma}_i)$, $i = 1, \dots, n$, where $\boldsymbol{\Sigma}_i$ is the variance-covariance matrix that captures the temporal correlation between the n_i responses, $y_i(t_{i1}), \dots, y_i(t_{in_i})$, for the i th subject.

NVC models (1.1) arise in many real applications. A prominent example is in longitudinal data analysis where we aim to model the response for the i th experimental subject at n_i different time points [34]. NVC models can also be used for functional data analysis where we wish to model smooth functional responses $y_i(t)$, $i = 1, \dots, n$, varying over a continuum $t \in \mathcal{T}$ [56]. See [31, 22] for examples of applications of these models.

There has been extensive frequentist work on fitting NVC models. Typical approaches to fitting (1.1) use local polynomial kernel smoothing [20, 72] or basis expansions [36, 54, 74] to estimate $\beta_k(t)$, $k = 1, \dots, p$. When the number of covariates p is large, one also often wants to impose a low-dimensional structure such as sparsity. In order to perform simultaneous function estimation and model selection, many authors have applied a penalty such as group SCAD [19] or group lasso [76] to the vectors of basis coefficients. See, e.g. [67, 68, 69]. These frequentist penalized NVC models do not account for the within-subject temporal correlations, essentially solving objective functions with $\boldsymbol{\varepsilon} = (\boldsymbol{\varepsilon}'_1, \dots, \boldsymbol{\varepsilon}'_n)' \sim \mathcal{N}_N(\mathbf{0}, \mathbf{I}_N)$. In low-dimensional settings and without regularizing the parameter space, [41] and [11] incorporated estimation of within-subject correlations into NVC models. However, to the best of our knowledge, no similar extension has been made for high-dimensional, penalized NVC models. While many researchers, e.g. [67, 68, 69, 74], have shown that consistent estimation of the

β_k 's and model selection consistency can still be achieved for penalized NVC models, failing to account for the error variances can nevertheless lead to invalid inferences and overfitting in finite samples [47, 51]. Thus, it seems prudent to explicitly model temporal dependence in NVC models.

While there are numerous theoretical results for frequentist NVC models, work on Bayesian NVC models has been primarily methodological. For example, Liu et al. [48] endow the smooth functions $\beta_k(t)$'s with a Gaussian process prior. Biller and Fahrmeir [6] and Huang et al. [37] use splines to model the $\beta_k(t)$'s in (1.1) and place multivariate normal priors on the groups of basis coefficients. Li et al. [44] place a scale-mixture of a multivariate normal priors known as the Bayesian group lasso prior on groups of basis coefficients. Unlike the frequentist penalized approaches, Liu et al. [48] and Li et al. [44] explicitly model the temporal dependence of the within-subject measurements by either including subject-specific random effects or by specifying a first-order autoregressive (AR(1)) covariance structure for the error terms $\varepsilon_i(t)$. In spite of the benefits of being able to incorporate temporal correlation into variable selection, existing Bayesian approaches to NVCs rely on Markov chain Monte Carlo (MCMC) to obtain posterior estimates of the $\beta_k(t)$'s. In high dimensions, however, MCMC can be very slow and even computationally impractical. In addition, hardly anything is known about the theoretical properties of Bayesian NVC models.

To address the aforementioned limitations, we adopt a Bayesian perspective, using spike-and-slab priors to induce sparsity in the estimates of the smooth functionals. Recently, there has been a rapid development in spike-and-slab lasso (SSL) methods to solve various high-dimensional problems, including (generalized) linear models [59, 63, 16, 2], factor analysis [58, 50], graphical models [25, 45, 26], and nonparametric additive regression [2]. Roughly speaking, SSL methodology endows regression coefficients with spike-and-slab priors such that the posterior mode gives exact sparsity. In this work, we extend the SSL methodology to functional and longitudinal data analysis. Our main contributions can be summarized as follows:

- We introduce the *nonparametric varying coefficient spike-and-slab lasso* (NVC-SSL) for Bayesian estimation and variable selection in NVC models. Our method provides several advantages over previously proposed methodology for high-dimensional varying coefficient models. Unlike frequentist penalized NVC models, the NVC-SSL can incorporate estimation of the within-subject correlation structure and borrow information across functional components through a *non*-separable beta-Bernoulli prior. Unlike other Bayesian NVC models, the NVC-

SSL does not need to use MCMC for estimation or posthoc thresholding for variable selection. Instead, our model can be implemented using a highly efficient expectation/maximization (EM) algorithm which performs simultaneous estimation and selection.

- We extend spike-and-slab lasso methodology to the functional regression setting, where the response is not just a nonlinear function of fixed covariates but *also* a function of time. We also propose a simple method to ensure that our model is robust and gives consistent estimates even when the within-subject covariance structure is misspecified. Previous work on the SSL did not address model misspecification, and our proposed approach can be used to ensure robustness for other spike-and-slab lasso methods.
- We derive posterior contraction rates for the functional components when the number of covariates p grows at nearly exponential rate with n , both when the correlation structure is correctly specified *and* when it is misspecified. To the best of our knowledge, there has been no previous theoretical work done for Bayesian NVC models. In this paper, we take a step towards narrowing this gap in the literature.

The rest of this paper is structured as follows. In Section 2, we introduce the NVC-SSL model. In Section 3, we derive a fast EM algorithm for rapidly obtaining estimates of the smooth functionals $\beta_k(t), k = 1, \dots, p$, under the NVC-SSL. In Section 4, we derive several attractive asymptotic properties of the NVC-SSL model when $p \gg n$. In Section 5, we introduce the robustified NVC-SSL method, which is robust to misspecification of the temporal correlation structure. In Section 6, we provide simulation studies of our method. Finally, in Section 7, we use our model to analyze a real data set.

1.1 Notation

We use the following notations for the rest of the paper. For two nonnegative sequences $\{a_n\}$ and $\{b_n\}$, we write $a_n \asymp b_n$ to denote $0 < \liminf_{n \rightarrow \infty} a_n/b_n \leq \limsup_{n \rightarrow \infty} a_n/b_n < \infty$. If $\lim_{n \rightarrow \infty} a_n/b_n = 0$, we write $a_n = o(b_n)$ or $a_n \prec b_n$. We use $a_n \lesssim b_n$ or $a_n = O(b_n)$ to denote that for sufficiently large n , there exists a constant $C > 0$ independent of n such that $a_n \leq Cb_n$. We write $a_n \vee b_n$ to denote $\max\{a_n, b_n\}$.

For a vector $\mathbf{v} \in \mathbb{R}^p$, we let $\|\mathbf{v}\|_2 := \sqrt{\sum_{i=1}^p v_i^2}$ and $\|\mathbf{v}\|_\infty := \max_i |v_i|$ denote its ℓ_2 and ℓ_∞ norms respectively. For a symmetric matrix \mathbf{A} , we let $\lambda_{\min}(\mathbf{A})$ and $\lambda_{\max}(\mathbf{A})$ denote its minimum and maximum eigenvalues

respectively. For a matrix $\mathbf{A} \in \mathbb{R}^{a \times b}$ with entries a_{ij} , $\|\mathbf{A}\|_F := \sqrt{\text{tr}(\mathbf{A}'\mathbf{A})} = \sqrt{\sum_{i=1}^a \sum_{j=1}^b a_{ij}^2}$ denotes its Frobenius norm, while $\|\mathbf{A}\|_2 := \sqrt{\lambda_{\max}(\mathbf{A}'\mathbf{A})}$ denotes its spectral norm.

2 The Nonparametric Varying Coefficient Spike-and-Slab Lasso

2.1 Basis Expansion and the NVC-SSL

Following the development in [67, 68, 69], we suppose that each coefficient function β_k in (1.1) can be approximated by g_k , a linear combination of d_k basis functions, i.e.

$$g_k(t) = \sum_{l=1}^{d_k} \gamma_{kl} B_{kl}(t), t \in \mathcal{T}, k = 1, \dots, p, \quad (2.1)$$

where $B_{kl}(t), t \in \mathcal{T}, l = 1, \dots, d_k$, are the basis functions. Then the model (1.1) can be approximated as

$$y_i(t_{ij}) \approx \sum_{k=1}^p \sum_{l=1}^{d_k} x_{ik}(t_{ij}) \gamma_{kl} B_{kl}(t_{ij}) + \varepsilon_i(t_{ij}), \quad (2.2)$$

for $i = 1, \dots, n$ and $j = 1, \dots, n_i$. Let $\mathbf{X} = [\mathbf{X}_1, \dots, \mathbf{X}_p]$, with

$$\mathbf{X}_k = (x_{1k}(t_{11}), \dots, x_{1k}(t_{1n_1}), \dots, x_{nk}(t_{n1}), \dots, x_{nk}(t_{nn_n}))'. \quad (2.3)$$

Further, we define $\mathbf{B}(t)$ as

$$\mathbf{B}(t) = \begin{pmatrix} B_{11}(t) & B_{12}(t) & \dots & B_{1d_1}(t) & 0 & \dots & 0 & 0 & \dots & 0 \\ \vdots & \vdots & & \vdots & \vdots & & \vdots & \vdots & & \vdots \\ 0 & 0 & \dots & 0 & 0 & \dots & B_{p1}(t) & B_{p2}(t) & \dots & B_{pd_p}(t) \end{pmatrix}, \quad (2.4)$$

and set $\mathbf{U} = (\mathbf{U}_{11}, \dots, \mathbf{U}_{1n_1}, \dots, \mathbf{U}_{n1}, \dots, \mathbf{U}_{nn_n})'$ with

$$\mathbf{U}_{ij}' = \mathbf{x}'(t_{ij}) \mathbf{B}(t_{ij}) \quad (2.5)$$

for $i = 1, \dots, n, j = 1, \dots, n_i$, where $\mathbf{x}'(t_{ij})$ denotes the row of \mathbf{X} corresponding to the j th observation for the i th subject.

Letting $\mathbf{Y} = (y_1(t_{11}), \dots, y_1(t_{1n_1}), \dots, y_n(t_{n1}), \dots, y_n(t_{nn_n}))'$ and $\boldsymbol{\varepsilon} = (\varepsilon'_1, \dots, \varepsilon'_n)'$, the model (1.1) can then be expressed in matrix form as

$$\mathbf{Y} - \boldsymbol{\delta} = \mathbf{U}\boldsymbol{\gamma} + \boldsymbol{\varepsilon}, \quad \boldsymbol{\varepsilon} \sim \mathcal{N}_N(\mathbf{0}, \boldsymbol{\Sigma}), \quad (2.6)$$

where $\boldsymbol{\gamma} = (\boldsymbol{\gamma}'_1, \dots, \boldsymbol{\gamma}'_p)'$, and $\boldsymbol{\gamma}_k = (\gamma_{k1}, \dots, \gamma_{kd_k})'$ is the d_k -dimensional vector of basis coefficients corresponding to the k th covariate. Meanwhile, $\boldsymbol{\Sigma} = \text{diag}(\boldsymbol{\Sigma}_1, \dots, \boldsymbol{\Sigma}_n)$ is an $N \times N$ block diagonal matrix, and $\boldsymbol{\delta}$ is an $N \times 1$ vector of lower-order bias, or the approximation error from using truncated basis functions of dimension d_k to approximate the β_k 's.

2.2 Model Formulation

For the NVC model (1.1), we assume that the within-subject covariance matrices have the structure, $\boldsymbol{\Sigma}_i = \sigma^2 \mathbf{R}_i(\rho)$, $i = 1, \dots, n$, where $\mathbf{R}_i(\rho)$ denotes that the correlation matrix \mathbf{R}_i is determined by a single parameter $\rho \in [0, 1]$. That is, we suppose that for $\boldsymbol{\varepsilon} = (\varepsilon'_1, \dots, \varepsilon'_n)'$,

$$\varepsilon_i \stackrel{\text{ind}}{\sim} \mathcal{N}_{n_i}(\mathbf{0}, \sigma^2 \mathbf{R}_i(\rho)), i = 1, \dots, n. \quad (2.7)$$

In longitudinal data analysis, it is customary to make this sort of simplifying assumption about the structure of the within-subject correlations in order to avoid overfitting and poor out-of-sample predictive performance. This general form subsumes many popular choices for covariance structures. For example, if we assume first-order autoregressive (AR(1)) structure, then the (j, k) th element of $\mathbf{R}_i(\rho)$ is $\rho^{|t_{ij} - t_{ik}|}$. For compound symmetry (CS), the (j, k) th element of $\mathbf{R}_i(\rho)$ is $\mathbb{I}(j = k) + \rho \mathbb{I}(j \neq k)$. For concreteness, we focus only on AR(1) and CS structures in this paper, noting that our model can be generalized to more exotic correlation structures. For example, if it is assumed that the data contains seasonal effects, the covariance structure (2.7) can be replaced with a seasonal ARIMA structure, and our method can be easily extended to estimate the additional seasonal parameters in the \mathbf{R}_i 's, as in [7].

The structural assumption (2.7) also makes estimation more computationally efficient, as the problem of estimating the within-subject error covariance matrices reduces to just estimating two unknowns (σ^2, ρ) . In Appendix B.1, we provide some guidelines for how to choose the appropriate covariance structure to use in our model. In Section 5, we also give a simple procedure to make the NVC-SSL model robust to possible misspecification of the error covariance structure.

Under the NVC-SSL model, we endow the vector of basis coefficients $\boldsymbol{\gamma} = (\boldsymbol{\gamma}'_1, \dots, \boldsymbol{\gamma}'_p)'$ in (2.6) with the *slope-and-slab group lasso* (SSGL) prior of [2],

$$\pi(\boldsymbol{\gamma}|\theta) = \prod_{k=1}^p [(1-\theta)\boldsymbol{\Psi}(\boldsymbol{\gamma}_k|\lambda_0) + \theta\boldsymbol{\Psi}(\boldsymbol{\gamma}_k|\lambda_1)], \quad (2.8)$$

where θ is a mixing proportion, or the expected proportion of nonzero $\boldsymbol{\gamma}_k$'s, and $\boldsymbol{\Psi}(\cdot|\lambda)$ denotes the group lasso density indexed by hyperparameter λ ,

$$\boldsymbol{\Psi}(\boldsymbol{\gamma}_k|\lambda) = \frac{\lambda^{d_k} e^{-\lambda\|\boldsymbol{\gamma}_k\|_2}}{2^{d_k} \pi^{(d_k-1)/2} \Gamma((d_k+1)/2)}, \quad k = 1, \dots, p.$$

The group lasso prior has been considered by several other authors ([2, 44, 42, 73] and can be derived as the marginal density of a multivariate normal scale-mixture, $\boldsymbol{\gamma}_k|\zeta \sim \mathcal{N}_{d_k}(\mathbf{0}_{d_k}, \zeta \mathbf{I}_{d_k})$, $\zeta \sim \mathcal{G}((d_k+1)/2, \lambda^2/2)$.

The SSGL prior (2.8), which we denote as $\mathcal{SSGL}(\lambda_0, \lambda_1, \theta)$ going forward, can be considered a two-group refinement of the group lasso [76]. Under the prior (2.8), the global posterior mode for $\boldsymbol{\gamma}$ may be exactly sparse, thereby allowing the $\mathcal{SSGL}(\lambda_0, \lambda_1, \theta)$ to perform joint estimation and variable selection [2]. In the present context, if the posterior mode $\hat{\boldsymbol{\gamma}}_k = \mathbf{0}_{d_k}$, then the k th functional component will be estimated as $\hat{\beta}_k(t) = \sum_{l=1}^{d_k} \hat{\gamma}_{kl} B_{kl}(t) = 0$ and thus thresholded out of the model. We typically set $\lambda_0 \gg \lambda_1$ in (2.8), so that the first mixture component (the spike) is heavily concentrated near $\mathbf{0}_{d_k}$ for each $k = 1, \dots, p$, while the slab stabilizes the posterior estimates of large coefficients, preventing them from being downward biased.

To model the uncertainty in θ in (2.8), we endow θ with a beta prior,

$$\theta \sim \mathcal{B}(a, b), \quad (2.9)$$

where (a, b) are fixed positive constants. Unlike frequentist penalties such as group lasso, this prior on θ ultimately renders our Bayesian penalty *non-separable* in the sense that the groups $\boldsymbol{\gamma}_k, k = 1, \dots, p$ are *a priori* dependent. This non-separability provides several benefits. First, the prior on θ allows the NVC-SSL model to *share* information across functional components and self-adapt to ensemble information about sparsity. Second, with appropriate choices for the hyperparameters in $\theta \sim \mathcal{B}(a, b)$, namely $a = 1, b = p$, our prior performs an automatic multiplicity adjustment [60] and favors parsimonious models in high dimensions.

To complete the model specification, we place independent priors on the parameters (σ^2, ρ) in (2.7) as

$$\sigma^2 \sim \mathcal{IG}(c_0/2, d_0/2), \quad (2.10)$$

where $c_0, d_0 > 0$ are small positive constants, and

$$\pi(\rho) = \sum_{h=1}^q q^{-1} \delta_{m_h}. \quad (2.11)$$

That is, ρ follows a discrete uniform distribution with q atoms $\{m_1, \dots, m_q\}$ where $0 \leq m_h < 1, 1 \leq h \leq q$. In our default implementation, we specify the support for $\pi(\rho)$ as $\{0, 0.1, \dots, 0.9\}$, though a finer grid could also be specified. This representation offers several advantages. First, the prior (2.11) puts *positive* mass at $\rho = 0$, so the NVC-SSL model can model i.i.d. errors, i.e. $\varepsilon \sim \mathcal{N}_N(\mathbf{0}, \sigma^2 \mathbf{I}_N)$, if there is no temporal correlation present. Second, as we illustrate in Section 3, placing a discrete uniform prior on ρ also facilitates more efficient computations from an optimization perspective.

3 Computational Strategy

3.1 Posterior Mode Estimation

We now detail how to implement the NVC-SSL model. Rather than relying on MCMC, we will target the maximum *a posteriori* (MAP) estimate for the basis coefficients, $\hat{\gamma}$. We may then take as our estimates for the smooth functionals as $\hat{\beta}_k(t) = \sum_{l=1}^d \hat{\gamma}_{kl} B_{kl}(t), k = 1, \dots, p$. For simplicity, we let the basis truncation parameters satisfy $d_1 = d_2 = \dots = d_p = d$ for some positive integer d . In Section 3.2, we describe how to select d .

Let Ξ denote the collection $\{\gamma, \theta, \sigma^2, \rho\}$. The log-posterior density for Ξ (up to an additive constant) is given by

$$\begin{aligned} \log \pi(\Xi | \mathbf{Y}) = & -\frac{N}{2} \log \sigma^2 - \frac{1}{2} \log |\mathbf{R}(\rho)| - \frac{\|\mathbf{R}^{-1/2}(\rho)(\mathbf{Y} - \mathbf{U}\gamma)\|_2^2}{2\sigma^2} \\ & + \sum_{k=1}^p \log \left((1 - \theta) \lambda_0^d e^{-\lambda_0 \|\gamma_k\|^2} + \theta \lambda_1^d e^{-\lambda_1 \|\gamma_k\|^2} \right) \\ & + (a - 1) \log \theta + (b - 1) \log(1 - \theta) \\ & - \left(\frac{c_0 + 2}{2} \right) \log \sigma^2 - \frac{d_0}{2\sigma^2} + \log \pi(\rho). \end{aligned} \quad (3.1)$$

Our objective is to maximize the log-posterior with respect to Ξ . We first introduce latent 0-1 indicators, $\boldsymbol{\tau} = (\tau_1, \dots, \tau_p)'$. Then we reparametrize

the $\mathcal{SSGL}(\lambda_0, \lambda_1, \theta)$ prior (2.8) as:

$$\begin{aligned}\pi(\boldsymbol{\gamma}|\boldsymbol{\tau}) &= \prod_{k=1}^p [(1 - \tau_k)\boldsymbol{\Psi}(\boldsymbol{\gamma}_k|\lambda_0) + \tau_k\boldsymbol{\Psi}(\boldsymbol{\gamma}_k|\lambda_1)], \\ \pi(\boldsymbol{\tau}|\theta) &= \prod_{k=1}^p \theta^{\tau_k} (1 - \theta)^{1 - \tau_k}.\end{aligned}\tag{3.2}$$

Let $\mathbf{R} := \mathbf{R}(\rho) = \text{diag}(\mathbf{R}_1(\rho), \dots, \mathbf{R}_n(\rho))$. The augmented log-posterior density for $(\boldsymbol{\Xi}, \boldsymbol{\tau})$ (up to an additive constant) is now given by

$$\begin{aligned}\log \pi(\boldsymbol{\Xi}, \boldsymbol{\tau}|\mathbf{Y}) &= -\frac{N}{2} \log \sigma^2 - \frac{1}{2} \log |\mathbf{R}(\rho)| - \frac{\|\mathbf{R}^{-1/2}(\rho)(\mathbf{Y} - \mathbf{U}\boldsymbol{\gamma})\|_2^2}{2\sigma^2} \\ &\quad + \sum_{k=1}^p \log \left((1 - \tau_k) \lambda_0^d e^{-\lambda_0 \|\boldsymbol{\gamma}_k\|_2} + \tau_k \lambda_1^d e^{-\lambda_1 \|\boldsymbol{\gamma}_k\|_2} \right) \\ &\quad + \left(a - 1 + \sum_{k=1}^p \tau_k \right) \log \theta + \left(b - 1 + p - \sum_{k=1}^p \tau_k \right) \log(1 - \theta) \\ &\quad - \left(\frac{c_0 + 2}{2} \right) \log \sigma^2 - \frac{d_0}{2\sigma^2} + \log \pi(\rho).\end{aligned}\tag{3.3}$$

It is straightforward to verify that $\mathbb{E}[\tau_k|\mathbf{Y}, \boldsymbol{\Xi}] = p_k^*(\boldsymbol{\gamma}_k, \theta)$, where

$$p_k^*(\boldsymbol{\gamma}_k, \theta) = \frac{\theta \boldsymbol{\Psi}(\boldsymbol{\gamma}_k|\lambda_1)}{\theta \boldsymbol{\Psi}(\boldsymbol{\gamma}_k|\lambda_1) + (1 - \theta) \boldsymbol{\Psi}(\boldsymbol{\gamma}_k|\lambda_0)}\tag{3.4}$$

is the conditional posterior probability that $\boldsymbol{\gamma}_k$ is drawn from the slab distribution rather than from the spike.

With the augmented log-posterior (3.3), we may now implement an EM algorithm to find the MAP estimator $\hat{\boldsymbol{\Xi}} = \{\hat{\boldsymbol{\gamma}}, \hat{\rho}, \hat{\theta}, \hat{\sigma}^2\}$. After initializing the parameters $\boldsymbol{\Xi}^{(0)}$, we iterate between the E-step and M-step until convergence. For the E-step, we compute $p_k^* := p^*(\boldsymbol{\gamma}_k^{(t-1)}, \theta^{(t-1)}) = \mathbb{E}[\tau_k|\mathbf{Y}, \boldsymbol{\Xi}^{(t-1)}]$, $k = 1, \dots, p$, given the previous estimate $\boldsymbol{\Xi}^{(t-1)}$. For the M-step, we then maximize the following objective function with respect to $\boldsymbol{\Xi}$:

$$\begin{aligned}\mathbb{E} \left[\log \pi(\boldsymbol{\Xi}|\mathbf{Y}) | \boldsymbol{\Xi}^{(t-1)} \right] &= -\frac{N}{2} \log \sigma^2 - \frac{1}{2} \log |\mathbf{R}(\rho)| - \frac{\|\mathbf{R}^{-1/2}(\rho)(\mathbf{Y} - \mathbf{U}\boldsymbol{\gamma})\|_2^2}{2\sigma^2} - \sum_{k=1}^p \lambda_k^* \|\boldsymbol{\gamma}_k\|_2 \\ &\quad + \left(a - 1 + \sum_{k=1}^p p_k^* \right) \log \theta + \left(b - 1 + p - \sum_{k=1}^p p_k^* \right) \log(1 - \theta)\end{aligned}$$

$$-\left(\frac{c_0+2}{2}\right)\log\sigma^2 - \frac{d_0}{2\sigma^2} + \log\pi(\rho), \quad (3.5)$$

where $\lambda_k^* = \lambda_1 p_k^* + \lambda_0(1 - p_k^*)$. The function (3.5) would be difficult to jointly maximize with respect to $(\gamma, \rho, \theta, \sigma^2)$ if $\pi(\rho)$ were a continuous density. However, by endowing ρ with a discrete uniform prior (2.11), our optimization is much simpler. With the prior (2.11), we may fix $\rho \in \{m_1, \dots, m_q\}$ and maximize (3.5) with respect to $(\gamma, \theta, \sigma^2)$ for each atom. In our implementation, each of these t optimizations is performed in parallel and the log-posterior for each $m_h, 1 \leq h \leq q$, is evaluated. We take as our modal estimate the $\hat{\rho}$ to be the m_h which maximizes $\log\pi(\hat{\gamma}, \hat{\theta}, \hat{\sigma}^2, \rho | \mathbf{Y}, \rho = m_h)$, the original non-augmented log-posterior (3.1).

It is clear from (3.5) that θ has the following closed form update in the M-step:

$$\theta^{(t)} = \frac{a - 1 + \sum_{k=1}^p p_k^*}{a + b + p - 2}. \quad (3.6)$$

Next, we update γ , holding $(\theta, \sigma^2, \rho) = (\theta^{(t)}, \sigma^{2(t-1)}, m_h)$ fixed. Let $\widetilde{\mathbf{Y}} = \mathbf{R}^{-1/2}(m_h)\mathbf{Y}$ and $\widetilde{\mathbf{U}} = \mathbf{R}^{-1/2}(m_h)\mathbf{U}$. To update γ , we solve the following optimization:

$$\gamma^{(t)} = \arg \max_{\gamma} -\frac{1}{2}\|\widetilde{\mathbf{Y}} - \widetilde{\mathbf{U}}\gamma\|_2^2 - \sum_{k=1}^p \sigma^2 \lambda_k^* \|\gamma_k\|_2. \quad (3.7)$$

Note that (3.7) is an adaptive group lasso problem with weights $\sigma^2 \lambda_k^*$, and it explicitly takes temporal correlation into account (through \mathbf{R}) in our estimate procedure for γ . This optimization can be solved with any standard (adaptive) group lasso algorithm [76, 32].

Finally, holding $(\gamma, \rho) = (\gamma^{(t)}, m_h)$ fixed, we update σ^2 , which has the following closed form:

$$\sigma^{2(t)} = \frac{d_0 + \|\widetilde{\mathbf{Y}} - \widetilde{\mathbf{U}}\gamma\|_2^2}{N + c_0 + 2}. \quad (3.8)$$

In order to obtain $\widetilde{\mathbf{Y}}$ and $\widetilde{\mathbf{U}}$ and evaluate the log posterior (3.1) for each atom $m_h, 1 \leq h \leq q$, in (2.11), we must invert \mathbf{R} , which is an $N \times N$ matrix. However, by exploiting the block structure of \mathbf{R} , we only need to perform n matrix inversions of the individual correlation matrices $\mathbf{R}_i, i = 1, \dots, n$, incurring total computational complexity of $\sum_{i=1}^n \mathcal{O}(n_i^3)$. Similarly, evaluating the log-determinant $\log|\mathbf{R}| = \sum_{k=1}^n \log|\mathbf{R}_i|$ requires $\sum_{i=1}^n \mathcal{O}(n_i^3)$ operations. In high dimensions, the number of within-subject repeated measurements n_i 's are typically smaller than both n and p , so performing these operations

is not particularly costly. However, if the n_i 's are so large that computing the inverses and log-determinants of the \mathbf{R}_i 's is prohibitive, then we recommend using the robustified NVC-SSL model in Section 5 with a working independence assumption (i.e. setting the “working” covariance matrices to be $\mathcal{N}_{n_i}(\mathbf{0}, \mathbf{I}_{n_i}), i = 1, \dots, n$). This way, we can estimate the functionals without needing to invert any within-subject covariance matrices.

To further improve computational efficiency, we compute the inverses and the log-determinants of the \mathbf{R}_i 's in parallel, so the computational complexity of these operations reduces to $\max_{1 \leq i \leq n} \mathcal{O}(n_i^3)$. For AR(1) with equispaced time points and CS error covariance structures, the computational complexity may be further reduced to $\max_{1 \leq i \leq n} \mathcal{O}(n_i)$ by using explicit formulas for the individual entries in \mathbf{R}_i^{-1} (see, e.g., p. 283 of [13]).

Unfortunately, the objective (3.5) is highly non-convex and the posterior is multimodal. In order to navigate the multimodal posterior efficiently and prevent our EM algorithm from terminating at a suboptimal mode, we need to take care in tuning the hyperparameters (λ_0, λ_1) and initializing (γ, σ^2) . In the interest of space, the complete details have been placed in Appendix A.1. To summarize briefly, however, we fix λ_1 at a small value so that the significant groups of basis coefficients receive minimal shrinkage. Meanwhile, we gradually increase λ_0 along a ladder of increasing values using a dynamic posterior exploration strategy [58, 59, 2]. This helps to ameliorate the issue of multimodality in the posterior by initially starting out with a relatively flat objective function that becomes “spikier” as we traverse the ladder of λ_0 's. By the time that the spikes have reappeared, the iterates will be more likely to have entered the basin of the dominant mode.

The complete algorithm for the NVC-SSL model is given in Algorithm 1 of Appendix A.1. Let $\mathbf{t} = (t_{11}, \dots, t_{1n_1}, \dots, t_{n1}, \dots, t_{nn_n})'$ be the vector of all observation times for all subjects. Once we have gotten the final modal estimate $\hat{\gamma}$, we can obtain the estimates for the smooth functionals as $\hat{\beta}_k(\mathbf{t}) = \sum_{l=1}^d \hat{\gamma}_{kl} B_{kl}(\mathbf{t}), k = 1, \dots, p$, where $\hat{\beta}_k(\mathbf{t})$ is a $N \times 1$ vector of $\hat{\beta}_k$ evaluated at all N time points in \mathbf{t} .

3.2 Selection of Degrees of Freedom

We also need to choose the degrees of freedom d (i.e. the number of basis functions to use). To do this, we use the Akaike information criterion with a correction for small sample sizes (AIC_c) [38]. This correction ensures that if the sample size is small, AIC_c will be reluctant to overfit. Let $\hat{S} \subset \{1, \dots, p\}$ denote the indices of the estimated nonzero subvectors of γ , with cardinality

$|\widehat{S}| = \widehat{s}$. In this context, the AIC_c is defined as

$$AIC_c = \log \left(\frac{\|\mathbf{R}^{-1/2}(\widehat{\rho})(\mathbf{Y} - \mathbf{U}\widehat{\gamma})\|_2^2}{N} \right) + 1 + \frac{2(\widehat{s} + 1)}{N - \widehat{s} - 2}, \quad (3.9)$$

where $(\widehat{\gamma}, \widehat{\rho})$ are the modal estimates under the NVC-SSL prior. Note that if (γ, ρ) were known, then the first term in (3.9) would be the maximum likelihood estimate (MLE) for $\log(\sigma^2)$. We select the d which minimizes AIC_c from a reasonable range of values.

In our numerical studies, we also found that simply fixing d to be sufficiently large (e.g., $d = 8$) gave excellent performance under the NVC-SSL model. Further tuning of d using AIC_c provided only modest improvements. This could possibly be attributed to the fact that the dynamic posterior exploration strategy from Section A.1 of the Supplementary Material already eliminates many spurious variables. In our simulations in Section 6, we use AIC_c to select d in order to make our comparisons with competing frequentist methods more transparent (where d was also similarly tuned). However, in practice, fitting the model with a default choice of $d = 8$ also works well.

4 Asymptotic Theory for the NVC-SSL

In this section, we prove several asymptotic properties about the NVC-SSL model. To the very best of our knowledge, these are the first theoretical results for Bayesian NVC models. All the proofs for these results can be found in Section E of the Supplementary Material. We assume that there is a true model,

$$y_i(t_{ij}) = \sum_{k=1}^p x_{ik}(t_{ij})\beta_{0k}(t_{ij}) + \varepsilon_i(t_{ij}), i = 1, \dots, n, j = 1, \dots, n_i, \quad (4.1)$$

where $\varepsilon_i \sim \mathcal{N}_{n_i}(\mathbf{0}, \sigma_0^2 \mathbf{R}_i(\rho_0))$, $i = 1, \dots, n$, for fixed $\sigma_0^2 \in (0, \infty)$ and $\rho_0 \in [0, 1)$. We let \mathbb{P}_0 denote the probability measure underlying the true model (4.1). We assume that the time interval $\mathcal{T} := [0, T]$ is finite and that $\beta_{0k}(t) \in \mathcal{C}^\alpha[0, T]$, $k = 1, \dots, p$. That is, the true functions are all at least α -times continuously differentiable in \mathcal{T} , for some $\alpha \in \mathbb{N}$.

As before, suppose that each $\beta_{0k}(t)$ in (4.1) can be approximated by a linear combination of basis functions,

$$g_{0k}(t) = \sum_{i=1}^{d_k} \gamma_{0kl} B_{kl}(t), t \in \mathcal{T}, k = 1, \dots, p, \quad (4.2)$$

where $\{B_{kl}, l = 1, \dots, d_k\}$ is a given basis system. Throughout this section, we assume that the basis functions are B-splines. However, our results also hold for other choices of basis functions [14]. For simplicity, we also assume that $d_1 = \dots d_p = d$, noting that this can be relaxed. Our theory will continue to hold if we allow different vector sizes d_k 's, provided that $\limsup_n d_{\max}/d_{\min} < \infty$, as in [36] and [69], and $d_{\max} \asymp n^{1/(2\alpha+1)}$. For each $g_{0k}(t), k = 1, \dots, p$, let the approximation error be given by

$$\kappa_{0k}(t) = \beta_{0k}(t) - g_{0k}(t) = \beta_{0k}(t) - \sum_{l=1}^d \gamma_{0kl} B_{kl}(t), t \in \mathcal{T}, k = 1, \dots, p,$$

and so model (4.1) can be written as

$$y_i(t_{ij}) = \sum_{k=1}^p \sum_{l=1}^d x_{ik}(t_{ij}) \gamma_{0kl} B_{kl}(t_{ij}) + \sum_{k=1}^p x_{ik}(t_{ij}) \kappa_{0k}(t_{ij}) + \varepsilon_i(t_{ij}). \quad (4.3)$$

Let δ_0 be an $N \times 1$ vector with entries, $\sum_{k=1}^p x_{ik}(\mathbf{t}) \kappa_{0k}(\mathbf{t})$. In matrix form, (4.1) can be expressed as

$$\mathbf{Y} = \mathbf{U} \gamma_0 + \delta_0 + \varepsilon, \quad \varepsilon \sim \mathcal{N}_N(\mathbf{0}, \sigma_0^2 \mathbf{R}(\rho_0)), \quad (4.4)$$

where \mathbf{U} is defined as in (2.5), $\gamma_0 = (\gamma'_{01}, \dots, \gamma'_{0p})'$ where γ_{0k} is a d -dimensional vector of the true coefficients in the basis expansion for the k th function, and $\mathbf{R}(\rho_0) = \text{diag}(\mathbf{R}_1(\rho_0), \dots, \mathbf{R}_n(\rho_0))$.

4.1 Dimensionality Recovery for the NVC-SSL Model

We first begin with a result on dimensionality. Under the NVC-SSL model, determining the number of nonzero functions $\beta_k(t)$ is equivalent to determining the number of d -dimensional vectors γ_k such that $\gamma_k \neq \mathbf{0}_d$. Since we used a continuous spike-and-slab prior (2.8) in our prior, our model assigns zero mass to exactly sparse vectors γ . To approximate the model size under the NVC-SSL model, we use the following generalized notion of sparsity [2]. For a small constant $\omega_d > 0$ which depends on d , we define the generalized inclusion indicator and generalized dimensionality, respectively, as

$$\nu_{\omega_d}(\gamma_k) = \mathbb{I}(\|\gamma_k\|_2 > \omega_d) \text{ and } |\boldsymbol{\nu}(\boldsymbol{\gamma})| = \sum_{k=1}^p \nu_{\omega_d}(\gamma_k). \quad (4.5)$$

For the threshold ω_d , we use the following:

$$\omega_d \equiv \omega_d(\lambda_0, \lambda_1, \theta) = \frac{1}{\lambda_0 - \lambda_1} \log \left[\frac{1 - \theta \lambda_0^d}{\theta \lambda_1^d} \right]. \quad (4.6)$$

As noted in [2], any d -dimensional vectors γ_k satisfying $\|\gamma_k\|_2 = \omega_d$ represent the intersection points between the spike and the slab densities in the $\mathcal{SSGL}(\lambda_0, \lambda_1, \theta)$ prior. For large λ_0 , the threshold ω_d rapidly approaches zero as n increases, so that $|\nu(\gamma)|$ provides a good approximation to $\#\{k : \gamma_k \neq \mathbf{0}_d\}$.

We first state the following regularity assumptions. We denote $\mathcal{H} := (0, \infty) \times [0, 1)$ as the parameter space for (σ^2, ρ) . Let $S_0 \subset \{1, \dots, p\}$ denote the set of indices of the true nonzero functions $\beta_{0k}(t)$ in (4.1), with cardinality $|S_0| = s_0$. Let $n_{\max} := \max\{n_1, \dots, n_n\}$ denote the maximum number of within-subject observations.

- (A1) n, p, s_0, N, n_{\max} , and d satisfy: $n \ll p$, $\log p = o(n)$, $s_0 = o((n/\log p) \vee n^{2\alpha/(2\alpha+1)})$, $N \asymp n \times n_{\max}$, $n_{\max} = O(1)$, $d \log n = o(\log p)$, and $d \asymp n^{1/(2\alpha+1)}$.
- (A2) The maximum signal size in γ_0 satisfies $\|\gamma_0\|_\infty = O(\log p)$.
- (A3) For \mathbf{U} in (4.4), define the matrix norm, $\|\mathbf{U}\|_* = \max_{1 \leq k \leq p} \|\mathbf{U}_k\|_2$, where \mathbf{U}_k is the submatrix of \mathbf{U} with d columns corresponding to the k th covariate. Suppose $\|\mathbf{U}\|_*^2 \asymp N$. Further, define the compatibility number $\phi_2(s)$ as

$$\phi_2(s) = \inf_{\gamma: 1 \leq |\nu(\gamma)| \leq s} \frac{\|\mathbf{U}\gamma\|_2}{\|\mathbf{U}\|_* \|\gamma\|_2},$$

and assume that for any constant $K > 0$, $\phi_2(Ks_0)$ is bounded away from zero.

- (A4) There exists a positive constant M such that $|x_{ik}(t_{ij})| \leq M$ for all $i = 1, \dots, n, j = 1, \dots, n_i, k = 1, \dots, p$.
- (A5) The eigenvalues of the within-subject correlation matrices satisfy

$$1 \lesssim \min_{1 \leq i \leq n} \lambda_{\min}(\mathbf{R}_i(\rho_0)) \leq \max_{1 \leq i \leq n} \lambda_{\max}(\mathbf{R}_i(\rho_0)) \lesssim 1.$$

- (A6) For any $(\sigma_1^2, \rho_1), (\sigma_2^2, \rho_2) \in \mathcal{H}$,

$$\begin{aligned} \max_{1 \leq i \leq n} \|\sigma_1^2 \mathbf{R}_i(\rho_1) - \sigma_2^2 \mathbf{R}_i(\rho_2)\|_F^2 &\leq \frac{1}{n} \|\sigma_1^2 \mathbf{R}(\rho_1) - \sigma_2^2 \mathbf{R}(\rho_2)\|_F^2 \\ &\lesssim n_{\max}^2 (\sigma_1^2 - \sigma_2^2)^2 + n_{\max}^4 \sigma_2^4 |\rho_1 - \rho_2|^2. \end{aligned}$$

Assumption (A1) allows the number of covariates p to grow at nearly exponential rate with sample size n . However, the true number of nonzero functions s_0 should grow slower than $\max\{n/\log p, n^{2\alpha/(2\alpha+1)}\}$. Assumption (A2) places a restriction on the maximum signal size in γ_0 and is mild. By Assumption (A3), p is allowed to grow at the rate $p = O(e^{n^u})$ for some $0 < u < 1$. Thus, Assumption (A2) allows the maximum entry (in absolute value) in $\gamma_0 \in \mathbb{R}^{dp}$ to be of the order $O(n^u)$. In practice, the basis coefficients are unlikely to be exceptionally large values. Further detailed discussion of the regularity conditions (A3)-(A6) is given in Appendix B.2.

With all these ingredients, we state our first result. This next theorem establishes that the NVC-SSL posterior concentrates on sparse models of dimension no larger than a constant multiple of the true model size.

Theorem 1 (dimensionality). *Under model (4.4), suppose that we endow (γ, σ^2) with the prior (2.8)-(2.10) and ρ with the prior, $\rho \sim \mathcal{U}(0, 1)$. For the $\mathcal{SSGL}(\lambda_0, \lambda_1, \theta)$ prior, we set $\lambda_0 = (1 - \theta)/\theta$ and $\lambda_1 \asymp 1/n$, and for the $\mathcal{B}(a, b)$ prior on θ , we set $a = 1, b = p^c, c > 2$. Suppose that Assumptions (A1)-(A6) hold. Then for sufficiently large $M_1 > 0$,*

$$\Pi(\gamma : |\nu(\gamma)| > M_1 s_0 | \mathbf{Y}) \rightarrow 0 \text{ a.s. } \mathbb{P}_0 \text{ as } n, p \rightarrow \infty.$$

Proof. Appendix E. □

Remark 1. *For practical implementation of the NVC-SSL model, we endowed the autocorrelation parameter ρ with a discrete uniform prior (2.11). For our theoretical analysis, we require the prior on ρ to be continuous. The $\mathcal{U}(0, 1)$ prior can be seen as a limiting case of letting $q \rightarrow \infty$ in (2.11).*

Theorem 1 shows that the expected posterior probability that the generalized dimension size $|\nu(\gamma)|$ is a constant multiple larger than the true model size s_0 asymptotically vanishes. We also have the following corollary which shows that if the within-subject covariance matrices follow AR(1) structure (for equally spaced time points) or compound symmetry, then the generalized dimensionality result of Theorem 1 holds.

Corollary 1. *Suppose the conditions for Theorem 1 hold. If either: a) the within-subject matrices have AR(1) structure, i.e. the (j, k) th entry of \mathbf{R}_i is $\mathbf{R}_i(j, k) = \rho_0^{|j-k|}$, or b) the within-subject covariance matrices have compound symmetry structure, i.e. the (j, k) th entry of \mathbf{R}_i is $\mathbf{R}_i(j, k) = \mathbb{1}(j = k) + \rho_0(j \neq k)$, then for sufficiently large $M_1 > 0$,*

$$\Pi(\gamma : |\nu(\gamma)| > M_1 s_0 | \mathbf{Y}) \rightarrow 0 \text{ a.s. } \mathbb{P}_0 \text{ as } n, p \rightarrow \infty.$$

Proof. In the proof of Theorem 10 in [39], it is shown that under the conditions on N and n_{\max} in Assumption (A1), the within-subject covariance matrices $\sigma_0^2 R_i(\rho_0)$ satisfy both Assumptions (A5)-(A6). Thus, by Theorem 1, the dimensionality result holds. \square

4.2 Posterior Contraction Rate for the NVC-SSL Model

In addition to guaranteeing that the NVC-SSL posterior concentrates on sparse models, we also prove that our model consistently estimates the true functions $\beta_0(t) = (\beta_{01}(t), \dots, \beta_{0p}(t))'$ as $n, p \rightarrow \infty$. Let $\beta_k(\mathbf{t})$ and $\beta_{0k}(\mathbf{t})$ denote $N \times 1$ vectors of β_k and β_{0k} evaluated at the N observed time points, $\mathbf{t} = (t_{11}, \dots, t_{1n_1}, \dots, t_{n1}, \dots, t_{nn_n})'$. Let $\beta(\mathbf{t}) = [\beta_1(\mathbf{t}), \dots, \beta_p(\mathbf{t})]$ and $\beta_0(\mathbf{t}) = [\beta_{01}(\mathbf{t}), \dots, \beta_{0p}(\mathbf{t})]$ denote $N \times p$ matrices with respective columns $\beta_k(\mathbf{t})$ and $\beta_{0k}(\mathbf{t})$, $1 \leq k \leq p$. We will position our results in terms of $\|\cdot\|_n$ neighborhoods of the truth, where

$$\|\beta(\mathbf{t}) - \beta_0(\mathbf{t})\|_n^2 = \frac{1}{n} \sum_{i=1}^n \frac{1}{n_i} \sum_{j=1}^{n_i} \sum_{k=1}^p [\beta_k(t_{ij}) - \beta_{0k}(t_{ij})]^2.$$

The next theorem establishes the posterior concentration rate under the NVC-SSL prior, while the next corollary shows that our posterior contraction result holds for NVC models with AR(1) and CS covariance structures.

Theorem 2 (contraction rate). *Under model (4.4), suppose that we endow (γ, σ^2) with the prior (2.8)-(2.10) and ρ with the prior, $\rho \sim \mathcal{U}(0, 1)$. For the $\mathcal{SSGL}(\lambda_0, \lambda_1, \theta)$ prior, we set $\lambda_0 = (1 - \theta)/\theta$ and $\lambda_1 \asymp 1/n$, and for the $\mathcal{B}(a, b)$ prior on θ , we set $a = 1, b = p^c, c > 2$. Suppose that Assumptions (A1)-(A6) hold. Then for $\epsilon_n^2 = s_0 \log p/n + s_0 n^{-2\alpha/(2\alpha+1)}$,*

$$\Pi(\beta : \|\beta(\mathbf{t}) - \beta_0(\mathbf{t})\|_n > M_2 \epsilon_n | \mathbf{Y}) \rightarrow 0 \text{ a.s. } \mathbb{P}_0 \text{ as } n, p \rightarrow \infty,$$

for some $M_2 > 0$.

Proof. Appendix E. \square

Corollary 2. *Suppose the conditions for Theorem 2 hold. If either: a) the within-subject matrices have AR(1) structure, i.e. the (j, k) th entry of \mathbf{R}_i is $\mathbf{R}_i(j, k) = \rho_0^{|j-k|}$, or b) the within-subject covariance matrices have compound symmetry structure, i.e. the (j, k) th entry of \mathbf{R}_i is $\mathbf{R}_i(j, k) = \mathbb{1}(j = k) + \rho_0(j \neq k)$, then*

$$\Pi(\beta : \|\beta(\mathbf{t}) - \beta_0(\mathbf{t})\|_n > M_2 \epsilon_n | \mathbf{Y}) \rightarrow 0 \text{ a.s. } \mathbb{P}_0 \text{ as } n, p \rightarrow \infty,$$

for some $M_2 > 0$ and $\epsilon_n = s_0 \log p/n + s_0 n^{-2\alpha/(2\alpha+1)}$.

Theorem 2 and Corollary 2 show that the posterior contraction rate $\epsilon_n^2 = s_0 \log p/n + s_0 n^{-2\alpha/(2\alpha+1)}$ under the NVC-SSL model is composed of two terms: a) the error due to variable selection uncertainty (reflected in the term $s_0 \log p/n$), and b) the approximation error due to using basis expansions to estimate the smooth functionals (reflected in the term $s_0 n^{-2\alpha/(2\alpha+1)}$). By Assumption (A1), $s_0 = o((n/\log p) \vee n^{2\alpha/(2\alpha+1)})$, and hence, both these terms tend towards zero as $n \rightarrow \infty$. This proves that the NVC-SSL model consistently estimates the true functionals $\beta_0(t) = (\beta_{01}(t), \dots, \beta_{0p}(t))'$.

Remark 2. *If we assume that the sparsity level $s_0 = O(1)$, then we can achieve the faster posterior convergence rate of $\epsilon_n^2 = \log p/n + n^{-2\alpha/(2\alpha+1)}$.*

5 The Robustified NVC-SSL Model

In Section 4, we showed that the NVC-SSL model consistently estimates the true $\beta_k(t)$'s in (4.1) as long as we have correctly specified the parametric covariance structure for the within-subject errors. In Appendix B.1, we detail several methods to determine how to choose the appropriate covariance structure for our model. Nevertheless, it is still possible to misspecify the covariance structure if the true correlation structure is very complicated, and this could lead to a loss of efficiency and statistical power [27].

One tempting remedy would be to extend the NVC-SSL model to estimate completely unstructured covariance matrices. That is, we could estimate all $N + \sum_{i=1}^n \binom{n_i}{2}$ parameters in the unknown within-subject covariance matrices, $\Sigma_1, \dots, \Sigma_n$ in (1.1). In Appendix D, we show that by placing inverse-Wishart priors on the Σ_i 's and appropriately modifying our EM algorithm in Section 3, the NVC-SSL model can be implemented for unstructured error covariance matrices. However, Appendix D also illustrates that this strategy leads to very poor out-of-sample prediction, largely because the model is overparametrized and lacks generalizability. For these reasons, we prefer *not* to use the unstructured NVC-SSL method.

To handle possible misspecification of the within-subject covariances, we instead turn to a recent stream of research on Bayesian fractional posteriors. Suppose that we have specified “working” (possibly misspecified) within-subject error covariance matrices S_1, \dots, S_n in (2.6), so that we do not need to estimate Σ . Then the only unknown parameters in (2.6) are the basis coefficients γ , which we endow with the hierarchical $\mathcal{SSGL}(\lambda_0, \lambda_1, \theta)$ prior (2.8)-(2.9). Let $L_\gamma(Y_i)$ be the likelihood for the i th subject with working error covariance matrix S_i , i.e. $Y_i \sim \mathcal{N}_{n_i}(U_i \gamma, S_i)$, where U_i denotes the submatrix of U in (2.5) with n_i rows corresponding to the i th subject. The

fractional posterior is obtained by raising the likelihood function by a factor $\xi \in (0, 1)$ in the Bayes formula,

$$\Pi_{n,\xi}(A|\mathbf{Y}) = \frac{\int_A \prod_{i=1}^n L_{\gamma}(\mathbf{Y}_i)^{\xi} \Pi(d\gamma)}{\int \prod_{i=1}^n L_{\gamma}(\mathbf{Y}_i)^{\xi} \Pi(d\gamma)}. \quad (5.1)$$

Fractional posteriors have gained much attention in the statistical literature recently due to their robustness to model misspecification [30, 49, 66, 5]. As discussed in [66], the fractional posterior can be interpreted as combining the original likelihood with a data-dependent prior that is divided by a portion of the likelihood. This data reweighting in the prior corrects for possible inconsistencies by attenuating the dependence of the model on the data (i.e. reducing the weights for parameter values that track the data too closely). It turns out that we can ensure consistent estimation of the $\beta_k(t)$'s in (1.1) for *any* $\xi \in (0, 1)$ in (5.1), *even when* the working covariance matrices $\mathbf{S}_1, \dots, \mathbf{S}_n$ are misspecified. We call this fractional posterior approach *the robustified NVC-SSL model*.

For a given $\xi \in (0, 1)$, we have $\Pi_{n,\xi}(\gamma, \theta|\mathbf{Y}) \propto \left[\prod_{i=1}^n L_{\gamma}(\mathbf{Y}_i)^{\xi} \right] \times \Pi(\gamma, \theta)$. Thus, it is straightforward to implement an EM algorithm which performs MAP estimation of the robustified NVC-SSL model. Once the working error covariance matrices have been specified, the EM algorithm only cycles through updates for (γ, θ) . This complete algorithm is given in Algorithm 2 of Appendix A.2.

5.1 Consistent Estimation Under the Robustified NVC-SSL Model

We now show that using the robustified NVC-SSL model is theoretically justified. In Section 4, we assumed that the model was well-specified with within-covariance matrices of the form, $\sigma_0^2 \mathbf{R}_i(\rho_0), i = 1, \dots, n$. In this section, we allow for more general forms for the Σ_i 's. That is, we suppose the true model is

$$\mathbf{Y} = \mathbf{U}\gamma_0 + \delta_0 + \varepsilon, \quad \varepsilon \sim \mathcal{N}(\mathbf{0}, \Sigma_0), \quad (5.2)$$

where $\Sigma_0 = \text{diag}(\Sigma_{01}, \dots, \Sigma_{0n})$. Recall that we have *pre-specified* working error covariances $(\mathbf{S}_1, \dots, \mathbf{S}_n)$, so we do not estimate Σ_0 . We first state the following mild regularity conditions, which are needed to ensure that $(\mathbf{S}_i, \Sigma_{0i}), i = 1, \dots, n$, are asymptotically well-behaved.

$$(B1) \quad 1 \lesssim \min_{1 \leq i \leq n} \lambda_{\min}(\mathbf{S}_i) \leq \max_{1 \leq i \leq n} \lambda_{\max}(\mathbf{S}_i) \lesssim 1.$$

$$(B2) \quad 1 \lesssim \min_{1 \leq i \leq n} \lambda_{\min}(\Sigma_{0i}) \leq \max_{1 \leq i \leq n} \lambda_{\max}(\Sigma_{0i}) \lesssim 1.$$

The next theorem establishes that under these conditions, the fractional posterior (5.1) contracts around the true functions $\beta_{0k}(t), k = 1, \dots, p$, at the same rate as that in Theorem 2, even if we have misspecified the working within-subject covariance matrices. The proof of this theorem can be found in Section E of the Supplementary Material.

Theorem 3. *Under model (5.2), suppose that we specify working covariance matrices $\mathbf{S}_1, \dots, \mathbf{S}_n$ and endow γ with the prior (2.8)-(2.9). For the $SSGL(\lambda_0, \lambda_1, \theta)$ prior, we set $\lambda_0 = (1 - \theta)/\theta$ and $\lambda_1 \asymp 1/n$, and for the $\mathcal{B}(a, b)$ prior on θ , we set $a = 1, b = p^c, c > 2$. Suppose that the working and true covariance matrices $(\mathbf{S}_i, \Sigma_{0i}), i = 1, \dots, n$, satisfy Assumptions (B1)-(B2) and that Assumptions (A1)-(A4) hold. Then for $\epsilon_n^2 = s_0 \log p/n + s_0 n^{-2\alpha/(2\alpha+1)}$, the fractional posterior satisfies*

$$\Pi_{n,\xi}(\beta : \|\beta(t) - \beta_0(t)\|_n > M_3 \epsilon_n | \mathbf{Y}) \text{ a.s. } \mathbb{P}_0 \text{ as } n, p \rightarrow \infty,$$

for any $0 < \xi < 1$ and some $M_3 > 0$.

Proof. Appendix E. □

5.2 Selecting the Working Correlation Structure and the Fractional Power

By Theorem 3, the robustified NVC-SSL model consistently estimates the true functions $\beta_k(t), k = 1, \dots, p$, even if the working covariance structure we have specified is incorrect. One may wonder: why not simply use the fractional posterior instead of specifying the parametric structure (2.7)? For example, we could simply specify a working independence structure (i.e. $\mathbf{S}_i = \mathbf{I}_{n_i}, i = 1, \dots, n$) and use the robustified NVC-SSL procedure detailed here. First, this will likely lead to a loss of statistical efficiency when temporal correlations are in fact present, potentially requiring large sample sizes n to achieve reasonable estimation [47]. Second, it is often reasonable to assume that temporal correlation decays with distance. Thus, the AR(1) structure, although perhaps simplistic, will at least be able to capture this aspect of the data, leading to a more efficient estimator for γ . Finally, the speed of the EM algorithm in Section 3 makes it computationally feasible for us to use both the likelihood and fractional likelihood-based approaches, so we can perform a sensitivity analysis to see which one gives better predictive performance.

As a default working covariance structure, we recommend setting the working covariance matrices \mathbf{S}_i 's as $\mathbf{S}_i = \hat{\sigma}^2 \mathbf{R}_i(\hat{\rho})$, where $\mathbf{R}_i(j, k) = \hat{\rho}^{|t_{ij} - t_{ik}|}$

and $(\hat{\sigma}^2, \hat{\rho})$ are empirical Bayes (EB) estimates. In Section A.2 of the Supplementary Material, we describe how to obtain these EB estimates. Once the \mathbf{S}_i 's have been specified, we can use Algorithm 2 in Section A.2 of the Supplementary Material to obtain MAP estimates under the fractional posterior (5.1).

Theorem 3 also shows that the fractional posterior $\Pi_{n,\xi}$ consistently estimates the true $\beta_k(t)$'s for *any* choice of $\xi \in (0, 1)$. However, in finite samples, the specific choice of ξ should be carefully tuned. We recommend tuning ξ using AIC_c (3.9) from Section 3.2. That is, for a discrete grid of values strictly between 0 and 1, we select the value for ξ that minimizes AIC_c . In our simulation studies, we used the grid $\xi \in \{0.5, 0.6, 0.7, 0.8, 0.9, 0.95, 0.99\}$. Choosing ξ in a more automatic, data-adaptive manner is a very challenging problem in high dimensions and a problem that we leave for future research.

6 Simulation Studies

Here, we conduct several simulation studies for the NVC-SSL and robustified NVC-SSL models under both correct specification and misspecification of the within-subject error covariance structures. All the methods that we considered, including the frequentist NVC methods, are implemented in the publicly available R package `NVCSSL`, which can be found on the Comprehensive R Archive Network. In Appendix C and Appendix D.2, we provide results for additional simulation studies.

6.1 Simulation Study for the Correctly Specified NVC-SSL Model

We generated data for $n = 50$ subjects from model (1.1) as follows. To simulate the observation times, we first sampled from $\{1, 2, \dots, 20\}$, where each time point has a 60 percent chance of being skipped. This way, we had very irregularly spaced data, with n_i being different for different subjects. We then added random perturbation from $\mathcal{U}(-0.5, 0.5)$ to the non-skipped time points.

To model the high-dimensional scenario, we set $p = 400$, with the first six variables x_{i1}, \dots, x_{i6} being the relevant ones. $x_{i1}(t)$ was simulated from $\mathcal{U}(t/10, 2 + t/10)$ for any given time point t ; $x_{ij}(t), j = 2, \dots, 5$, conditioned on $x_{i1}(t)$, were i.i.d. drawn from a normal distribution with mean zero and variance $(1 + x_{i1}(t))/(2 + x_{i1}(t))$; x_{i6} , independent of $x_{ij}, j = 1, \dots, 5$ was normal with mean $1.5 \exp(t/40)$ and variance 1. For $k = 7, \dots, 400$, each $x_{ik}(t)$, independent of the others, was drawn from a multivariate normal

distribution with covariance structure $\text{cov}(x_{ik}(t), x_{ik}(s)) = \rho^{-|t-s|}$, with $\rho = 0.5$. The coefficient functions were

$$\begin{aligned}\beta_1(t) &= 10 \sin\left(\frac{\pi t}{15}\right), \beta_2(t) = 5 \cos\left(\frac{\pi t}{15}\right), \beta_3(t) = -1 + 2 \sin\left(\frac{\pi(t-25)}{8}\right), \\ \beta_4(t) &= 1 + 2 \cos\left(\frac{\pi(t-25)}{15}\right), \beta_5(t) = 2 + \frac{10e^{t-10}}{1+e^{t-10}}, \beta_6(t) = -4 + \frac{(20-t)^3}{2000}, \\ \beta_7(t) &= \dots = \beta_{400}(t) = 0.\end{aligned}$$

To generate the random errors $\varepsilon_i \stackrel{\text{ind}}{\sim} \mathcal{N}_{n_i}(\mathbf{0}, \sigma^2 \mathbf{R}_i(\rho))$, $i = 1, \dots, n$, we considered AR(1) and CS structures, i.e. the (j, k) th entry of $\mathbf{R}_i(\rho)$ was either $\rho^{|t_{ij}-t_{ik}|}$ or $\mathbb{I}(j = k) + \rho\mathbb{I}(j \neq k)$ respectively. We fixed $\sigma^2 = 1$ and varied $\rho \in \{0, 0.4, 0.8\}$ so that we could evaluate our method under no, moderate, and strong temporal correlation.

We evaluated estimation error, out-of-sample prediction error, and variable selection performance for the posterior modal estimates. For estimation error, we computed the rescaled mean squared error $100 \times \text{MSE}$, where $\text{MSE} = (1/Np) \sum_{k=1}^p \sum_{i=1}^n \sum_{j=1}^{n_i} (\hat{\beta}_k(t_{ij}) - \beta_{0k}(t_{ij}))^2$. For prediction error, we generated 50 new observations $(\mathbf{Y}_{\text{new}}, \mathbf{t}_{\text{new}}, \mathbf{X}_{\text{new}})$, calculated a new \mathbf{U} matrix (2.5), and computed mean squared prediction error $\text{MSPE} = (1/N) \|\mathbf{Y}_{\text{new}} - \mathbf{U}_{\text{new}} \hat{\gamma}\|_2^2$. Finally, to evaluate variable selection performance, we calculated the F1 score, which is defined as:

$$\text{F1} = \frac{2 \times \text{precision} \times \text{recall}}{\text{precision} + \text{recall}},$$

where $\text{precision} = \text{TP}/(\text{TP} + \text{FP})$, $\text{recall} = \text{TP}/(\text{TP} + \text{FN})$, and TP, FP, and FN denote the number of true positives, false positives, and false negatives respectively. A higher F1 score indicates that the model does a better job including relevant functions $\beta_k(t)$, while excluding irrelevant ones.

For the NVC-SSL model, we fixed the slab parameter $\lambda_1 = 1$ in the $\mathcal{SSGL}(\lambda_0, \lambda_1, \theta)$ prior (2.8) and used the dynamic posterior exploration strategy detailed in Appendix A.1 to tune the spike parameter λ_0 . Specifically, we tuned λ_0 from the ladder $I = \{5, 10, 15, 20, 25, 30, 40, 50, 60, 70, 80, 90, 100\}$. We set $a = 1, b = p$ in the prior (2.9) on θ so that θ is small with high probability, and we set $c_0 = 1, d_0 = 1$ in the prior (2.10) on σ^2 , so that the prior was weakly informative. The discrete uniform prior on ρ (2.11) had support $\{0, 0.1, \dots, 0.9\}$. Finally, the degrees of freedom d was chosen from the range $\{4, \dots, 12\}$ to minimize the AIC_c criterion (3.9).

With $p = 400$ and $4 \leq d \leq 12$, we estimated a total of between 1600 and 4800 unknown basis coefficients in γ . Thus, it would be quite time-consuming to implement this model using MCMC. However, with the EM

AR(1)									
	$\rho = 0$			$\rho = 0.4$			$\rho = 0.8$		
	100× MSE	MSPE	F1	100× MSE	MSPE	F1	100× MSE	MSPE	F1
NVC-SSL	0.18	1.81	0.90	0.11	1.50	0.93	0.09	1.72	0.98
NVC-gLASSO	1.42	6.64	0.94	1.42	6.35	0.92	1.41	6.27	0.94
NVC-gSCAD	0.67	3.63	0.91	0.69	3.44	0.91	0.69	3.45	0.92
NVC-gMCP	0.65	3.55	0.89	0.70	3.47	0.88	0.67	3.37	0.89

CS									
	$\rho = 0$			$\rho = 0.4$			$\rho = 0.8$		
	100× MSE	MSPE	F1	100× MSE	MSPE	F1	100× MSE	MSPE	F1
NVC-SSL	0.19	2.21	0.90	0.12	1.84	0.94	0.03	1.45	0.99
NVC-gLASSO	1.42	6.34	0.94	1.43	6.25	0.93	1.41	6.29	0.93
NVC-gSCAD	0.68	3.30	0.92	0.70	3.57	0.91	0.66	3.24	0.92
NVC-gMCP	0.71	3.39	0.89	0.69	3.51	0.89	0.65	3.23	0.89

Table 1: Rescaled MSE, MSPE, and F1 results for our numerical simulations, averaged across 100 replications.

algorithm we introduced in Section 3, we obtained MAP estimates for $\hat{\gamma}$ (and thus estimates of $\hat{\beta}_k(t), k = 1, \dots, p$) in a fraction of the time it would take to perform MCMC.

We compared our method to the group lasso (gLASSO), group smoothly clipped absolute deviation (gSCAD), and group minimax concave penalty (gMCP) [76, 35]. For high-dimensional NVC models, these models solve the following optimization problem:

$$\hat{\gamma} = \arg \max_{\gamma} \frac{1}{2} \|\mathbf{Y} - \mathbf{U}\gamma\|_2^2 + \sum_{k=1}^p \text{pen}_{\lambda}(\gamma_k),$$

where \mathbf{U} is defined as in (2.5) and $\text{pen}_{\lambda}(\cdot)$ is a penalty function that depends on a tuning parameter λ . These methods have been considered by numerous authors [67, 68, 69]. Unlike the NVC-SSL model, however, the penalty function $\text{pen}_{\lambda}(\cdot)$ is fully separable. Further, these penalized frequentist methods all ignore the within-subject temporal correlations. We choose (λ, d) to minimize the AIC_c criterion $AIC_c = \|\mathbf{Y} - \mathbf{U}\hat{\gamma}\|_2^2/N + 1 + 2(\hat{s} + 1)/(N - \hat{s} - 2)$, where \hat{s} is the estimated number of nonzero functions.

Table 1 reports the MSE, MSPE, and F1 score averaged across 100 replications. For both the AR(1) or CS within-subject error structures, the NVC-SSL has much lower estimation error and prediction error than the competing methods. This suggests two things: 1) that it is beneficial to use a *non*-separable and self-adaptive penalty (as the NVC-SSL does through the prior on the mixing proportion θ (2.9)), and 2) that estimation and predictive performance both improve when we account for the within-subject

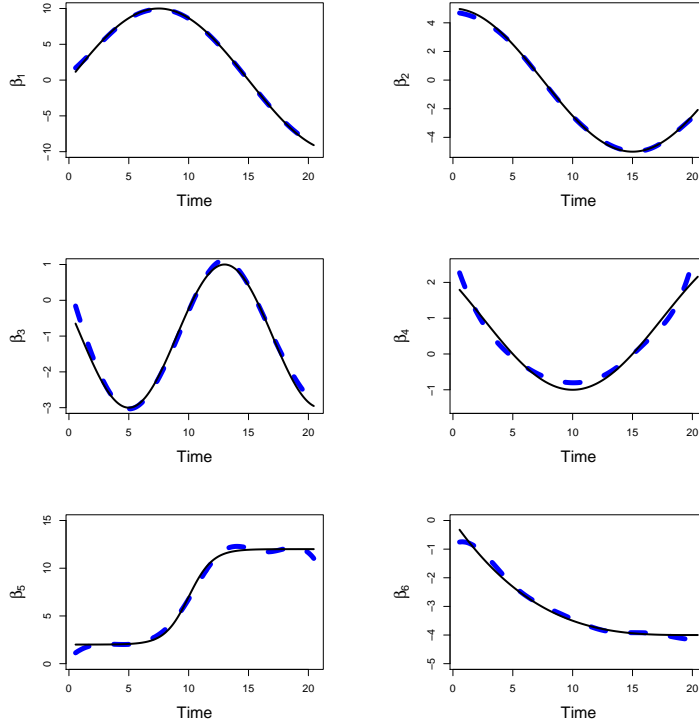


Figure 1: Plots of the estimates for $\beta_k(t)$, $k = 1, \dots, 6$, under the NVC-SSL model when the error terms follow AR(1) structure with $\rho = 0.8$. The true functions are the solid lines and the NVC-SSL estimates are the dashed lines.

correlations in our estimation procedure. In terms of variable selection, when there was no temporal correlation ($\rho = 0$), the NVC-gLASSO method had the highest F1 score. However, when temporal correlation was present (a more realistic scenario), the NVC-SSL model performed the best. In particular, when the correlation was high ($\rho = 0.8$), the NVC-SSL model had an F1 score close to 1 for both AR(1) and CS error structures, indicating that our model almost always selected the correct nonzero functions while excluding the spurious ones.

Figure 1 plots the NVC-SSL model's estimates of the nonzero functions $\beta_k(t)$, $k = 1, \dots, 6$, for one of the AR(1) simulations when $\rho = 0.8$ (dashed lines) against the true functions (solid lines). Figure 1 illustrates that the NVC-SSL model was able to estimate the unknown functions very accurately in the presence of high temporal correlation.

	$100 \times \text{MSE}$	MSPE	F1
Robustified NVC-SSL	0.10	1.84	0.99
NVC-gLASSO	1.38	6.15	0.94
NVC-gSCAD	0.65	3.22	0.92
NVC-gMCP	0.63	3.14	0.89

Table 2: MSE, MSPE, and F1 score for the robustified NVC-SSL model, compared to NVC-gLASSO, NVC-gSCAD, and NVC-gMCP. The results are averaged across 100 replications.

6.2 Simulation Study for the Robustified NVC-SSL Model Under Misspecification

Our simulation results in Section 6.1 partly relied on the fact that we correctly specified the error covariance structure. Here, we demonstrate that the robustified NVC-SSL model introduced in Section 5 gives excellent performance even when we have misspecified the working covariance structure. In Appendix D.2, we provide an additional simulation study of the robustified NVC-SSL model under both heteroscedasticity and incorrectly specified covariance structure.

We kept all the same simulation settings as those in Section 6.1, except for the random errors $\varepsilon_i, i = 1, \dots, n$. The random errors were generated from $\varepsilon_i \sim \mathcal{N}_{n_i}(\mathbf{0}, \sigma^2 \mathbf{T}_i)$, where $\sigma^2 = 1$ and the \mathbf{T}_i 's had Toeplitz structure,

$$\mathbf{T}_i = \begin{pmatrix} 1 & \rho_1 & \rho_2 & \cdots & \rho_{n_i-1} \\ \rho_1 & 1 & \rho_1 & & \vdots \\ \rho_2 & \rho_1 & 1 & \ddots & \rho_2 \\ \vdots & & \ddots & \ddots & \rho_1 \\ \rho_{n_i-1} & \cdots & \rho_2 & \rho_1 & 1 \end{pmatrix}.$$

The off-diagonal correlations $\rho_1, \dots, \rho_{n_i-1}$ were generated randomly from $\mathcal{U}(0, 0.9)$ and the \mathbf{T}_i 's were constrained to be positive-definite. In this case, neither the AR(1) or CS structure was correctly specified, and the within-subject correlation matrices were characterized by multiple correlation parameters and had the possibility of long-range dependence.

We fit the robustified NVC-SSL model with degrees of freedom $d = 8$ and a working covariance structure of AR(1). We chose the fractional power ξ from the grid, $\xi \in \{0.5, 0.6, 0.7, 0.8, 0.9, 0.95, 0.99\}$ to minimize AIC_c (3.9). We used Algorithm 2 in Section A.2 of the Supplementary Material to obtain

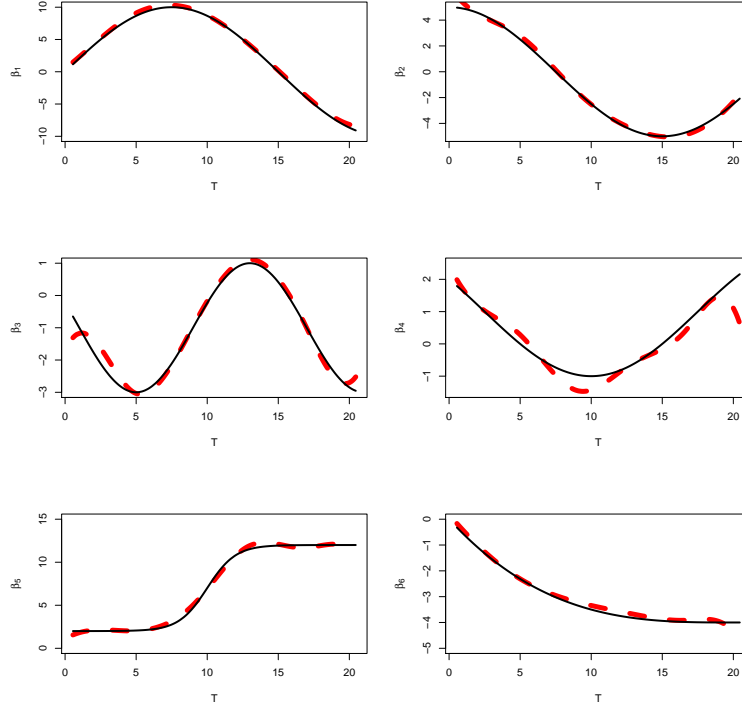


Figure 2: Plots of the estimates for $\beta_k(t)$, $k = 1, \dots, 6$, under the robustified NVC-SSL model when the error terms have a Toeplitz structure. The true functions are the solid lines and the robustified NVC-SSL estimates are the dashed lines.

the MAP estimates for our model. Table 2 reports our results averaged across 100 replications, compared to the NVC-gLASSO, NVC-gSCAD, and NVC-gMCP models. We see that the robustified NVC-SSL had much better estimation, prediction, and variable selection accuracy than the frequentist approaches, despite the fact that we misspecified the working covariance error structure. Figure 2 plots the function estimates under the robustified NVC-SSL model (dashed lines) against the true regression functions (solid lines) for one experiment. We see that the robustified NVC-SSL model was able to recover the larger signals $(\beta_1, \beta_2, \beta_5)$ nearly perfectly, while also recovering the smaller signals (β_3, β_4) fairly well.

7 Yeast Cell Cycle Data Analysis

The cell cycle is a tightly regulated set of processes by which cells grow, replicate their DNA, segregate their chromosomes, and divide into daughter cells. Transcription factors (TFs) are sequence-specific DNA binding proteins which regulate the transcription of genes from DNA to mRNA by binding specific DNA sequences. To better understand how TFs regulate the cell cycle, we applied our proposed NVC-SSL procedure to a data set of cell-cycle regulated yeast genes and associated TFs.

The data that we used comes from the α -factor synchronized cultures of Spellman et al. [62] and the CHIP-chip data of Lee et al. [43]. Spellman et al. [62] measured genome-wide mRNA levels for 6,178 yeast open reading frames (ORFs) over approximately two cell cycle periods, with measurements at 7-minute intervals for 119 minutes (for a total of 18 time points). The data of Lee et al. [43] contains binding information of $p = 96$ TFs which elucidates which TFs bind to promoter sequences of genes across the yeast genome. We aimed to fit the varying coefficient model,

$$y_{ij} = \sum_{k=1}^{96} x_{ik}\beta_k(t_{ij}) + \varepsilon_{ij}, i = 1, \dots, n, j = 1, \dots, 18. \quad (7.1)$$

where y_{ij} denotes the mRNA level for the i th gene at the j th time point. Previous works for fitting (7.1) assumed that the error terms ε_{ij} 's were independent for all i and j [68, 69]. However, de Lichtenberg et al. [15] identified 113 yeast genes most likely to be periodically expressed (or to display periodicities over time) in small-scale experiments, including 104 genes used by [62]. This suggests that at least some genes display temporal correlation, and the independence assumptions previously used are not always appropriate.

From the data sets in [62] and [43], we extracted the 104 genes identified as periodically expressed by [15]. After excluding genes with missing values in either of the experiments, we were left with $n = 47$ genes. Thus, we have $p > n$. Since our data consisted of equispaced time points, we first conducted the Durbin-Watson (DW) test [40] to test whether the errors followed a stationary first order autoregression. The DW test concluded that there was significant autocorrelation of lag one in the data (i.e. reject $H_0 : \rho = 0$). We then fit the NVC-SSL model with AR(1) covariance structure and regularization parameters $\lambda = 1$ and λ_0 ranging on an equally spaced grid from 25 to 400. We compared our results to the NVC-gLASSO, NVC-gSCAD, and NVC-gMCP approaches.

Table 3 shows our results for in-sample prediction error and number of TFs selected. The NVC-SSL model selected 37 TFs. NVC-gSCAD selected

	MSPE	Number of TFs Selected
NVC-SSL	0.071	37
NVC-gLASSO	0.073	75
NVC-gSCAD	0.087	32
NVC-gMCP	0.066	75

Table 3: Predictive accuracy and number of transcription factors selected by the NVC-SSL model, compared with NVC-gLASSO, NVC-gSCAD, and NVC-gMCP.

the most parsimonious model (32 TFs), but it had the worst predictive accuracy. Meanwhile, the NVC-gMCP model had the best predictive accuracy, but it selected a highly non-sparse model (75 out of 96 TFs). Our results demonstrate that the NVC-SSL model was able to achieve both relative parsimony *and* predictive accuracy.

Of the 37 TFs selected by NVC-SSL, 15 TFs were also selected by the other three methods. Figure 3 gives the names of these 15 TFs and plots their estimated transcriptional effects over time. In Section F of the Supplementary Material, we provide the names and plots of the estimated effects for the remaining 22 TFs selected by the NVC-SSL model. We also compare our findings to several existing results on the yeast cell cycle process in the literature in Appendix F.

8 Discussion

In this paper, we have introduced the nonparametric varying coefficient spike-and-slab lasso, a new Bayesian approach for estimation and variable selection in high-dimensional NVC models. The NVC-SSL extends the spike-and-slab lasso methodology [59] to the functional regression setting with dependent responses. Under model (1.1), the NVC-SSL performs simultaneous estimation and variable of the functional components. Moreover, the NVC-SSL simultaneously estimates the covariance structure of the responses, whereas previously proposed frequentist penalized approaches to NVC models have ignored these temporal correlations. Unlike frequentist approaches, the NVC-SSL model also employs a *non*-separable penalty which allows for automatic model complexity control and self-adaptivity to the true level of sparsity in the data.

We introduced an efficient EM algorithm to obtain maximum *a posteriori* estimates, thus allowing us to bypass the use of MCMC. We provided

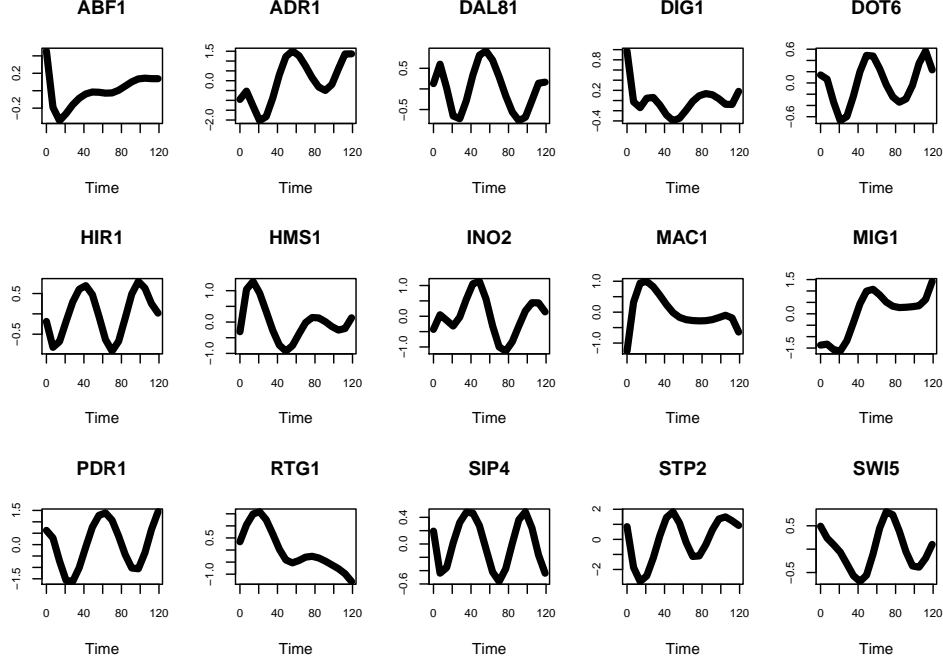


Figure 3: Plots of the estimated transcriptional effects over time for the 15 TFs selected by NVC-SSL that were also selected by NVC-gLASSO, NVC-gSCAD, and NVC-gMCP.

theoretical support for the NVC-SSL by deriving posterior contraction rates when $p \gg n$. Finally, we introduced the robustified NVC-SSL model and showed theoretically and empirically that it consistently estimates the true functionals even when the within-subject covariance structure has been misspecified. Our technique may be useful for other spike-and-slab lasso models where potential model misspecification is a concern.

There are a few directions for future research. In this paper, we have only considered univariate functions of time. A possible direction for future research is to extend the NVC-SSL model for modeling *multivariate* functions of both time and space, i.e. $\beta_k := \beta_k(\mathbf{s}, t), k = 1, \dots, p$, where $\mathbf{s} \in \mathcal{S}$ and \mathcal{S} is some (possibly multi-dimensional) spatial domain. This would widen the use of our methodology for spatiotemporal models.

Finally, the issue of model robustness deserves further attention. One open issue is how to determine a more automatic, data-driven value for $\xi > 0$ in the fractional posterior of Section 5. When the parameter space is low-

dimensional (e.g. a single scalar), several researchers, e.g. [33, 30, 49], have proposed data-driven methods based on optimizing the expected gain in information from using a fractional likelihood or by minimizing a posterior expected loss function. These approaches require calculating expectations, which will be very computationally intensive and unstable when the parameter space is large. In the present context, we would need to perform dp numerical integrations over the unknown parameters in γ to obtain these sort of data-driven values for ξ . Obtaining an automatic, data-driven estimate for ξ in a computationally feasible way is an interesting question for future research.

Alternative approaches for ensuring model robustness are also worth exploring. In the frequentist setting, a common approach for working around misspecification of correlation structure is to use generalized estimating equations (GEEs), or pseudolikelihood methods [46, 77, 12, 23]). GEEs do *not* require the response to be normally distributed and only require the user to specify a “working” covariance structure. GEEs are known to consistently estimate the unknown parameters even if the covariance structure is misspecified [46, 12, 23]. It would be interesting to explore the use of GEEs for Bayesian varying coefficient models. Under the Bayesian paradigm, replacing the likelihood with a pseudolikelihood would not yield a true posterior, but it is possible that the resultant “pseudo-posterior” would achieve both excellent finite-sample performance and posterior contraction at the (near) optimal rate [1]. We leave these investigations for future work.

Acknowledgments

The bulk of this work was done when the first listed author was a post-doc at the Perelman School of Medicine, University of Pennsylvania, under the mentorship of the last two authors. The authors are grateful to the Editor, the Associate Editor, and two anonymous referees for their helpful and insightful comments which led to a substantially improved article. The authors are grateful to Seonghyun Jeong for helpful discussions.

Funding

Dr. Ray Bai and Dr. Mary Boland were funded in part by generous funding from the Perelman School of Medicine, University of Pennsylvania. The work of Ray Bai and Yong Chen was supported in part by National Institutes of Health grants 1R01LM012607 (R.B., Y.C.) and 1R01AI130460 (Y.C.).

References

- [1] Atchadé, Y. A. (2017). On the contraction properties of some high-dimensional quasi-posterior distributions. *The Annals of Statistics*, 45(5):2248–2273.
- [2] Bai, R., Moran, G. E., Antonelli, J. L., Chen, Y., and Boland, M. R. (2020). Spike-and-slab group lassos for grouped regression and sparse generalized additive models. *Journal of the American Statistical Association* (to appear).
- [3] Banerjee, N. and Zhang, M. Q. (2003). Identifying cooperativity among transcription factors controlling the cell cycle in yeast. *Nucleic Acids Research*, 31(23):7024–7031.
- [4] Basu, S. and Michailidis, G. (2015). Regularized estimation in sparse high-dimensional time series models. *The Annals of Statistics*, 43(4):1535–1567.
- [5] Bhattacharya, A., Pati, D., and Yang, Y. (2019). Bayesian fractional posteriors. *The Annals of Statistics*, 47(1):39–66.
- [6] Biller, C. and Fahrmeir, L. (2001). Bayesian varying-coefficient models using adaptive regression splines. *Statistical Modelling*, 1(3):195–211.
- [7] Birrell, C. L., Steel, D. G., and Lin, Y.-X. (2011). Seasonal adjustment of an aggregate series using univariate and multivariate basic structural models. *Journal of Statistical Theory and Practice*, 5(2):179–205.
- [8] Bühlmann, P. and van de Geer, S. (2011). *Statistics for High-Dimensional Data: Methods, Theory and Applications*. Springer Publishing Company, Incorporated, 1st edition.
- [9] Cai, Z., Fan, J., and Li, R. (2000). Efficient estimation and inferences for varying-coefficient models. *Journal of the American Statistical Association*, 95(451):888–902.
- [10] Castillo, I., Schmidt-Hieber, J., and van der Vaart, A. (2015). Bayesian linear regression with sparse priors. *The Annals of Statistics*, 43(5):1986–2018.
- [11] Chen, H. and Wang, Y. (2011). A penalized spline approach to functional mixed effects model analysis. *Biometrics*, 67(3):861–870.

- [12] Chen, Y., Ning, J., and Cai, C. (2015). Regression analysis of longitudinal data with irregular and informative observation times. *Biostatistics*, 16(4):727–739.
- [13] Christensen, R., Johnson, W., Branscum, A., and Hanson, T. E. (2011). *Bayesian Ideas and Data Analysis: An Introduction for Scientists and Statisticians*. CRC Press.
- [14] De Boor, C. (2001). *A Practical Guide to Splines; rev. ed.* Applied mathematical sciences. Springer, Berlin.
- [15] de Lichtenberg, U., Jensen, L. J., Fausbøll, A., Jensen, T. S., Bork, P., and Brunak, S. (2005). Comparison of computational methods for the identification of cell cycle-regulated genes. *Bioinformatics*, 21(7):1164–1171.
- [16] Deshpande, S. K., Ročková, V., and George, E. I. (2019). Simultaneous variable and covariance selection with the multivariate spike-and-slab lasso. *Journal of Computational and Graphical Statistics*, 28(4):921–931.
- [17] Diggle, P. J., Heagerty, P., Liang, K.-Y., and Zeger, S. L. (2002). *Analysis of Longitudinal Data*. Oxford University Press.
- [18] Dobriban, E. and Fan, J. (2016). Regularity properties for sparse regression. *Communications in Mathematics and Statistics*, 4(1):1–19.
- [19] Fan, J. and Li, R. (2001). Variable selection via nonconcave penalized likelihood and its oracle properties. *Journal of the American Statistical Association*, 96(456):1348–1360.
- [20] Fan, J. and Zhang, J.-T. (2000a). Two-step estimation of functional linear models with applications to longitudinal data. *Journal of the Royal Statistical Society. Series B (Statistical Methodology)*, 62(2):303–322.
- [21] Fan, J. and Zhang, W. (2000b). Simultaneous confidence bands and hypothesis testing in varying-coefficient models. *Scandinavian Journal of Statistics*, 27(4):715–731.
- [22] Fan, J. and Zhang, W. (2008). Statistical methods with varying coefficient models. *Statistics and Its Interface*, 1(1):179–195.
- [23] Fang, E. X., Ning, Y., and Li, R. (2019). Test of significance for high-dimensional longitudinal data. *The Annals of Statistics (to appear)*.

- [24] Farouki, R. T. (2012). The Bernstein polynomial basis: A centennial retrospective. *Computer Aided Geometric Design*, 29(6):379 – 419.
- [25] Gan, L., Narisetty, N. N., and Liang, F. (2019a). Bayesian regularization for graphical models with unequal shrinkage. *Journal of the American Statistical Association*, 114(527):1218–1231.
- [26] Gan, L., Yang, X., Narisetty, N., and Liang, F. (2019b). Bayesian joint estimation of multiple graphical models. In Wallach, H., Larochelle, H., Beygelzimer, A., d’Alché Buc, F., Fox, E., and Garnett, R., editors, *Advances in Neural Information Processing Systems 32*, pages 9799–9809. Curran Associates, Inc.
- [27] George, B. and Aban, I. (2015). Selecting a separable parametric spatiotemporal covariance structure for longitudinal imaging data. *Statistics in Medicine*, 34(1):145–161.
- [28] Ghosal, S. and van der Vaart, A. (2017). *Fundamentals of Nonparametric Bayesian Inference*. Cambridge Series in Statistical and Probabilistic Mathematics. Cambridge University Press.
- [29] Greene, W. H. (2003). *Econometric Analysis*. Pearson Education.
- [30] Grünwald, P. (2012). The safe bayesian. In Bshouty, N. H., Stoltz, G., Vayatis, N., and Zeugmann, T., editors, *Algorithmic Learning Theory*, pages 169–183, Berlin, Heidelberg. Springer Berlin Heidelberg.
- [31] Hastie, T. and Tibshirani, R. (1993). Varying-coefficient models. *Journal of the Royal Statistical Society: Series B (Statistical Methodology)*, 55(4):757–796.
- [32] Hastie, T., Tibshirani, R., and Wainwright, M. (2015). *Statistical Learning with Sparsity: The Lasso and Generalizations*. Chapman & Hall/CRC.
- [33] Holmes, C. C. and Walker, S. G. (2017). Assigning a value to a power likelihood in a general Bayesian model. *Biometrika*, 104(2):497–503.
- [34] Hoover, D. R., Rice, J. A., Wu, C. O., and Yang, L.-P. (1998). Non-parametric smoothing estimates of time-varying coefficient models with longitudinal data. *Biometrika*, 85(4):809–822.
- [35] Huang, J., Breheny, P., and Ma, S. (2012). A selective review of group selection in high-dimensional models. *Statistical Science*, 27(4):481–499.

- [36] Huang, J. Z., Wu, C. O., and Zhou, L. (2004). Polynomial spline estimation and inference for varying coefficient models with longitudinal data. *Statistica Sinica*, 14:763–788.
- [37] Huang, Z., Li, J., Nott, D., Feng, L., Ng, T.-P., and Wong, T.-Y. (2015). Bayesian estimation of varying-coefficient models with missing data, with application to the singapore longitudinal aging study. *Journal of Statistical Computation and Simulation*, 85(12):2364–2377.
- [38] Hurvich, C. M., Simonoff, J. S., and Tsai, C.-L. (1998). Smoothing parameter selection in nonparametric regression using an improved Akaike information criterion. *Journal of the Royal Statistical Society. Series B (Statistical Methodology)*, 60(2):271–293.
- [39] Jeong, S. and Ghosal, S. (2020). Unified Bayesian asymptotic theory for sparse linear regression. *preprint*.
- [40] King, M. L. (1992). *Introduction to Durbin and Watson (1950, 1951) Testing for Serial Correlation in Least Squares Regression. I, II*, pages 229–236. Springer New York, New York, NY.
- [41] Krafty, R. T., Gimotty, P. A., Holtz, D., Coukos, G., and Guo, W. (2008). Varying coefficient model with unknown within-subject covariance for analysis of tumor growth curves. *Biometrics*, 64:1023–1031.
- [42] Kyung, M., Gill, J., Ghosh, M., and Casella, G. (2010). Penalized regression, standard errors, and Bayesian lassos. *Bayesian Analysis*, 5(2):369–411.
- [43] Lee, T. I., Rinaldi, N. J., Robert, F., Odom, D. T., Bar-Joseph, Z., Gerber, G. K., Hannett, N. M., Harbison, C. T., Thompson, C. M., Simon, I., Zeitlinger, J., Jennings, E. G., Murray, H. L., Gordon, D. B., Ren, B., Wyrick, J. J., Tagne, J.-B., Volkert, T. L., Fraenkel, E., Gifford, D. K., and Young, R. A. (2002). Transcriptional regulatory networks in *saccharomyces cerevisiae*. *Science*, 298(5594):799–804.
- [44] Li, J., Wang, Z., Li, R., and Wu, R. (2015). Bayesian group lasso for nonparametric varying-coefficient models with application to functional genome-wide association studies. *The Annals of Applied Statistics*, 9(2):640–664.
- [45] Li, Z., McCormick, T., and Clark, S. (2019). Bayesian joint spike-and-slab graphical lasso. In Chaudhuri, K. and Salakhutdinov, R., editors,

- Proceedings of the 36th International Conference on Machine Learning*, volume 97 of *Proceedings of Machine Learning Research*, pages 3877–3885, Long Beach, California, USA. PMLR.
- [46] Liang, K.-Y. and Zeger, S. L. (1986). Longitudinal data analysis using generalized linear models. *Biometrika*, 73(1):13–22.
 - [47] Liang, K. Y. and Zeger, S. L. (1993). Regression analysis for correlated data. *Annual Review of Public Health*, 14(1):43–68.
 - [48] Liu, S. H., Bobb, J. F., Henn, B. C., Gennings, C., Schnaas, L., Tellez-Rojas, M., Bellinger, D., Arora, M., Wright, R. O., and Coull, B. A. (2018). Bayesian varying coefficient kernel machine regression to assess neurodevelopmental trajectories associated with exposure to complex mixtures. *Statistics in Medicine*, 25(3):665–683.
 - [49] Miller, J. W. and Dunson, D. B. (2019). Robust Bayesian inference via coarsening. *Journal of the American Statistical Association*, 114(527):1113–1125.
 - [50] Moran, G. E., Ročková, V., and George, E. I. (2019a). Spike-and-slab lasso biclustering. *preprint*.
 - [51] Moran, G. E., Ročková, V., and George, E. I. (2019b). Variance prior forms for high-dimensional Bayesian variable selection. *Bayesian Analysis*, 14(4):1091–1119.
 - [52] Ning, B., Jeong, S., and Ghosal, S. (2020). Bayesian linear regression for multivariate responses under group sparsity. *Bernoulli*, 3(26):2353–2382.
 - [53] Pourahmadi, M. (2002). Graphical diagnostics for modeling unstructured covariance matrices. *International Statistical Review*, 70(3):395–417.
 - [54] Qu, A. and Li, R. (2006). Quadratic inference functions for varying-coefficient models with longitudinal data. *Biometrics*, 62:379–391.
 - [55] Raskutti, G., Wainwright, M. J., and Yu, B. (2010). Restricted eigenvalue properties for correlated gaussian designs. *Journal of Machine Learning Research*, 11:2241–2259.
 - [56] Rice, J. A. (2004). Functional and longitudinal data analysis: Perspectives on smoothing. *Statistica Sinica*, 14(3):631–647.

- [57] Ročková, V. and George, E. I. (2014). EMVS: The EM approach to bayesian variable selection. *Journal of the American Statistical Association*, 109(506):828–846.
- [58] Ročková, V. and George, E. I. (2016). Fast Bayesian factor analysis via automatic rotations to sparsity. *Journal of the American Statistical Association*, 111(516):1608–1622.
- [59] Ročková, V. and George, E. I. (2018). The spike-and-slab LASSO. *Journal of the American Statistical Association*, 113(521):431–444.
- [60] Scott, J. G. and Berger, J. O. (2010). Bayes and empirical-Bayes multiplicity adjustment in the variable-selection problem. *The Annals of Statistics*, 38(5):2587–2619.
- [61] Simon, I., Barnett, J., Hannett, N., Harbison, C. T., Rinaldi, N. J., Volkert, T. L., Wyrick, J. J., Zeitlinger, J., Gifford, D. K., Jaakkola, T. S., and Young, R. A. (2001). Serial regulation of transcriptional regulators in the yeast cell cycle. *Cell*, 106(6):697 – 708.
- [62] Spellman, P. T., Sherlock, G., Zhang, M. Q., Iyer, V. R., Anders, K., Eisen, M. B., Brown, P. O., Botstein, D., and Futcher, B. (1998). Comprehensive identification of cell cycle-regulated genes of the yeast *Saccharomyces cerevisiae* by microarray hybridization. *Molecular Biology of the Cell*, 9(12):3273–3297. PMID: 9843569.
- [63] Tang, Z., Shen, Y., Zhang, X., and Yi, N. (2017). The spike-and-slab lasso generalized linear models for prediction and associated genes detection. *Genetics*, 205(1):77–88.
- [64] Tibshirani, R. (1996). Regression shrinkage and selection via the lasso. *Journal of the Royal Statistical Society, Series B*, 58:267–288.
- [65] Tsai, H.-K., Lu, H. H.-S., and Li, W.-H. (2005). Statistical methods for identifying yeast cell cycle transcription factors. *Proceedings of the National Academy of Sciences*, 102(38):13532–13537.
- [66] Walker, S. and Hjort, N. L. (2001). On Bayesian consistency. *Journal of the Royal Statistical Society: Series B (Statistical Methodology)*, 63(4):811–821.
- [67] Wang, H. and Xia, Y. (2009). Shrinkage estimation of the varying coefficient model. *Journal of the American Statistical Association*, 104(486):747–757.

- [68] Wang, L., Li, H., and Huang, J. Z. (2008). Variable selection in nonparametric varying-coefficient models for analysis of repeated measurements. *Journal of the American Statistical Association*, 103(484):1556–1569.
- [69] Wei, F., Huang, J., and Li, H. (2011). Variable selection and estimation in high-dimensional varying-coefficient models. *Statistica Sinica*, 21:1515–1540.
- [70] Wei, R., Reich, B. J., Hoppin, J. A., and Ghosal, S. (2020). Sparse Bayesian additive nonparametric regression with application to health effects of pesticides mixtures. *Statistica Sinica*, 30:55–79.
- [71] Winer, B. J., Brown, D. R., and Michels, K. M. (1991). *Statistical Principles in Experimental Design*. McGraw-Hill Humanities/Social Sciences/Languages, 3 edition.
- [72] Wu, C. O. and Chiang, C.-T. (2000). Kernel smoothing on varying coefficient models with longitudinal dependent variable. *Statistica Sinica*, 10(2):433–456.
- [73] Xu, X. and Ghosh, M. (2015). Bayesian variable selection and estimation for group lasso. *Bayesian Analysis*, 10(4):909–936.
- [74] Xue, L. and Qu, A. (2012). Variable selection in high-dimensional varying-coefficient models with global optimality. *Journal of Machine Learning Research*, 13(1):1973–1998.
- [75] Yoo, W. W. and Ghosal, S. (2016). Supremum norm posterior contraction and credible sets for nonparametric multivariate regression. *The Annals of Statistics*, 44(3):1069–1102.
- [76] Yuan, M. and Lin, Y. (2006). Model selection and estimation in regression with grouped variables. *Journal of the Royal Statistical Society: Series B (Statistical Methodology)*, 68(1):49–67.
- [77] Zeger, S. L. and Liang, K.-Y. (1986). Longitudinal data analysis for discrete and continuous outcomes. *Biometrics*, 42(1):121–130.
- [78] Zhang, C.-H. (2010). Nearly unbiased variable selection under minimax concave penalty. *The Annals of Statistics*, 38(2):894–942.
- [79] Zhou, S., Shen, X., and Wolfe, D. (1998). Local asymptotics for regression splines and confidence regions. *The Annals of Statistics*, 26(5):1760–1782.

A Additional Computational Details for Implementation

A.1 Initialization and Dynamic Posterior Exploration

For the usual (non-robustified) NVC-SSL model, we initialize our EM algorithm at $\gamma^{(0)} = \mathbf{0}_{pd}$ and $\theta^{(0)} = 0.5$. Following [51], we also initialize $\sigma^{2(0)}$ to be the mode of a scaled inverse chi-squared distribution with degrees of freedom $\nu = 3$ and scale parameter chosen such that the sample variance of \mathbf{Y} corresponds to the 90th quantile of the prior.

We fix the slab hyperparameter λ_1 to be a small constant so that the slab density has considerable spread. Having a diffuse slab with fixed λ_1 allows vectors with large coefficients to escape the pull of the spike. As a default, we recommend setting $\lambda_1 = 1$, though we have found that our model’s performance is not very sensitive to the specific choice of λ_1 as long as it is much smaller than the spike hyperparameter λ_0 .

A potential issue we face with the EM algorithm is multimodality. The posterior distribution under the NVC-SSL prior will typically be multimodal when $p \gg n$ and $\lambda_0 \gg \lambda_1$, and thus, any MAP finding algorithm is prone to becoming entrapped at a suboptimal local mode for γ . To mitigate this issue, we employ *dynamic posterior exploration* to increase the chances of finding more optimal modes [59, 57, 2]. If we set the spike hyperparameter λ_0 to be too small, then many negligible γ_k ’s will tend to be selected in our model. To eliminate these suboptimal non-sparse modes, we gradually increase λ_0 along a ladder of L increasing values, $I = \{\lambda_0^1, \dots, \lambda_0^L\}$. For each λ_0^s in the ladder, we reinitialize $(\gamma, \theta, \sigma^2, \rho^2)$ using the MAP estimate $(\hat{\gamma}_{s-1}, \hat{\theta}_s, \hat{\sigma}_{s-1}^2, \hat{\rho}_{s-1})$ from the previous spike parameter λ_0^{s-1} as a “warm start.” As we increase λ_0 along the ladder, the posterior becomes “spikier,” with the spikes absorbing more and more negligible parameter estimates. By the time the spikes have reappeared (when $\lambda_0 \gg \lambda_1$), the sequential reinitialization strategy ensures that we will be more likely to be in the basin of the dominant mode.

For large enough λ_0 , this dynamic posterior exploration approach also eventually stabilizes so that further increases in λ_0 do not change the solution. We recommend $I = \{5, 10, 15, 20, 25, 30, 40, 50, 60, 70, 80, 90, 100\}$. We have found this choice to work well in a variety of simulation and real data settings. Of course, the practitioner may perform a sensitivity analysis with different choices of ladders for λ_0 .

The complete algorithm with dynamic posterior exploration is given in Algorithm 1. Step 3 of the algorithm is computed in parallel for each $m_h \in$

Algorithm 1 Nonparametric Varying Coefficient Spike-and-Slab Lasso

Input: grid of increasing λ_0 values $I = \{\lambda_0^1, \dots, \lambda_0^L\}$ and initial values $\boldsymbol{\gamma}^* = \boldsymbol{\gamma}^{(0)}$, $\theta^* = \theta^{(0)}$, $\sigma^{2*} = \sigma^{2(0)}$

For $s = 1, \dots, L$:

1. Set iteration counter $t_s = 0$
2. Initialize $\boldsymbol{\gamma}^* = \boldsymbol{\gamma}^{(t_{s-1})}$, $\theta^* = \theta^{(t_{s-1})}$, $\sigma^{2*} = \sigma^{2(t_{s-1})}$
3. For each m_h in m_1, \dots, m_q :
 - (a) Set $\rho = m_h$ and set $\tilde{\mathbf{Y}} = \mathbf{R}^{-1/2}(m_h)\mathbf{Y}$ and $\tilde{\mathbf{U}} = \mathbf{R}^{-1/2}(m_h)\mathbf{U}$.
 - (b) While $\text{diff} > \varepsilon$
 - i. Increment t_s
 - E-step:**
 - ii. Compute $\lambda_k^* = \lambda_1 p_k^{*(t_{s-1})} + \lambda_0(1 - p_k^{*(t_{s-1})})$, $k = 1, \dots, p$, where $p_k^{*(t_{s-1})} = p^*(\boldsymbol{\gamma}_k^{(t_{s-1})}, \theta^{(t_{s-1})})$ as in (3.4)
 - M-step:**
 - iii. Update $\theta^{(t_s)}$ given $\rho = m_h$ according to (3.6)
 - iv. Update $\boldsymbol{\gamma}^{(t_s)}$ given $\rho = m_h$ by solving (3.7)
 - v. Update $\sigma^{2(t_s)}$ given $\rho = m_h$ according to (3.8)
 - vi. $\text{diff} = \|\boldsymbol{\gamma}^{(t_s)} - \boldsymbol{\gamma}^{(t_{s-1})}\|_2$
 - (c) Evaluate $\log \pi(\boldsymbol{\gamma}^{(t_s)}, \theta^{(t_s)}, \sigma^{2(t_s)}, \rho | \mathbf{Y}, \rho = m_h)$ as in (3.1)
 4. Set $\rho^{(t_s)}$ equal to the m_h that maximizes $\log \pi(\boldsymbol{\gamma}^{(t_s)}, \theta^{(t_s)}, \sigma^{2(t_s)}, \rho | \mathbf{Y}, \rho = m_h)$, and set the corresponding $(\boldsymbol{\gamma}^{(t_s)}, \theta^{(t_s)}, \sigma^{2(t_s)})$ given $\rho^{(t_s)}$ to be the final values for $(\boldsymbol{\gamma}^{(t_s)}, \theta^{(t_s)}, \sigma^{2(t_s)})$

Return $\hat{\beta}_k(\mathbf{t}) = \sum_{l=1}^d \hat{\gamma}_{kl} B_{kl}(\mathbf{t})$, $k = 1, \dots, p$.

$\{m_1, \dots, m_q\}$ to accelerate computing time. Letting \mathbf{Y}_i and \mathbf{U}_i denote the subvector of \mathbf{Y} and submatrix of \mathbf{U} corresponding to the i th subject, we also compute $\tilde{\mathbf{Y}}_i = \mathbf{R}_i^{-1/2} \mathbf{Y}_i$, and $\tilde{\mathbf{U}}_i = \mathbf{R}_i^{-1/2} \mathbf{U}_i$, $i = 1, \dots, n$, in parallel and then combine them into a single $\tilde{\mathbf{Y}}$ and $\tilde{\mathbf{U}}$ respectively.

A.2 EM Algorithm for the Robustified NVC-SSL Model

In this section, we describe the EM algorithm for the robustified NVC-SSL model introduced in Section 5. Note that in this case, we have pre-specified n working within-subject error covariance matrices $\mathbf{S}_1, \dots, \mathbf{S}_n$, so the only unknowns we need to estimate in our model are $(\boldsymbol{\gamma}, \theta)$. Similarly as in Section 3.1, we first introduce the latent binary indicators $\boldsymbol{\tau} = (\tau_1, \dots, \tau_p)'$ and reparametrize the $\mathcal{SSGL}(\lambda_0, \lambda_1, \theta)$ prior as in (3.2). Let

$\mathbf{S} = \text{diag}(\mathbf{S}_1, \dots, \mathbf{S}_n)$. Given a fractional power $\xi \in (0, 1)$, the log-fractional posterior for $(\boldsymbol{\gamma}, \theta, \boldsymbol{\tau})$ (up to an additive constant) is then

$$\begin{aligned} \log \pi_{n,\xi}(\boldsymbol{\gamma}, \theta, \boldsymbol{\tau} | \mathbf{Y}) &= -\frac{\xi}{2} \sum_{i=1}^n \log |\mathbf{S}_i| - \frac{\xi}{2} \|\mathbf{S}^{-1/2}(\mathbf{Y} - \mathbf{U}\boldsymbol{\gamma})\|_2^2 \\ &\quad + \sum_{k=1}^p \log \left((1 - \tau_k) \lambda_0^d e^{-\lambda_0 \|\boldsymbol{\gamma}_k\|_2} + \tau_k \lambda_1^d e^{-\lambda_1 \|\boldsymbol{\gamma}_k\|_2} \right) \\ &\quad + \left(a - 1 + \sum_{k=1}^p \tau_k \right) \log \theta + \left(b - 1 + p - \sum_{k=1}^p \tau_k \right) \log(1 - \theta). \end{aligned} \quad (\text{A.1})$$

For the robustified NVC-SSL EM algorithm, we iterate between E-step and M-step until convergence after initializing $(\boldsymbol{\gamma}^{(0)}, \theta^{(0)})$. For the E-step, we compute $p_k^*(\boldsymbol{\gamma}_k^{(t)}, \theta^{(t)}) = \mathbb{E}[\tau_k | \mathbf{Y}, \boldsymbol{\gamma}^{(t-1)}, \theta^{(t-1)}]$, $k = 1, \dots, p$, where $p_k^*(\boldsymbol{\gamma}, \theta)$ is defined as in (3.4). For the M-step, we then maximize the following objective function with respect to $(\boldsymbol{\gamma}, \theta)$:

$$\begin{aligned} \mathbb{E}[\log \pi_{n,\xi}(\boldsymbol{\gamma}, \theta | \mathbf{Y}) | \boldsymbol{\gamma}^{(t-1)}, \theta^{(t-1)}] &= -\frac{\xi}{2} \|\mathbf{S}^{-1/2}(\mathbf{Y} - \mathbf{U}\boldsymbol{\gamma})\|_2^2 - \sum_{k=1}^p \lambda_k^* \|\boldsymbol{\gamma}_k\|_2 + \left(a - 1 + \sum_{k=1}^p p_k^* \right) \log \theta \\ &\quad + \left(b - 1 + p - \sum_{k=1}^p p_k^* \right) \log(1 - \theta). \end{aligned} \quad (\text{A.2})$$

From (A.2), it is clear that $\theta^{(t)}$ has the same update in the M-step as (3.6). Let $\check{\mathbf{Y}} = \mathbf{S}^{-1/2}\mathbf{Y}$ and $\check{\mathbf{U}} = \mathbf{S}^{-1/2}\mathbf{U}$. To update $\boldsymbol{\gamma}$, we solve the following optimization:

$$\boldsymbol{\gamma}^{(t)} = \arg \max_{\boldsymbol{\gamma}} -\frac{1}{2} \|\check{\mathbf{Y}} - \check{\mathbf{U}}\boldsymbol{\gamma}\|_2^2 - \sum_{k=1}^p \frac{\lambda_k^*}{\xi} \|\boldsymbol{\gamma}_k\|_2, \quad (\text{A.3})$$

which is also an adaptive group lasso problem with group-specific weights λ_k^*/ξ and can be solved with the usual block coordinate ascent algorithms.

For the robustified NVC-SSL EM algorithm, we initialize $\boldsymbol{\gamma}^{(0)} = \mathbf{0}_{dp}$ and $\theta^{(0)} = 0.5$. In the $\mathcal{SSGL}(\lambda_0, \lambda_1, \theta)$ prior, we fix the slab hyperparameter λ_1 to be a small constant and pursue the same dynamic posterior exploration strategy with regard to λ_0 that was outlined in Section A.1. For the working covariance matrices $\mathbf{S}_1, \dots, \mathbf{S}_n$, we opt to use the working AR(1) structure

Algorithm 2 Robustified NVC-SSL

Input: grid of increasing λ_0 values $I = \{\lambda_0^1, \dots, \lambda_0^L\}$, working covariance matrices $\mathbf{S}_1, \dots, \mathbf{S}_n$, fractional power $\xi \in (0, 1)$, and initial values $\boldsymbol{\gamma}^* = \boldsymbol{\gamma}^{(0)}$, $\boldsymbol{\theta}^* = \boldsymbol{\theta}^{(0)}$,

Compute $\mathbf{S}_1^{-1/2}, \dots, \mathbf{S}_n^{-1/2}$ and set $\check{\mathbf{Y}} = \mathbf{S}^{-1/2}\mathbf{Y}$ and $\check{\mathbf{U}} = \mathbf{S}^{-1/2}\mathbf{U}$.

For $s = 1, \dots, L$:

1. Set iteration counter $t_s = 0$
2. Initialize $\boldsymbol{\gamma}^* = \boldsymbol{\gamma}^{(t_{s-1})}$, $\boldsymbol{\theta}^* = \boldsymbol{\theta}^{(t_{s-1})}$
3. While $\text{diff} > \varepsilon$
 - (a) Increment t_s
 - E-step:**
 - (b) Compute $\lambda_k^* = \lambda_1 p_k^{*(t_{s-1})} + \lambda_0(1 - p_k^{*(t_{s-1})})$, $k = 1, \dots, p$, where $p_k^{*(t_{s-1})} = p^*(\boldsymbol{\gamma}_k^{(t_{s-1})}, \boldsymbol{\theta}^{(t_{s-1})})$ as in (3.4)
 - M-step:**
 - (c) Update $\boldsymbol{\theta}^{(t_s)}$ according to (3.6)
 - (d) Update $\boldsymbol{\gamma}^{(t_s)}$ by solving (A.3)
 - (e) $\text{diff} = \|\boldsymbol{\gamma}^{(t_s)} - \boldsymbol{\gamma}^{(t_{s-1})}\|_2$

Return $\hat{\beta}_k(\mathbf{t}) = \sum_{l=1}^d \hat{\gamma}_{kl} B_{kl}(\mathbf{t})$, $k = 1, \dots, p$.

$\mathbf{S}_i = \sigma^2 \mathbf{R}_i(\rho)$, $i = 1, \dots, n$, where $\mathbf{R}_i(j, k) = \rho^{-|t_{ij} - t_{ik}|}$. To determine empirical Bayes estimates for (σ^2, ρ) , we first take an initial estimate of $\hat{\boldsymbol{\gamma}}$ based on a standard group lasso fit. We then choose the (σ^2, ρ) which maximizes the marginal log-likelihood for $\mathbf{Y} \sim \mathcal{N}(\mathbf{U}\hat{\boldsymbol{\gamma}}, \sigma^2 \mathbf{R}(\rho))$, i.e.

$$\max_{\sigma^2 \in (0, \infty), \rho \in (0, 1)} -\frac{N}{2} \log \sigma^2 - \frac{1}{2} \sum_{i=1}^n \log |\mathbf{R}_i(\rho)| - \frac{\sum_{i=1}^n \|\mathbf{R}_i^{-1/2}(\rho)(\mathbf{Y}_i - \mathbf{U}_i \hat{\boldsymbol{\gamma}})\|_2^2}{2\sigma^2},$$

where \mathbf{Y}_i and \mathbf{U}_i denote the subvector of \mathbf{Y} and submatrix of \mathbf{U} for the i th subject. The complete algorithm for the robustified NVC-SSL model is given in Algorithm 2. Note that we only need to compute $\mathbf{S}_1, \dots, \mathbf{S}_n$, $\mathbf{S}_1^{-1/2}, \dots, \mathbf{S}_n^{-1/2}$, $\check{\mathbf{Y}}$, and $\check{\mathbf{U}}$ *once* before we begin the EM algorithm. If the number of within-subject observations n_i is prohibitively large, then we can also set the \mathbf{S}_i 's to be the identity matrices \mathbf{I}_{n_i} , $i = 1, \dots, n$, (i.e. employ a working independence structure) to avoid the cost of computing matrix determinants or matrix inverses.

B Additional Discussion of the NVC-SSL Model

B.1 Determining the Appropriate Error Covariance Structure to Use

The NVC-SSL model described in Section 2.2 requires the user to specify the error covariance structure (AR(1) or CS). In order to determine which one to use, we can first obtain the residuals $\hat{y}(t_{ij}) - y(t_{ij})$ from a regression fit (e.g. a regression with the standard group lasso). Then we can construct empirical variogram plots, scatterplot matrices, or correlograms of the residuals to give us an idea of the underlying error covariance structure [17, 53].

In particular, empirical variograms and correlograms of the residuals (see Chapter 5 of [17] and the review article by [53]) are widely used in practice to determine the appropriate covariance structure to use for modeling longitudinal and spatial data. If the residual variogram or correlogram shows decaying correlation with distance, then we may specify the AR(1) structure for the NVC-SSL model. On the other hand, if these plots suggest equicorrelation, then we may specify the CS structure.

Besides graphical procedures such as variograms and scatterplots, there are several tests to formally test for first-order autoregressive or compound symmetry structure. For equispaced time points, the Durbin-Watson significance test can be used to test for AR(1) error structure [40]. For compound symmetry, a formal hypothesis test based on expanding the likelihood ratio with a correction factor C is given in [71]. Note that because the NVC-SSL model allows for ρ in (2.7) to be estimated as $\hat{\rho} = 0$ (as seen in the support $\{0, 0.1, \dots, 0.9\}$ for the prior (2.11)), our model can *also* model the case of i.i.d. errors with no temporal correlation.

B.2 Discussion of Regularity Assumptions (A3)-(A6) for the Asymptotic Theory

Here, we provide a detailed discussion of the regularity assumptions (A3)-(A6) used for the asymptotic theory in Section 4.

Assumption (A3) is a compatibility (or restricted eigenvalue) condition used to control the eigenstructure of the design matrix \mathbf{U} and is frequently invoked in sparse regression problems [8, 10]. When $p \gg n$, the smallest eigenvalue of \mathbf{U} is necessarily zero. To ensure estimability of $\boldsymbol{\gamma}$ in this scenario, the restricted eigenvalue condition (A3) ensures that the smallest eigenvalue of the submatrix of \mathbf{U} corresponding to nonzero groups of basis coefficients is bounded away from zero. A similar sparse Riesz condition on

\mathbf{U} was also used for high-dimensional frequentist penalized nonparametric varying coefficient models in [69].

The restricted eigenvalue condition is known to hold with high probability when the rows of \mathbf{U} are independent and sub-Gaussian [55]. Recently, Basu and Michailidis [4] showed that under temporal dependence, the restricted eigenvalue also holds with high probability (Propositions 3.1 and 4.2 of [4]) if the rows of the design matrix are generated from a stable Gaussian autoregressive-moving-average process (ARMA(p, q)) of any orders p, q . Note that ARMA models subsume autoregressive (AR(p)) models and moving average (MA(q)) models as special cases.

In our case, Condition (A3) will hold if the covariates in $\mathbf{X} = [\mathbf{X}_1, \dots, \mathbf{X}_p]$ from (2.3) are either independent and sub-Gaussian *or* if the rows of \mathbf{X} are dependent and generated from stable Gaussian ARMA processes. Outside of covariates generated under these specific conditions, it can be difficult to verify Assumption (A3). However, for normal linear regression with i.i.d. errors, it is *also* NP-hard to verify restricted eigenvalue conditions outside of a certain class of matrices with independent, sub-Gaussian rows [18]. It is reassuring that the result in [4] applies to a wide class of stochastic matrices with temporal dependence between rows. This suggests that the condition (A3) may not be overly restrictive at all.

We also remark that if we are interested in *prediction* error loss, then we do not need to impose *any* restricted eigenvalue conditions on the design matrix \mathbf{U} . The average prediction error can be expressed as $\frac{1}{N} \|\widehat{\mathbf{Y}} - \mathbf{Y}\|_2^2 = \frac{1}{N} \|\mathbf{U}\hat{\boldsymbol{\gamma}} - \mathbf{U}\boldsymbol{\gamma}_0\|_2^2$. Lemma 3 shows that

$$\mathbb{E}_0 \Pi \left(\frac{1}{N} \|\mathbf{U}(\boldsymbol{\gamma} - \boldsymbol{\gamma}_0)\|_2^2 \geq M \epsilon_n^2 | \mathbf{Y} \right) \rightarrow 0 \text{ as } n \rightarrow \infty,$$

for some $M > 0$ and $\epsilon_n^2 = s_0 \log p/n + s_0 n^{-2\alpha/(2\alpha+1)}$. Recall that under Assumption (A1), $\epsilon_n^2 \rightarrow 0$ as $n \rightarrow \infty$, and thus, under average prediction error loss, we can consistently recover \mathbf{Y} without eigenvalue conditions on \mathbf{U} . However, a compatibility condition on \mathbf{U} , as in Assumption (A3), is mandatory if we want to convert an ℓ_2 -norm concentration result for the mean vector $\mathbf{U}\boldsymbol{\gamma}$ to an ℓ_2 -norm concentration result for $\boldsymbol{\gamma}$ itself (which then implies posterior contraction for the functionals).

Assumption (A4) assumes that all the covariates are uniformly bounded. This is a standard assumption in the asymptotic theory for varying coefficient models and has been employed by multiple authors in the theory for frequentist NVC models [36, 68, 74, 69]. As noted by [74], it is needed even in the case where p is fixed. Additionally, as noted in [69], the condition (A4) is often satisfied in practice. For example, this condition will be satisfied

automatically if the time range \mathcal{T} is a finite, closed interval and the $x(t)$'s are generated from continuous functions of t . Then by the boundedness theorem, there exists $M > 0$ so that $|x(t)| \leq M$ for all $t \in \mathcal{T}$. In practice, the covariates are also often standardized (e.g. to lie in $[0, 1]$ or to have mean zero and standard deviation one), in which case they are bounded.

Finally, Assumptions (A5) and (A6) ensure that the within-subject covariance matrices $\sigma^2 \mathbf{R}_i(\rho), i = 1, \dots, n$, are asymptotically well-behaved in some sense. In particular, Assumption (A5) states that the true within-subject correlation matrices should have eigenvalues that are bounded away from zero and infinity for all n . Assumption (A6) ensures that for n subjects, the maximum squared Frobenius norm for the difference between two covariance matrices of dimension $n_i \times n_i$ can be bounded above by a function of n_{\max} . In Theorem 10 of [39], it is shown that these two conditions hold for a wide class of covariance matrices, including compound symmetry, moving average (MA), and AR(1) covariance matrices. Thus, the conditions (A5)-(A6) can be considered mild.

C Additional Simulation Studies

In this section, we provide additional simulation studies assessing the performance of the NVC-SSL model when: (i) some of the nonzero functions are either linear or constant (non-time varying), (ii) the number of within-subject observations n_i exceeds sample size n for all $i = 1, \dots, n$, and (iii) the insignificant covariates are strongly correlated with the significant ones. In our experiments, we found that our results were not very sensitive to the choice of basis dimension d . Hence, we use $d = 8$ for all of the methods.

C.1 Estimating Linear and Non-Time Varying Significant Functions

Here, we assess whether the NVC-SSL model can recover significant functions that are either perfectly linear or non-time varying. Our simulation settings were the same as those in Section 6.1 with $n = 50$ and $p = 400$, except we changed the true nonzero functions $\beta_k(t), k = 1, \dots, 6$, to be:

$$\begin{aligned}\beta_1(t) &= 2t - 10, \beta_2(t) = 5 \cos\left(\frac{\pi t}{15}\right), \beta_3(t) = -1 + 2 \sin\left(\frac{\pi(t-25)}{8}\right), \\ \beta_4(t) &= -2.5, \beta_5(t) = 10, \beta_6(t) = -t/3, \\ \beta_7(t) &= \dots = \beta_{400}(t) = 0.\end{aligned}$$

AR(1)									
	$\rho = 0$			$\rho = 0.4$			$\rho = 0.8$		
	100× MSE	MSPE	F1	100× MSE	MSPE	F1	100× MSE	MSPE	F1
NVC-SSL	0.40	5.05	0.99	0.39	4.63	0.99	0.28	4.79	0.99
NVC-gLASSO	7.21	22.96	0.91	7.09	23.65	0.93	7.28	23.97	0.91
NVC-gSCAD	6.10	24.06	0.80	5.15	20.98	0.84	5.48	21.58	0.82
NVC-gMCP	6.37	25.38	0.75	6.11	25.65	0.76	5.99	24.48	0.76

CS									
	$\rho = 0$			$\rho = 0.4$			$\rho = 0.8$		
	100× MSE	MSPE	F1	100× MSE	MSPE	F1	100× MSE	MSPE	F1
NVC-SSL	0.44	5.35	0.99	0.41	4.73	0.99	0.29	4.95	0.99
NVC-gLASSO	7.29	24.01	0.93	7.39	24.51	0.92	7.10	22.97	0.93
NVC-gSCAD	5.81	24.35	0.82	5.58	22.63	0.82	5.33	21.76	0.84
NVC-gMCP	5.93	25.07	0.77	6.28	26.06	0.75	5.74	23.64	0.78

Table C.1: Rescaled MSE, MSPE, and F1 results for our numerical simulations where some of the functions were perfectly linear or constant, averaged across 100 replications.

That is, β_1 and β_6 were linear functions, while β_4 and β_5 were constant functions.

Table C.1 reports our results averaged across 100 simulations. We see that for all the different levels of temporal correlation, the NVC-SSL model obtained the lowest estimation error, the lowest out-of-sample prediction error, and the highest variable selection accuracy. In particular, we found that the other nonconvex methods, NVC-gSCAD and NVC-gMCP, had more difficulty recovering the constant functions, which explains their lower F1 score. In Figure C.1, we plot the function estimates for $\beta_k(t)$, $k = 1, \dots, 6$, under the NVC-SSL model (dashed lines) against the true functions (solid lines). We see that the NVC-SSL model does a fairly good job estimating the linear functions β_1 and β_6 , as well as the constant functions β_4 and β_5 .

Based on our results, we conclude that B-splines are a flexible enough class of basis functions to model both *non*-time varying covariates and perfectly linear functionals. However, if we know *a priori* that the functions have to obey certain shape constraints (e.g. linearity or monotonicity), we can instead use different basis functions that will enforce these constraints, such as piecewise linear splines [29] or Bernstein polynomials [24].

It may also be worthwhile to perform formal hypothesis tests $H_0 : \beta_k(t) = c$ for each $\beta_k(t)$, $k = 1, \dots, p$, prior to fitting the model. Examples of these tests include bootstrap-based tests [9] and generalized likelihood ratio tests [21]. Then if any of the p covariates are determined to be non-time varying, the NVC-SSL model can be straightforwardly extended to the

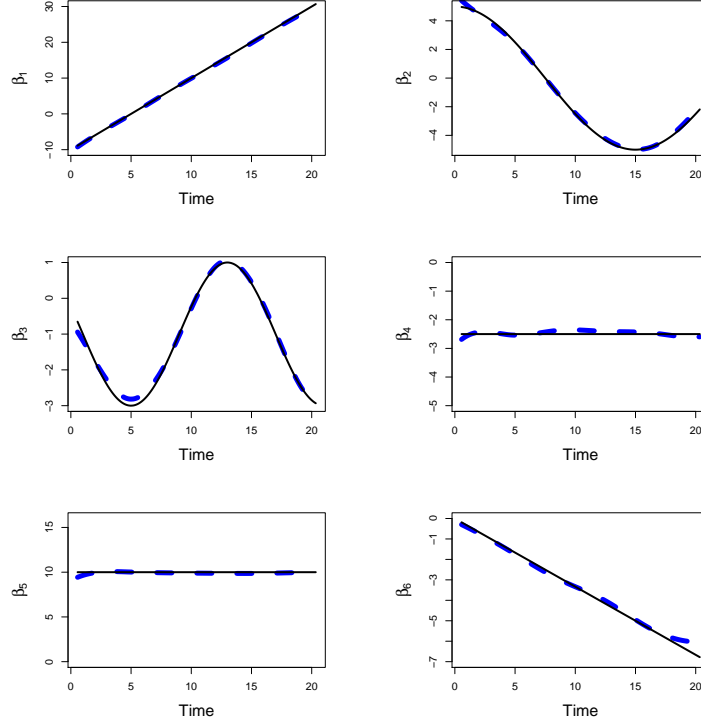


Figure C.1: Plots of the estimates for $\beta_k(t), k = 1, \dots, 6$, under the NVC-SSL model when the error terms follow CS structure with $\rho = 0.8$, and $\beta_1, \beta_4, \beta_5$, and β_6 are either linear or constant (non-time varying) functions. The true functions are the solid lines and the NVC-SSL estimates are the dashed lines.

semiparametric model,

$$y_i(t_{ij}) = \mathbf{z}_i' \boldsymbol{\theta} + \sum_{k=1}^{p-q} x_{ik}(t_{ij}) \beta_k(t_{ij}) + \varepsilon_i(t_{ij}),$$

where $\mathbf{z}_i = (z_{i1}, \dots, z_{iq})' \in \mathbb{R}^q$ is a q -dimensional vector (with $q < p$) with *non-time* varying covariates. In this case, a separate prior could be put on $\boldsymbol{\theta}$, and the EM algorithm detailed in Section 3.1 can be modified straightforwardly to update $\boldsymbol{\theta}$ at each iteration.

AR(1)									
	$\rho = 0$			$\rho = 0.4$			$\rho = 0.8$		
	100× MSE	MSPE	F1	100× MSE	MSPE	F1	100× MSE	MSPE	F1
NVC-SSL	0.04	0.12	0.77	0.03	0.08	0.82	0.03	0.07	0.80
NVC-gLASSO	17.86	3.48	0.78	17.95	3.47	0.78	18.06	3.50	0.79
NVC-gSCAD	13.45	2.41	0.68	16.91	3.05	0.63	13.50	2.43	0.67
NVC-gMCP	13.64	2.46	0.70	10.43	1.88	0.75	12.61	2.28	0.72

CS									
	$\rho = 0$			$\rho = 0.4$			$\rho = 0.8$		
	100× MSE	MSPE	F1	100× MSE	MSPE	F1	100× MSE	MSPE	F1
NVC-SSL	0.04	0.13	0.76	0.03	0.09	0.82	0.03	0.10	0.82
NVC-gLASSO	17.75	3.46	0.79	17.88	3.48	0.78	17.93	3.48	0.79
NVC-gSCAD	17.60	3.18	0.61	14.98	2.72	0.64	18.40	3.29	0.60
NVC-gMCP	16.96	3.06	0.65	14.58	2.65	0.68	15.69	2.82	0.66

Table C.2: Rescaled MSE, MSPE, and F1 results for our numerical simulations where $n_i > n$ for all $i = 1, \dots, n$.

C.2 Number of Within-Subject Observations Exceeds Sample Size

To derive our asymptotic results for the NVC-SSL model in Section 4, we required the number of within-subject observations n_i to be much smaller than sample size for large n . However, for *finite* samples, the issue of $n_i > n$ poses no practical issues. In this section, we demonstrate that the NVC-SSL model is suitable to use when the number of repeated measures is large compared to sample size, and indeed, it often outperforms competing methods when $n_i > n$.

We used the same simulation as those in Section 6.1, except we generated the data for only $n = 20$ subjects, and the within-subject time points were set to be 80 equispaced time points from 0.25 to 20, i.e. $t_{ij} = 0.25, 0.5, 0.75, 1, \dots, 20$, for all $i = 1, \dots, n$. This resulted in $n_i = 80$, and thus $n_i > n$ for all $i = 1, \dots, n$.

Table C.2 reports our results, averaged across 100 replications. We see that the NVC-SSL mode has much lower estimation and prediction error than the other methods. When there is no temporal correlation, the NVC-gLASSO method does slightly better for variable selection. However, when temporal correlations are present, NVC-SSL does the best.

C.3 Strong Correlation Between All Covariates

In our previous simulation settings, we assumed that the noise covariates were uncorrelated with the significant ones. Here, we assess the performance

AR(1)									
	$\rho = 0$			$\rho = 0.4$			$\rho = 0.8$		
	100× MSE	MSPE	F1	100× MSE	MSPE	F1	100× MSE	MSPE	F1
NVC-SSL	3.52	1.70	0.74	3.39	1.87	0.73	4.18	1.90	0.76
NVC-gLASSO	16.08	3.50	0.55	17.68	4.03	0.55	16.75	3.80	0.54
NVC-gSCAD	2.45	0.85	0.91	2.64	0.92	0.91	3.07	1.04	0.91
NVC-gMCP	1.71	0.72	0.95	1.75	0.76	0.94	1.58	0.76	0.95

CS									
	$\rho = 0$			$\rho = 0.4$			$\rho = 0.8$		
	100× MSE	MSPE	F1	100× MSE	MSPE	F1	100× MSE	MSPE	F1
NVC-SSL	3.65	1.67	0.75	3.81	1.93	0.75	4.07	1.90	0.76
NVC-gLASSO	16.79	3.76	0.53	16.89	3.86	0.56	17.25	3.99	0.54
NVC-gSCAD	3.28	1.10	0.90	3.39	1.03	0.90	2.91	0.98	0.91
NVC-gMCP	2.09	0.89	0.94	1.71	0.73	0.95	1.67	0.75	0.95

Table C.3: Rescaled MSE, MSPE, and F1 results for our numerical simulations where all the covariates are strongly correlated.

of the NVC-SSL model when all of the covariates – significant or not – are correlated with each other. We generated data for $n = 40$ subjects and $p = 100$ covariates, where the first six functions were set to the same ones as those in Section 6.1, and the rest of the functions were set equal to zero. To generate the correlated covariates, we generated the design matrix \mathbf{X} so that the rows of \mathbf{X} were drawn from a multivariate normal $\mathcal{N}_p(\mathbf{0}, \mathbf{\Omega})$, where the (j, k) th entry of $\mathbf{\Omega}$ was $\omega_{jk} = \rho^{|j-k|}$, and $\rho = 0.8$ for high correlation. The rest of the simulation settings were the same as those in Section 6.1.

Table C.3 reports our results averaged across 100 replications. In this case, NVC-SSL and NVC-gLASSO did not perform as well as NVC-gSCAD or NVC-gMCP. This is because NVC-SSL and NVC-gLASSO tended to have higher false discovery rates when all the covariates were heavily correlated. Thus, their precisions and F1 scores were lower. Based on our experiments, it appears as though NVC-gSCAD and NVC-gMCP are much better able to navigate multicollinearity between noise variables and significant variables than the ℓ_2 or ℓ_2 -type methods.

When there is weak correlation between the active set of functions and the non-significant functions, the NVC-SSL model often outperforms its competitors. Our experiments in this section shed light on the need for greater improvements and refinements to the NVC-SSL model. Extending the NVC-SSL model so that it can adapt better to the scenario of multicollinearity between active and inactive covariate functions is a topic for future research.

D The NVC-SSL Model Under Completely Unstructured Error Covariance Structure

D.1 The Unstructured NVC-SSL Model

As discussed in Section 2.2 and Section 5, it is not recommended to assume completely unstructured within-subject error covariance matrices $\Sigma_1, \dots, \Sigma_n$ in the model (2.6), since this leads to a heavily overparametrized model with $N + \sum_{i=1}^n \binom{n_i}{2}$ unknown parameters in $\Sigma = \text{diag}(\Sigma_1, \dots, \Sigma_n)$.

Nevertheless, the NVC-SSL model *can* be extended to accommodate this situation. In this case, we place the usual hierarchical $\mathcal{SSGL}(\lambda_0, \lambda_1, \theta)$ prior (2.8)-(2.9) on the basis coefficients γ in (2.6) and treat the Σ_i 's as unknown with priors placed on them. In particular, for each $\Sigma_i, i = 1, \dots, n$, we place an independent inverse-Wishart prior,

$$\pi(\Sigma_i) \sim \mathcal{IW}(m_i, \Omega_i), \quad (\text{D.1})$$

where $m_i > n_i - 1$ is the degrees of freedom and $\Omega_i \succ 0$ is an $n_i \times n_i$ positive-definite scale matrix.

As in Section 3.1, we first introduce the latent binary indicators $\tau = (\tau_1, \dots, \tau_p)'$ and reparametrize the $\mathcal{SSGL}(\lambda_0, \lambda_1, \theta)$ prior as in (3.2). Let Ξ denote the collection $\{\gamma, \theta, \Sigma_1, \dots, \Sigma_n\}$. The log-posterior density for Ξ (up to an additive constant) is given by

$$\begin{aligned} \log \pi(\Xi | \mathbf{Y}) = & -\frac{1}{2} \sum_{i=1}^n \log |\Sigma_i| - \frac{\|\Sigma^{-1/2}(\mathbf{Y} - \mathbf{U}\gamma)\|_2^2}{2} \\ & + \sum_{k=1}^p \log \left((1 - \tau_k) \lambda_0^d e^{-\lambda_0 \|\gamma_k\|_2} + \tau_k \lambda_1^d e^{-\lambda_1 \|\gamma_k\|_2} \right) \\ & + \left(a - 1 + \sum_{k=1}^p \tau_k \right) \log \theta + \left(b - 1 + p - \sum_{k=1}^p \tau_k \right) \log(1 - \theta) \\ & - \sum_{i=1}^n \left[\frac{m_i + n_i + 1}{2} \log |\Sigma_i| + \frac{1}{2} \text{tr}(\Omega_i \Sigma_i^{-1}) \right]. \end{aligned} \quad (\text{D.2})$$

For the unstructured NVC-SSL EM algorithm, we iterate between E-step and M-step until convergence. For the E-step, we compute $p_k^*(\gamma_k^{(t)}, \theta^{(t)}) = \mathbb{E}[\tau_k | \mathbf{Y}, \gamma^{(t-1)}, \theta^{(t-1)}], k = 1, \dots, p$, where $p_k^*(\gamma, \theta)$ is defined as in (3.4). For the M-step, we then maximize the following objective function with respect to Ξ :

$$\begin{aligned}
& \mathbb{E} \left[\log \pi(\Xi | \mathbf{Y}) | \Xi^{(t-1)} \right] \\
&= -\frac{\|\Sigma^{-1/2}(\mathbf{Y} - \mathbf{U}\boldsymbol{\gamma})\|_2^2}{2} - \frac{1}{2} \sum_{i=1}^n \left[(m_i + n_i + 2) \log |\Sigma_i| + \text{tr}(\mathbf{\Omega}_i \Sigma_i^{-1}) \right] \\
&\quad - \sum_{k=1}^p \lambda_k^* \|\boldsymbol{\gamma}_k\|_2 + \left(a - 1 + \sum_{k=1}^p p_k^* \right) \log \theta \\
&\quad + \left(b - 1 + p - \sum_{k=1}^p p_k^* \right) \log(1 - \theta). \tag{D.3}
\end{aligned}$$

From (D.3), it is clear that $\theta^{(t)}$ has the same update in the M-step as (3.6). To update $\boldsymbol{\gamma}$, we hold $(\theta, \Sigma) = (\theta^{(t)}, \Sigma^{(t-1)})$ fixed. We compute $\bar{\mathbf{Y}} = \Sigma^{-1/2} \mathbf{Y}$ and $\bar{\mathbf{U}} = \Sigma^{-1/2} \mathbf{U}$ and solve the following optimization:

$$\boldsymbol{\gamma}^{(t)} = \arg \max_{\boldsymbol{\gamma}} -\frac{1}{2} \|\bar{\mathbf{Y}} - \bar{\mathbf{U}} \boldsymbol{\gamma}\|_2^2 - \sum_{k=1}^p \lambda_k^* \|\boldsymbol{\gamma}_k\|_2, \tag{D.4}$$

which is an adaptive group lasso problem with group-specific weights λ_k^* .

Finally, holding $(\theta, \boldsymbol{\gamma}) = (\theta^{(t)}, \boldsymbol{\gamma}^{(t)})$ fixed, we update each $\Sigma_i, i = 1, \dots, n$. Let \mathbf{Y}_i denote the subvector of \mathbf{Y} with n_i entries corresponding to the i th subject and \mathbf{U}_i the submatrix of \mathbf{U} with the n_i rows corresponding to the i th subject. Examining (D.3), we see that the M-step for updating Σ_i entails maximizing the following function with respect to Σ_i :

$$f(\Sigma_i) = -(\mathbf{Y}_i - \mathbf{U}_i \boldsymbol{\gamma})' \Sigma_i^{-1} (\mathbf{Y}_i - \mathbf{U}_i \boldsymbol{\gamma}) + (m_i + n_i + 2) \log |\Sigma_i^{-1}| - \text{tr}(\mathbf{\Omega}_i \Sigma_i^{-1}).$$

Taking the derivative of $f(\Sigma_i)$ with respect to Σ_i^{-1} and solving the equation $\frac{df(\Sigma)}{d\Sigma_i^{-1}} = \mathbf{0}_{n_i \times n_i}$ gives us the closed form update for $\Sigma_i^{(t)}, i = 1, \dots, n$,

$$\Sigma_i^{(t)} = \frac{1}{m_i + n_i + 2} [\mathbf{\Omega}_i + (\mathbf{Y}_i - \mathbf{U}_i \boldsymbol{\gamma})(\mathbf{Y}_i - \mathbf{U}_i \boldsymbol{\gamma})'], \quad i = 1, \dots, n. \tag{D.5}$$

For the unstructured NVC-SSL EM algorithm, we initialize $\boldsymbol{\gamma}^{(0)} = \mathbf{0}_{dp}$, $\boldsymbol{\theta}^{(0)} = 0.5$, and $\Sigma^{(0)} = \mathbf{I}_N$, i.e. all the $\Sigma_i^{(0)}$'s are the identity matrix. For the hyperparameters in the $\mathcal{IW}(m_i, \mathbf{\Omega}_i)$ priors on the Σ_i 's, we recommend using $m_i = n_i$ and $\mathbf{\Omega}_i = \mathbf{I}_{n_i}$ as default choices. These choices of hyperparameters ensure that the update for $\Sigma_i^{(t)}$ is nearly the same as the empirical covariance matrix estimate for $\Sigma_i^{(t)}$. In the $\mathcal{SSGL}(\lambda_0, \lambda_1, \theta)$ prior, we fix the hyperparameter λ_1 to be a small constant and pursue the same dynamic

Algorithm 3 Unstructured NVC-SSL

Input: grid of increasing λ_0 values $I = \{\lambda_0^1, \dots, \lambda_0^L\}$ and initial values $\gamma^* = \gamma^{(0)}$, $\theta^* = \theta^{(0)}$, $\Sigma_1^{(0)}, \dots, \Sigma_n^{(0)}$.

For $s = 1, \dots, L$:

1. Set iteration counter $t_s = 0$
2. Initialize $\gamma^* = \gamma^{(t_{s-1})}$, $\theta^* = \theta^{(t_{s-1})}$, $\Sigma^* = \Sigma^{(t_{s-1})}$
3. While $\text{diff} > \varepsilon$
 - (a) Increment t_s
 - E-step:**
 - (b) Compute $\lambda_k^* = \lambda_1 p_k^{*(t_s-1)} + \lambda_0(1 - p_k^{*(t_s-1)})$, $k = 1, \dots, p$, where $p_k^{*(t_s-1)} = p^*(\gamma_k^{(t_s-1)}, \theta^{(t_s-1)})$ as in (3.4)
 - M-step:**
 - (c) Update $\theta^{(t_s)}$ according to (3.6)
 - (d) Compute $\bar{\mathbf{Y}} = (\Sigma^{(t_s-1)})^{-1/2} \mathbf{Y}$ and $\bar{\mathbf{U}} = (\Sigma^{(t_s-1)})^{-1/2} \mathbf{U}$.
 - (e) Update $\gamma^{(t_s)}$ by solving (D.4)
 - (f) For $i = 1, \dots, n$:
 - i. Update $\Sigma_i^{(t_s)}$ according to (D.5)
 - (g) $\text{diff} = \|\gamma^{(t_s)} - \gamma^{(t_s-1)}\|_2$

Return $\hat{\beta}_k(\mathbf{t}) = \sum_{l=1}^d \hat{\gamma}_{kl} B_{kl}(\mathbf{t})$, $k = 1, \dots, p$.

posterior exploration strategy with regard to λ_0 that was outlined in Section A.1. The complete algorithm for the unstructured NVC-SSL model is given in Algorithm 3.

D.2 Simulation Study of the Unstructured NVC-SSL Model

In this section, we evaluate the performance of the unstructured NVC-SSL model, compared to the robustified NVC-SSL model and frequentist approaches. For our simulations, we generated data for $n = 50$ subjects and $p = 200$ covariates. We set the first six functions $\beta_k(t)$, $k = 1, \dots, 6$ to be the same as those in Section 6.2 and set the rest of them equal to zero. We also generated time points t_{ij} , $i = 1, \dots, n$, $j = 1, \dots, n_i$ and the covariates $x_{ik}(t_{ij})$ using the same settings as those in Section 6.2.

To generate the within-subject errors ε_i , $i = 1, \dots, n$, we did the following:

1. For each $i = 1, \dots, n$, draw a random variable u_i from Bernoulli(0.5).

	100× MSE	MSPE	F1
Unstructured NVC-SSL	4.72	45.53	0.87
Robustified NVC-SSL	0.18	1.76	0.99
NVC-gLASSO	2.83	6.21	0.94
NVC-gSCAD	1.40	3.54	0.91
NVC-gMCP	1.32	3.41	0.89

Table D.1: MSE, MSPE, and F1 score for the unstructured NVC-SSL model and the robustified NVC-SSL model, compared to NVC-gLASSO, NVC-gSCAD, and NVC-gMCP. The results are averaged across 100 replications.

2. If $u_i = 0$, generate $\varepsilon_i \sim \mathcal{N}_{n_i}(\mathbf{0}, \sigma_i^2 \mathbf{R}_i(\rho))$, where σ_i^2 is drawn from $\mathcal{U}(0.5, 2.5)$, ρ is drawn from $\mathcal{U}(0, 0.95)$, and \mathbf{R}_i follows an AR(1) structure.
3. If $u_i = 1$, generate $\varepsilon_i \sim \mathcal{N}_{n_i}(\mathbf{0}, \sigma_i^2 \mathbf{R}_i(\rho))$, where σ_i^2 is drawn from $\mathcal{U}(0.5, 2.5)$, ρ is drawn from $\mathcal{U}(0, 0.95)$, and \mathbf{R}_i follows a CS structure.

Under these simulation settings, we had both heteroscedasticity (i.e. the variance σ_i^2 was different for each i th subject), as well as subjects with different error covariance structures.

Table D.1 reports the results averaged across 100 simulations for the unstructured NVC-SSL model, compared to the robustified NVC-SSL model and the frequentist approaches. For the robustified NVC-SSL model, we specified a working AR(1) structure, while the frequentist methods implicitly assume a working independence structure.

Table D.1 shows that the unstructured NVC-SSL model performed worse than the other methods which had misspecified the temporal correlation structure. This is not surprising because a model with many more parameters (in this case, $N + \sum_{i=1}^n \binom{n_i}{2}$ more parameters) is inherently more difficult to estimate and is thus more likely to give more unstable results, regardless of whether a frequentist or a Bayesian approach is adopted. In the frequentist setup, attempting to simultaneously solve for the MLE's of $(\gamma, \Sigma_1, \dots, \Sigma_n)$ subject to the constraints that $\Sigma_i \succ 0, i = 1, \dots, n$, (i.e. all the Σ_i 's are positive-definite) is also very likely to give poorer estimates than simply maximizing an objective function for γ . In addition, as shown in Table D.1, the prediction error was *much* higher for the unstructured NVC-SSL model than for the other methods. This is because the unstructured NVC-SSL model fails to provide a generalizable fit for new data sets.

On the other hand, Table D.1 also shows that the robustified NVC-SSL

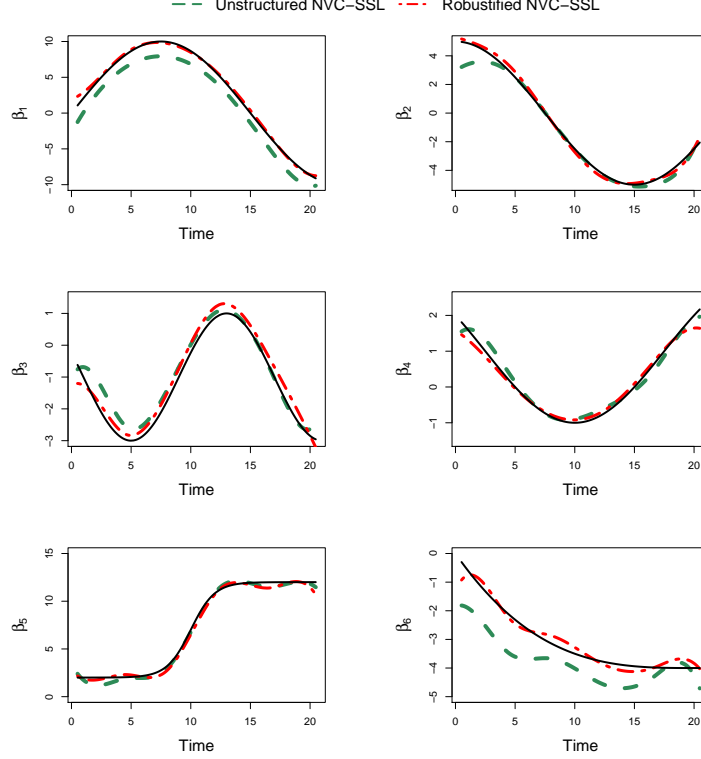


Figure D.1: Plots of the estimates for $\beta_k(t)$, $k = 1, \dots, 6$, under the unstructured NVC-SSL model and the robustified NVC-SSL model (dashed lines) plotted against the true functions (solid lines).

gave the best performance across all performance metrics, with much lower MSE, lower MSPE, and nearly perfect variable selection results. Figure D.1 plots the fits for the unstructured NVC-SSL and robustified NVC-SSL models (dashed lines) against the true functions for one experiment. We see that both the unstructured NVC-SSL and robustified NVC-SSL seem to give decent estimates of the true regression functions. However, as shown by the MSPE's in Table D.1, the fit from the robustified NVC-SSL model was much more generalizable to new data. Our numerical experiments provide further empirical support for using the robustified NVC-SSL model over the unstructured NVC-SSL model when there is doubt about the true temporal correlation structure.

E Proofs of Main Results

In this section, we provide proofs for all the asymptotic results in Sections 4 and 5. Throughout, we use the following notation. For two densities f and g , let $K(f, g) = \int f \log(f/g)$ and $V(f, g) = \int f |\log(f/g) - K(f, g)|^2$ denote the Kullback-Leibler (KL) divergence and variation respectively. Denote the Rényi divergence of order $1/2$ as $\rho(f, g) = -\log \int f^{1/2} g^{1/2} d\nu$. Finally, define the ε -covering number for a set Ω with semimetric d as the minimum number of d -balls of radius ε needed to cover Ω and denote the ε -covering number as $N(\varepsilon, \Omega, d)$ and the metric entropy as $\log N(\varepsilon, \Omega, d)$.

E.1 Proofs for Theorem 1

We first prove a lemma and then proceed to the proof of Theorem 1.

Lemma 1. *Let $f \sim \mathcal{N}_N(\mathbf{U}\boldsymbol{\gamma}, \sigma^2 \mathbf{R}(\rho))$ and $f_0 \sim \mathcal{N}_N(\mathbf{U}\boldsymbol{\gamma}_0 + \boldsymbol{\delta}_0, \sigma_0^2 \mathbf{R}(\rho_0))$. Under model (4.4), suppose that we endow $(\boldsymbol{\gamma}, \sigma^2)$ with the prior (2.8)-(2.10) and ρ with the prior, $\rho \sim \mathcal{U}(0, 1)$. For the $\mathcal{SSGL}(\lambda_0, \lambda_1, \theta)$ prior, we set $\lambda_0 = (1 - \theta)/\theta$ and $\lambda_1 \asymp 1/n$, and for the $\mathcal{B}(a, b)$ prior on θ , we set $a = 1, b = p^c, c > 2$. Suppose that Assumptions (A1)-(A6) hold. Then $\sup_{\boldsymbol{\gamma}_0, \sigma_0^2, \rho_0} \mathbb{P}_0(\mathcal{E}_n^c) \rightarrow 0$, where the set \mathcal{E}_n is*

$$\mathcal{E}_n \equiv \left\{ \int \int \int \frac{f(\mathbf{Y})}{f_0(\mathbf{Y})} d\Pi(\boldsymbol{\gamma}) d\Pi(\sigma^2) d\Pi(\rho) \geq e^{-C_1 n \epsilon_n^2} \right\},$$

for some constant $C_1 > 0$ and $\epsilon_n^2 = s_0 \log p/n + s_0 n^{-2\alpha/(2\alpha+1)}$.

Proof of Lemma 1. By Lemma 8.10 of [28], this statement will be proven if we can show that

$$\Pi \left(K(f_0, f) \leq n \epsilon_n^2, V(f_0, f) \leq n \epsilon_n^2 \right) \gtrsim \exp(-C_1 n \epsilon_n^2). \quad (\text{E.1})$$

For $\mathbf{R}_i^* = (\sigma^2/\sigma_0^2) \mathbf{R}_{0i}^{-1/2} \mathbf{R}_i \mathbf{R}_{0i}^{-1/2}, i = 1, \dots, n$, denote the ordered eigenvalues of \mathbf{R}_i^* by $\lambda_{ij}, 1 \leq j \leq n_i$ and let $\mathbf{R}^* = \text{diag}(\mathbf{R}_1^*, \dots, \mathbf{R}_n^*)$. Using Lemma 9 of [39] and noting that the n subjects are independent, we have that

$$K(f_0, f) = \frac{1}{2} \left\{ \sum_{i=1}^n \sum_{j=1}^{n_i} (\lambda_{ij} - 1 - \log \lambda_{ij}) + \frac{\|\mathbf{R}^{-1/2}(\mathbf{U}(\boldsymbol{\gamma} - \boldsymbol{\gamma}_0) - \boldsymbol{\delta}_0)\|_2^2}{\sigma^2} \right\},$$

$$V(f_0, f) = \left[\sum_{i=1}^n \sum_{j=1}^{n_i} \frac{(1 - \lambda_{ij})^2}{2} \right] + \frac{\sigma_0^2}{(\sigma^2)^2} \|\mathbf{R}_0^{1/2} \mathbf{R}^{-1}(\mathbf{U}(\boldsymbol{\gamma} - \boldsymbol{\gamma}_0) - \boldsymbol{\delta}_0)\|_2^2.$$

Define the sets,

$$\begin{aligned}\mathcal{A}_1 &= \left\{ (\sigma^2, \rho) : \sum_{i=1}^n \sum_{j=1}^{n_i} (\lambda_{ij} - 1 - \log \lambda_{ij}) \leq n\epsilon_n^2, \sum_{i=1}^n \sum_{j=1}^{n_i} (1 - \lambda_{ij})^2 \leq n\epsilon_n^2 \right\}, \\ \mathcal{A}_2 &= \left\{ (\gamma, \sigma^2, \rho) : \frac{\|\mathbf{R}^{-1/2}(\mathbf{U}(\gamma - \gamma_0) - \boldsymbol{\delta}_0)\|_2^2}{\sigma^2} \leq n\epsilon_n^2, \right. \\ &\quad \left. \frac{\sigma_0^2}{(\sigma^2)^2} \|\mathbf{R}_0^{1/2} \mathbf{R}^{-1}(\mathbf{U}(\gamma - \gamma_0) - \boldsymbol{\delta}_0)\|_2^2 \leq \frac{n\epsilon_n^2}{2} \right\}.\end{aligned}$$

Then $\Pi(K(f_0, f)) \leq n\epsilon_n^2$, $V(f_0, f) \leq n\epsilon_n^2 = \Pi(\mathcal{A}_2|\mathcal{A}_1)\Pi(\mathcal{A}_1)$. We will consider $\Pi(\mathcal{A}_1)$ and $\Pi(\mathcal{A}_2|\mathcal{A}_1)$ separately. Arguing as in Lemma 1 of [39], we may expand $\log \lambda_{ij}$ in the powers of $(1 - \lambda_{ij})$ to get $\lambda_{ij} - 1 - \log \lambda_{ij} \sim (1 - \lambda_{ij})^2/2$. Using Lemma 1 of [39], we also have that $\sum_{i=1}^n \sum_{j=1}^{n_i} (1 - \lambda_{ij})^2 \lesssim \sum_{i=1}^n \|\sigma^2 \mathbf{R}_i(\rho) - \sigma_0^2 \mathbf{R}_0(\rho_0)\|_F^2 = \|\sigma^2 \mathbf{R}(\rho) - \sigma_0^2 \mathbf{R}_0(\rho_0)\|_F^2$. Altogether, we have as a lower bound for $\Pi(\mathcal{A}_1)$,

$$\begin{aligned}\Pi(\mathcal{A}_1) &\geq \Pi\left((\sigma^2, \rho) : \|\sigma^2 \mathbf{R}(\rho) - \sigma_0^2 \mathbf{R}_0(\rho_0)\|_F^2 \leq b_1^2 n \epsilon_n^2\right) \\ &\gtrsim \Pi\left((\sigma^2, \rho) : n_{\max}^2 (\sigma^2 - \sigma_0^2)^2 + n_{\max}^4 \sigma_0^4 |\rho - \rho_0|^2 \leq b_1^2 n^2 \epsilon_n^2\right) \\ &\geq \Pi\left(\sigma^2 : |\sigma^2 - \sigma_0^2| \leq \frac{b_1 n \epsilon_n}{\sqrt{2} n_{\max}}\right) \Pi\left(\rho : |\rho - \rho_0| \leq \frac{b_1 n \epsilon_n}{\sqrt{2} \sigma_0^2 n_{\max}^2}\right) \\ &\gtrsim \exp(-C_1 n \epsilon_n^2/2),\end{aligned}\tag{E.2}$$

for some constants $b_1 > 0$ and $C_1 > 0$. The second line of the display comes from Assumption (A6) and the final line comes from the fact that σ^2 and ρ follow inverse gamma and uniform priors respectively.

Next, we focus on bounding $\Pi(\mathcal{A}_2|\mathcal{A}_1)$ from below. Arguing as in Lemma 5.1 of [52], $\mathcal{A}_1 \supset \{\|\sigma^{-2} \mathbf{R}^{-1}(\rho) - \sigma_0^2 \mathbf{R}_0^{-1}(\rho_0)\|_F \leq \epsilon_n/b_2\}$ for some constant $b_2 > 0$ and sufficiently large n , which then implies that $\|\sigma^{-2} \mathbf{R}^{-1}(\rho)\|_2 \lesssim 1$ and $\|\mathbf{R}^*\|_2 \lesssim 1$ (by using suitably modified arguments from the proof of Lemma 5.1 in [52]). Thus, conditional on \mathcal{A}_1 , the left-hand sides for both inequalities in the set \mathcal{A}_2 may be bounded above by a constant multiple of $\|\mathbf{U}(\gamma - \gamma_0) - \boldsymbol{\delta}_0\|_2^2$. Let $r_n^2 := \epsilon_n^2 - s_0 n^{-2\alpha/(2\alpha+1)} = s_0 \log p/n$. For some constants $b_3, b_4 > 0$, we thus have as a lower bound for $\Pi(\mathcal{A}_2|\mathcal{A}_1)$,

$$\begin{aligned}\Pi(\mathcal{A}_2|\mathcal{A}_1) &\gtrsim \Pi\left(\gamma : \|\mathbf{U}(\gamma - \gamma_0) - \boldsymbol{\delta}_0\|_2^2 \leq \frac{n\epsilon_n^2}{2b_3}\right) \\ &\geq \Pi\left(\gamma : \|\mathbf{U}(\gamma - \gamma_0)\|_2^2 + \|\boldsymbol{\delta}_0\|_2^2 \leq \frac{n\epsilon_n^2}{4b_3}\right)\end{aligned}$$

$$\begin{aligned}
&\geq \Pi \left(\gamma : \|\mathbf{U}\|_*^2 \left(\sum_{k=1}^p \|\gamma_k - \gamma_{0k}\|_2 \right)^2 + N s_0 n^{-2\alpha/(2\alpha+1)} \leq \frac{n\epsilon_n^2}{4b_3} \right) \\
&\gtrsim \Pi \left(\gamma : \left(\sum_{k=1}^p \|\gamma_k - \gamma_{0k}\|_2 \right)^2 + \frac{s_0 n^{-2\alpha/(2\alpha+1)}}{4b_4^2} \leq \frac{\epsilon_n^2}{4b_4^2} \right) \\
&= \Pi \left(\gamma : \sum_{k=1}^p \|\gamma_k - \gamma_{0k}\|_2 \leq \frac{r_n}{2b_4} \right) \\
&\geq \int_0^1 \Pi_{S_0} \left(\sum_{k \in S_0} \|\gamma_k - \gamma_{0k}\|_2 \leq \frac{r_n}{4b_4} \middle| \theta \right) \Pi_{S_0^c} \left(\sum_{k \in S_0^c} \|\gamma_k\|_2 \leq \frac{r_n}{4b_4} \middle| \theta \right) d\pi(\theta) \\
&\geq \int_0^1 \left\{ \Pi_{S_0} \left(\|\gamma_{S_0} - \gamma_{0S_0}\|_2^2 \leq \frac{r_n^2}{16b_4^2 s_0} \middle| \theta \right) \right\} \left\{ \Pi_{S_0^c} \left(\|\gamma_{S_0^c}\|_2^2 \leq \frac{r_n^2}{16b_4^2(p-s_0)} \middle| \theta \right) \right\} d\pi(\theta) \\
&\gtrsim \exp(-C_1 n \epsilon_n^2 / 2). \tag{E.3}
\end{aligned}$$

In the third line of the display, we used Assumption (A1) that $d \asymp n^{1/(\alpha+1)}$ and the fact that we used B-splines as the basis functions. In particular, for the true zero functions $\beta_{0k}(t) = 0, k \in S_0^c$, we have that the approximation error from a d -dimensional basis expansion is $\kappa_{0k}(t) = 0$ (since in this case, the basis expansion can approximate $\beta_{0k}(t)$ *exactly*, i.e. $\gamma_{0k} = \mathbf{0}_d$ for $k \in S_0^c$). Thus, the total approximation error for the p basis expansions satisfies $\|\sum_{k=1}^p \kappa_{0k}(\mathbf{t})\|_2^2 = \|\sum_{k \in S_0} \kappa_{0k}(\mathbf{t})\|_2^2$. By properties of B-splines, the choice of $d \asymp n^{1/(\alpha+1)}$ and the assumption of uniform boundedness of the covariates in Assumption (A4), we have that the bias δ_0 satisfies $\|\delta_0\|_2^2 \lesssim N s_0 n^{-2\alpha/(2\alpha+1)}$ (see, e.g., [79, 70, 75]). The fourth line of the display comes from Assumption (A5) that $\|\mathbf{U}\|_*^2 \asymp N$ and Assumption (A1) that $N \asymp n \times n_{\max}$ and $n_{\max} = O(1)$. The sixth line comes from the fact that conditional on θ , the $\mathcal{SSGL}(\lambda_0, \lambda_1, \theta)$ prior is separable, i.e. $\pi(\gamma|\theta) = \pi_{S_0}(\gamma|\theta)\pi_{S_0^c}(\gamma|\theta)$, and the seventh line follows from an application of the Cauchy-Schwarz inequality. The final inequality of the display can be obtained by suitably modifying the arguments used to prove (D.24) in the proof of Theorem 2 of [2].

Combining (E.2)-(E.3), we have that

$$\Pi(\mathcal{A}_2|\mathcal{A}_1) \gtrsim \exp(-C_1 n \epsilon_n^2 / 2) \exp(-C_1 n \epsilon_n / 2) = \exp(-C_1 n \epsilon_n^2),$$

and thus the Kullback-Leibler condition (E.1) holds. Therefore, invoking Lemma 8.10 of [28], $\mathbb{P}_0(\mathcal{E}_n^c) \rightarrow 0$, where \mathcal{E}_n was defined in the lemma. \square

Proof of Theorem 1. Let $\mathcal{E}_n = \left\{ \int \int \int \frac{f(\mathbf{Y})}{f_0(\mathbf{Y})} d\Pi(\gamma) d\Pi(\sigma^2) d\Pi(\rho) \geq e^{-C_1 n \epsilon_n^2} \right\}$, where ϵ_n^2 is defined in Lemma 1. Define the set $\mathcal{B}_n = \{\gamma : |\nu(\gamma)| \leq C_2 s_0\}$,

where $C_2 > C_1$. Then we have

$$\mathbb{E}_0 \Pi(\mathcal{B}_n^c | \mathbf{Y}) \leq \mathbb{E}_0 \Pi(\mathcal{B}_n^c | \mathbf{Y}) \mathbb{1}_{\mathcal{E}_n} + \mathbb{P}_0(\mathcal{E}_n^c). \quad (\text{E.4})$$

By Lemma 1, $\mathbb{P}_0(\mathcal{E}_n^c) \rightarrow 0$ as $n \rightarrow \infty$, so to prove that $\mathbb{E}_0 \Pi(\mathcal{B}_n^c | \mathbf{Y}) \rightarrow 0$, it suffices to show that $\mathbb{E}_0 \Pi(\mathcal{B}^c | \mathbf{Y}) \mathbb{1}_{\mathcal{E}_n} \rightarrow 0$. Now,

$$\Pi(\mathcal{B}_n^c | \mathbf{Y}) = \frac{\int \int \int_{\mathcal{B}_n^c} \frac{f(\mathbf{Y})}{f_0(\mathbf{Y})} d\Pi(\gamma) d\Pi(\sigma^2) d\Pi(\rho)}{\int \int \int \frac{f(\mathbf{Y})}{f_0(\mathbf{Y})} d\Pi(\gamma) d\Pi(\sigma^2) d\Pi(\rho)}. \quad (\text{E.5})$$

On the event \mathcal{E}_n , the denominator in (E.5) is bounded below by $e^{-C_1 n \epsilon_n^2}$. An upper bound for the expected value of the numerator is

$$\mathbb{E}_0 \left(\int \int \int_{\mathcal{B}_n^c} \frac{f(\mathbf{Y})}{f_0(\mathbf{Y})} d\Pi(\gamma) d\Pi(\sigma^2) d\Pi(\rho) \right) \leq \int_{\mathcal{B}_n^c} d\Pi(\gamma) = \Pi(|\nu(\gamma)| > C_2 s_0). \quad (\text{E.6})$$

Using the same arguments as those used to prove (D.34) in the proof of Theorem 2 of [2], we have

$$\Pi(\gamma : |\nu(\gamma)| > C_2 s_0) \prec e^{-C_2 n \epsilon_n^2}. \quad (\text{E.7})$$

Combining (E.6)-(E.7), we have that $\mathbb{E}_0 \Pi(\mathcal{B}_n^c | \mathbf{Y}) \mathbb{1}_{\mathcal{E}_n} \prec e^{-(C_2 - C_1) n \epsilon_n^2} \rightarrow 0$, since $C_2 > C_1$. This completes the proof. \square

E.2 Proofs for Theorem 2

In this section, we follow a technique recently developed by [52, 39]. We first prove posterior contraction with respect to average Rényi divergence of order 1/2 in Lemma 2. Then we use our result to derive a posterior contraction rate for γ under prediction loss in Lemma 3, which will imply the result in Theorem 2.

Lemma 2 (posterior contraction with respect to the average Rényi divergence). *Let $f \sim \mathcal{N}_N(\mathbf{U}\gamma, \sigma^2 \mathbf{R}(\rho))$ and $f_0 \sim \mathcal{N}_N(\mathbf{U}\gamma_0 + \boldsymbol{\delta}_0, \sigma_0^2 \mathbf{R}(\rho_0))$. Under model (4.4), suppose that we endow (γ, σ^2) with the prior (2.8)-(2.10) and ρ with the prior, $\rho \sim \mathcal{U}(0, 1)$. For the $\mathcal{SSGL}(\lambda_0, \lambda_1, \theta)$ prior, we set $\lambda_0 = (1 - \theta)/\theta$ and $\lambda_1 \asymp 1/n$, and for the $\mathcal{B}(a, b)$ prior on θ , we set $a = 1, b = p^c, c > 2$. Suppose that Assumptions (A1)-(A6) hold. Then*

$$\sup_{\gamma_0} \mathbb{E}_0 \Pi \left(\frac{1}{n} \rho(f, f_0) \geq M_3 \epsilon_n^2 | \mathbf{Y} \right) \rightarrow 0 \text{ as } n, p \rightarrow \infty,$$

for some $M_3 > 0$, where $\epsilon_n^2 = s_0 \log p/n + s_0 n^{-2\alpha/(2\alpha+1)}$.

Proof of Lemma 2. Let $\mathcal{B}_n = \{|\nu(\gamma)| \leq M_1 s_0\}$ For every $\epsilon > 0$, we have

$$\mathbb{E}_0 \Pi \left(\frac{1}{n} \rho(f, f_0) > \epsilon | \mathbf{Y} \right) \leq \mathbb{E}_0 \Pi \left(\gamma \in \mathcal{B}_n : \frac{1}{n} \rho(f, f_0) > \epsilon | \mathbf{Y} \right) + \mathbb{E}_0 \Pi(\mathcal{B}_n^c | \mathbf{Y}). \quad (\text{E.8})$$

By Theorem 1, the second term in (E.8) goes to zero. Thus, to prove posterior contraction for $\frac{1}{n} \rho(f, f_0)$, it suffices to prove that the first term in (E.8) tends to zero for $\epsilon = M_3 \epsilon_n^2$.

To prove that $\mathbb{E}_0 \Pi(\gamma \in \mathcal{B}_n : \frac{1}{n} \rho(f, f_0) > M_3 \epsilon_n^2 | \mathbf{Y}) \rightarrow 0$, we will first show the existence of a sieve \mathcal{F}_n such that

$$\Pi(\mathcal{B}_n \setminus \mathcal{F}_n) \leq \exp(-(1 + C_1)n\epsilon_n^2), \quad (\text{E.9})$$

where C_1 is the constant from Lemma 1. Then on \mathcal{B}_n , we will construct a test function φ_n such that

$$\begin{aligned} \mathbb{E}_{f_0} \varphi_n &\lesssim e^{-n\epsilon_n^2}, \\ \sup_{f \in \mathcal{F}_n : \rho(f_0, f) > M_3 n \epsilon_n^2} \mathbb{E}_f (1 - \varphi_n) &\lesssim e^{-n\epsilon_n^2/16}. \end{aligned} \quad (\text{E.10})$$

Finally, we will show that the metric entropy $\log N(\epsilon_n, \mathcal{B}_n \cap \mathcal{F}_n, \rho(\cdot))$ can be asymptotically bounded above by a constant of $n\epsilon_n^2$, which will complete the proof (see Sections D.2 and D.3 of [28] for more details).

Let $C_2 > 0$. Consider the sieve,

$$\mathcal{F}_n = \left\{ (\gamma, \sigma^2, \rho) : \max_{1 \leq j \leq p} \|\gamma_j\|_2 \leq \frac{nd}{\lambda_1}, 0 < \sigma^2 \leq e^{C_2 n \epsilon_n^2}, e^{-C_2 n \epsilon_n^2} \leq \rho \leq 1 - e^{-C_2 n \epsilon_n^2} \right\}. \quad (\text{E.11})$$

Then

$$\begin{aligned} \Pi(\mathcal{B}_n \setminus \mathcal{F}_n) &\leq \sum_{S: s \leq M_1 s_0} \sum_{j \in S} \Pi(\|\gamma_j\|_2 > nd/\lambda_1) \\ &\quad + \Pi(\sigma^2 > e^{C_2 n \epsilon_n^2}) + \Pi(\rho < e^{-C_2 n \epsilon_n^2}) + \Pi(\rho > 1 - e^{-C_2 n \epsilon_n^2}). \end{aligned} \quad (\text{E.12})$$

Since the priors on σ^2 and ρ are inverse gamma and $\mathcal{U}(0, 1)$ priors respectively, it is easy to verify that the last three terms on the right-hand side of (E.12) are upper bounded by $e^{-C_3 n \epsilon_n^2}$ for some $C_3 > 0$. Thus, it suffices to show that the probability of the first term on the right-hand side of (E.12) is upper bounded by $e^{-C_4 n \epsilon_n^2}$ for some $C_4 > 0$.

Note that because $\lambda_0 \gg \lambda_1$, we have that for large n , $\pi(\gamma_j | \theta) < (1 - \theta) \Psi(\gamma_j | \lambda_1) + \theta \Psi(\gamma_j | \lambda_1) = \Psi(\gamma_j | \lambda_1)$. Let $\tilde{\pi}(\gamma_j)$ denote $\Psi(\gamma_j | \lambda_1)$, i.e. the

group lasso density with the slab hyperparameter λ_1 . Note that for any $\gamma_j \sim \Psi(\gamma_j|\lambda)$, $\|\gamma_j\|_2$ is distributed as a gamma density with shape parameter d and scale parameter λ . Thus, using the arguments in the proof of Theorem 3.1 of Ning et al. [52] to upper bound the tail probability of a gamma density, we have

$$\begin{aligned}\Pi(\|\gamma_j\|_2 > nd/\lambda_1) &\leq \check{\Pi}(\|\gamma_j\|_2 > nd/\lambda_1) \\ &\leq \exp(-\lambda_1(nd/\lambda_1) + d) = \exp(-d(n-1)).\end{aligned}$$

Thus, for some $C_4 > 0$, we may upper bound for the first term in (E.12) as

$$\begin{aligned}\sum_{S:s \leq M_1 s_0} \sum_{j \in S} \Pi(\|\gamma_j\|_2 > nd/\lambda_1) &\leq \exp(\log(M_1 s_0) - d(n-1)) \\ &< \exp\left(\log(M_1 s_0) + d - s_0 \log p - s_0 n^{1/(2\alpha+1)}\right) \\ &\prec e^{-C_4 n \epsilon_n^2},\end{aligned}\tag{E.13}$$

where the second line of the display follows from the fact that $s_0 \log p = o(n)$ and the fact that $n(s_0 n^{-2\alpha/(2\alpha+1)}) = s_0 n^{1/(2\alpha+1)} = o(nd)$ by our assumptions on s_0 and d in Assumption (A1). The last line follows from the definition of $n\epsilon_n^2$ and the fact that the first two terms in the exponent of the third line are dominated by the last two terms. Thus, combining (E.13) with the upper bounds for the last three terms in (E.12), we may choose some $C_4 > C_1 + 1$, so that (E.9) holds. This proves (E.9).

We now show the existence of a test so that (E.10) also holds. As in [52, 39], we first consider the most powerful Neyman-Pearson test $\phi_n = \mathbb{1}\{f_1/f_0 \geq 1\}$. Following the arguments in [52, 39], if the average Rényi divergence between f_0 and f_1 is bigger than ϵ_n^2 , then

$$\begin{aligned}\mathbb{E}_{f_0} \phi_n &\leq e^{-n\epsilon_n^2}, \\ \mathbb{E}_{f_1} (1 - \phi_n) &\leq e^{-n\epsilon_n^2}.\end{aligned}\tag{E.14}$$

From the second inequality in (E.14), we apply the Cauchy-Schwarz inequality to get

$$\mathbb{E}_f(1 - \phi_n) \leq \{\mathbb{E}_{f_1}(1 - \phi_n)\}^{1/2} \left\{ \mathbb{E}_{f_1} \left(\frac{f}{f_1} \right)^2 \right\}^{1/2}.\tag{E.15}$$

Next, we show that $\mathbb{E}_{f_1}(f/f_1)^2$ is bounded above by $e^{7n\epsilon_n^2/8}$ for every density with parameters $(\gamma_1, \sigma_1^2, \rho_1)$ such that

$$\begin{aligned}\|U(\gamma - \gamma_1)\|_2^2 &\leq \frac{n\epsilon_n^2}{16}, \\ \frac{1}{n} \|\sigma^2 \mathbf{R}(\rho) - \sigma_1^2 \mathbf{R}(\rho_1)\|_F^2 &\leq \frac{\epsilon_n^4}{4n_{\max}^2},\end{aligned}\tag{E.16}$$

Denote $\mathbf{R}_i^* = (\sigma_1^2/\sigma^2)\mathbf{R}_i^{-1/2}(\rho)\mathbf{R}_i(\rho_1)\mathbf{R}_i^{-1/2}(\rho)$. We have by Assumptions (A5)-(A6) that for any such densities satisfying (E.16),

$$\begin{aligned} \max_{1 \leq i \leq n} \|\mathbf{R}_i^* - \mathbf{I}_{n_i}\|_2 &\leq \max_{1 \leq i \leq n} \|\sigma^{-2}\mathbf{R}_i^{-1}(\rho)\|_2 \|\sigma^2\mathbf{R}_i(\rho) - \sigma_1^2\mathbf{R}_i(\rho_1)\|_2 \\ &\lesssim \frac{1}{\sqrt{n}} \|\sigma^2\mathbf{R}(\rho) - \sigma_1^2\mathbf{R}(\rho_1)\|_F \\ &\lesssim \frac{\epsilon_n^2}{2n_{\max}}. \end{aligned}$$

Further, $\max_{1 \leq i \leq n} \|\mathbf{R}_i^* - \mathbf{I}_{n_i}\|_2$ is bounded below by $\max_{1 \leq i \leq n} |\text{eig}_k(\mathbf{R}_i^*) - 1|$ for every $k \leq n_i$, where eig_k denotes the k th ordered eigenvalue of \mathbf{R}_i^* . Thus, we have

$$1 - \frac{\epsilon_n^2}{2n_{\max}} \leq \min_{1 \leq i \leq n} \lambda_{\min}(\mathbf{R}_i^*) \leq \min_{1 \leq i \leq n} \lambda_{\max}(\mathbf{R}_i^*) \leq 1 + \frac{\epsilon_n^2}{2n_{\max}}. \quad (\text{E.17})$$

Since $\epsilon_n^2/n_{\max} \rightarrow 0$, (E.17) implies that $2\mathbf{R}_i^* - \mathbf{I}_{n_i}$ is nonsingular for every $i \leq n$, and hence, for every density f_1 with $(\gamma_1, \sigma_1^2, \rho_1)$ satisfying (E.16), we have

$$\begin{aligned} \mathbb{E}_{f_1}(f/f_1)^2 &= \prod_{i=1}^n \left\{ \det(\mathbf{R}_i^*)^{1/2} \det(2\mathbf{I}_{n_i} - \mathbf{R}_i^{*-1})^{-1/2} \right\} \\ &\quad \times \exp \left\{ \sum_{i=1}^n \|(2\mathbf{R}_i^* - \mathbf{I}_{n_i})^{-1/2} \sigma^{-1/2} [\mathbf{R}_i^{-1/2}(\rho)] (\mathbf{U}^i(\gamma - \gamma_1))\|_2^2 \right\}. \end{aligned} \quad (\text{E.18})$$

Arguing as in (S12) in the proof of Lemma 2 of [39], we have that

$$\prod_{i=1}^n \det(\mathbf{R}_i^*)^{1/2} \det(2\mathbf{I}_{n_i} - \mathbf{R}_i^{*-1})^{-1/2} \leq e^{3n\epsilon_n^2/4}. \quad (\text{E.19})$$

Further, for every density f_1 with $(\gamma_1, \sigma_1^2, \rho_1)$ satisfying (E.16), we have that the exponent term in (E.18) is bounded above by

$$\max_{1 \leq i \leq n} \|(2\mathbf{R}_i^* - \mathbf{I}_{n_i})^{-1}\|_2 \max_{1 \leq i \leq n} \|\sigma^{-2}\mathbf{R}_i^{-1}(\rho)\|_2 \|\mathbf{U}(\gamma - \gamma_1)\|_2^2 \leq \frac{n\epsilon_n^2}{8}, \quad (\text{E.20})$$

since $\max_{1 \leq i \leq n} \|(2\mathbf{R}_i^* - \mathbf{I}_{n_i})^{-1}\|_2 \leq 2$ for large n , and moreover, by Assumption (A5), $\max_{1 \leq i \leq n} \|\sigma^{-2}\mathbf{R}_i^{-1}\|_2 \lesssim 1$. Combining (E.19)-(E.20), $\mathbb{E}_{f_1}(f/f_1)^2$ in (E.18) is bounded above by $e^{7n\epsilon_n^2/8}$ for every density f_1 with $(\gamma_1, \sigma_1^2, \rho_1)$ satisfying (E.16).

Thus, if we plug in the upper bound of $e^{7n\epsilon_n^2/8}$ for $\mathbb{E}_{f_1}(f/f_1)^2$ and the upper bound of $e^{-n\epsilon_n^2}$ for $\mathbb{E}_{f_1}(1 - \phi_n)$ (given in (E.14)) into the right-hand side of (E.15), we obtain $\mathbb{E}_f(1 - \phi_n) \leq e^{-n\epsilon_n^2/16}$ for sufficiently large n . Combining this with the first inequality of (E.14) shows that the desired exponentially powerful test φ_n satisfying (E.10) is obtained by taking the *maximum* of all tests ϕ_n constructed above, for each piece required to cover the sieve.

To complete the proof, we need to show that the metric entropy of each piece (i.e. the densities satisfying f_1 satisfying (E.16)) needed to cover the sieve \mathcal{F}_n in (E.11) can be asymptotically bounded above by a constant multiple of $n\epsilon_n^2$ (see Lemma D.3 of [28]). Note that on \mathcal{B}_n , $\|\mathbf{U}(\gamma - \gamma_1)\|_2^2 \leq \|\mathbf{U}\|_*^2 (\sum_{k=1}^p \|\gamma_k - \gamma_{1k}\|_2)^2 \leq \|\mathbf{U}\|_*^2 (s_{\gamma - \gamma_1} \sqrt{d} \|\gamma - \gamma_1\|_\infty)^2 \lesssim 4NdM_1^2 s_0^2 \|\gamma - \gamma_1\|_\infty^2$. Additionally, by Assumption (A6), the left-hand side of the second inequality in (E.16) can be bounded from above by $n_{\max}^2(\sigma^2 - \sigma_1^2)^2 + e^{4C_2 n \epsilon_n^2} n_{\max}^4 (\rho - \rho_1)^2$ on \mathcal{F}_n . Thus, for densities f_1 satisfying (E.16), the metric entropy can be bounded above by

$$\begin{aligned} & \log N \left(\frac{\sqrt{n}\epsilon_n}{8M_1 s_0 \sqrt{d} \sqrt{N}}, \left\{ \gamma : |\nu(\gamma)| \leq M_1 s_0, \max_{1 \leq j \leq p} \|\gamma_j\|_2 \leq nd/\lambda_1 \right\}, \|\cdot\|_\infty \right) \\ & + \log N \left(\frac{\epsilon_n^2}{\sqrt{8}n_{\max}^2}, \left\{ \sigma^2 : 0 < \sigma^2 \leq e^{C_2 n \epsilon_n^2} \right\}, |\cdot| \right) \\ & + \log N \left(\frac{\epsilon_n^2}{\sqrt{8}n_{\max}^3 e^{2C_2 n \epsilon_n^2}}, \left\{ \rho : 0 < \rho < 1 \right\}, |\cdot| \right). \end{aligned} \quad (\text{E.21})$$

One can easily verify that the last two terms in (E.21) are upper bounded by a constant multiple of $n\epsilon_n^2$. Let δ_n be the radius in the first term in (E.21). Note that because $\{\gamma : \|\gamma - \gamma_0\|_\infty \leq nd/\lambda_1\} \subset \{\gamma : \max_{1 \leq j \leq p} \|\gamma_j\|_2 \leq nd/\lambda_1\}$, we can upper bound the first term in (E.21) by

$$\begin{aligned} & N \left(\delta_n, \left\{ \gamma : |\nu(\gamma)| \leq M_1 s_0, \|\gamma - \gamma_0\|_\infty \leq \frac{nd}{\lambda_1} \right\}, \|\cdot\|_\infty \right) \\ & \leq \binom{p}{M_1 s_0} \left(\frac{3nd}{\delta_n \lambda_1} \right)^{M_1 d s_0}. \end{aligned} \quad (\text{E.22})$$

Using the fact that $\binom{p}{M_1 s_0} \leq p^{M_1 s_0}$, the logarithm of (E.22) may be upper bounded by

$$M_1 s_0 \log p + M_1 d s_0 \log \left(\frac{3nd}{\delta_n \lambda_1} \right) \asymp M_1 s_0 \log p + M_1 d s_0 \log \left(\frac{3n^2 d}{\delta_n} \right)$$

$$\begin{aligned}
&\lesssim M_1 s_0 \log p + M_1 s_0 d \log \left(\frac{24 M_1 s_0^{1/2} d^{3/2} n^{5/2}}{(\log p)^{1/2}} \right) \\
&\lesssim M_1 s_0 \log p + C_5 s_0 d \log n \lesssim n \epsilon_n^2,
\end{aligned} \tag{E.23}$$

for some $C_5 > 0$, where we used the fact that $\lambda_1 \asymp 1/n$ in the first line of the display. In the second line, we used the definition of δ_n , Assumption (A1) that $N \asymp n$, and the fact that $\epsilon_n > \sqrt{s_0 \log p/n}$. In the third line, we used the fact that the second log term is of the same order as $\log n$ by our assumptions on s_0 , d , and p . The final line also follows from Assumption (A1) that $d \log n \prec \log p$. Therefore, from (E.21)-(E.23), the metric entropy for the densities satisfying (E.16) can be bounded above by a constant multiple of $n \epsilon_n^2$. Therefore, the first term on the right-hand side of (E.8) tends to zero as $n, p \rightarrow \infty$ and this completes the proof. \square

Lemma 3 (posterior contraction with respect to prediction loss). *Assume the same conditions as those in Lemma 2. Then*

$$\sup_{\gamma_0} \mathbb{E}_0 \Pi \left(\gamma : \|\mathbf{U}(\gamma - \gamma_0)\|_2 \geq M_4 \sqrt{N} \epsilon_n \right) \rightarrow 0 \text{ as } n, p \rightarrow \infty,$$

for some $M_4 > 0$ and $\epsilon_n^2 = s_0 \log p/n + s_0 n^{-2\alpha/(2\alpha+1)}$.

Proof of Lemma 3. By Lemma 2, we have posterior contraction with respect to average Rényi divergence $n^{-1} \rho(f, f_0)$. Note that

$$\begin{aligned}
\frac{1}{n} \rho(f, f_0) &= -\frac{1}{n} \left[\sum_{i=1}^n \log \left\{ \frac{[\det(\sigma^2 \mathbf{R}_i(\rho))]^{1/4} [\det(\sigma_0^2 \mathbf{R}_i(\rho_0))]^{1/4}}{\det((\sigma^2 \mathbf{R}_i(\rho) + \sigma_0^2 \mathbf{R}_i(\rho_0))/2)^{1/2}} \right\} \right] \\
&\quad + \frac{1}{4n} \|(\sigma^2 \mathbf{R}(\rho) + \sigma_0^2 \mathbf{R}(\rho_0))^{-1} (\mathbf{U}(\gamma - \gamma_0) - \boldsymbol{\delta}_0)\|_2^2.
\end{aligned}$$

Then $n^{-1} \rho(f, f_0) \lesssim \epsilon_n^2$ implies that

$$\frac{1}{n} \sum_{i=1}^n \log \left\{ \frac{[\det(\sigma^2 \mathbf{R}_i(\rho))]^{1/4} [\det(\sigma_0^2 \mathbf{R}_i(\rho_0))]^{1/4}}{\det((\sigma^2 \mathbf{R}_i(\rho) + \sigma_0^2 \mathbf{R}_i(\rho_0))/2)^{1/2}} \right\} \lesssim \epsilon_n^2, \tag{E.24}$$

and

$$\frac{1}{4n} \|(\sigma^2 \mathbf{R}(\rho) + \sigma_0^2 \mathbf{R}(\rho_0))^{-1} (\mathbf{U}(\gamma - \gamma_0) - \boldsymbol{\delta}_0)\|_2^2 \lesssim \epsilon_n^2. \tag{E.25}$$

As in the proof of Theorem 3 of [39], define g as

$$g^2(\sigma^2 \mathbf{R}_i(\rho), \sigma_0^2 \mathbf{R}_i(\rho_0)) = 1 - \frac{[\det(\sigma^2 \mathbf{R}_i(\rho))]^{1/4} [\det(\sigma_0^2 \mathbf{R}_i(\rho_0))]^{1/4}}{\det((\sigma^2 \mathbf{R}_i(\rho) + \sigma_0^2 \mathbf{R}_i(\rho_0))/2)^{1/2}}.$$

Then using the inequality $\log x \leq x - 1$, (E.25) implies that

$$\epsilon_n^2 \gtrsim -\frac{1}{n} \sum_{i=1}^n \log[1 - g^2(\sigma^2 \mathbf{R}_i(\rho), \sigma_0^2 \mathbf{R}_i(\rho_0))] \geq \frac{1}{n} \sum_{i=1}^n g^2(\sigma^2 \mathbf{R}_i(\rho), \sigma_0^2 \mathbf{R}_i(\rho_0)).$$

By Lemma 10 of [39], $g^2(\sigma^2 \mathbf{R}_i(\rho), \sigma_0^2 \mathbf{R}_i(\rho_0)) \gtrsim \|\sigma^2 \mathbf{R}_i(\rho) - \sigma_0^2 \mathbf{R}_i(\rho_0)\|_F^2$ when $\epsilon_n^2 \rightarrow 0$, and therefore, we have that

$$\epsilon_n^2 \gtrsim \frac{1}{n} \|\sigma^2 \mathbf{R}(\rho) - \sigma_0^2 \mathbf{R}(\rho_0)\|_F^2 \geq \max_{1 \leq i \leq n} \|\sigma^2 \mathbf{R}_i(\rho) - \sigma_0^2 \mathbf{R}_i(\rho_0)\|_2^2,$$

where the second line of the display comes from Assumption (A6). By Assumption (A5) of the bounded eigenvalues of $\mathbf{R}(\rho_0)$, we also have

$$\begin{aligned} \max_{1 \leq i \leq n} \|\sigma^2 \mathbf{R}_i(\rho) + \sigma_0^2 \mathbf{R}_i(\rho_0)\|_2^2 &\leq 2 \max_{1 \leq i \leq n} \|\sigma^2 \mathbf{R}_i(\rho) - \sigma_0^2 \mathbf{R}_i(\rho_0)\|_2^2 + 8 \max_{1 \leq i \leq n} \|\sigma_0^2 \mathbf{R}_i(\rho_0)\|_2^2 \\ &\lesssim \epsilon_n^2 + 1. \end{aligned} \quad (\text{E.26})$$

Thus, combining (E.25)-(E.26), we have

$$\begin{aligned} \epsilon_n^2 &\geq \frac{1}{4n} \left(\max_{1 \leq i \leq n} \|\sigma^2 \mathbf{R}_i(\rho) + \sigma_0^2 \mathbf{R}_i(\rho_0)\|_2^{-2} \right) \|\mathbf{U}(\boldsymbol{\gamma} - \boldsymbol{\gamma}_0) - \boldsymbol{\delta}_0\|_2^2 \\ &\gtrsim \frac{1}{n} \|\mathbf{U}(\boldsymbol{\gamma} - \boldsymbol{\gamma}_0) - \boldsymbol{\delta}_0\|_2^2 / (1 + \epsilon_n^2), \end{aligned}$$

and thus $\rho(f, f_0) \lesssim n\epsilon_n^2$ implies that

$$\begin{aligned} \sqrt{n}\epsilon_n &\gtrsim \|\mathbf{U}(\boldsymbol{\gamma} - \boldsymbol{\gamma}_0) - \boldsymbol{\delta}_0\|_2 / (1 + \epsilon_n^2)^{1/2} \\ &\geq (\|\mathbf{U}(\boldsymbol{\gamma} - \boldsymbol{\gamma}_0)\|_2 - \|\boldsymbol{\delta}_0\|_2) / (1 + \epsilon_n^2)^{1/2} \\ &\gtrsim \|\mathbf{U}(\boldsymbol{\gamma} - \boldsymbol{\gamma}_0)\|_2 - M_5 \sqrt{Ns_0} n^{-\alpha/(2\alpha+1)} \\ &\gtrsim \|\mathbf{U}(\boldsymbol{\gamma} - \boldsymbol{\gamma}_0)\|_2 - M_5 \sqrt{N}\epsilon_n, \end{aligned} \quad (\text{E.27})$$

for some $M_5 > 0$. In the third line of the above display, we used the fact that $\|\boldsymbol{\delta}_0\|_2 \lesssim \sqrt{Ns_0} n^{-\alpha/(2\alpha+1)}$ by Assumptions (A1) and (A4) and the fact that we used B-splines in our basis expansion. Thus, we have from (E.27) that the posterior is asymptotically supported on the event, $\{\boldsymbol{\gamma} : \|\mathbf{U}(\boldsymbol{\gamma} - \boldsymbol{\gamma}_0)\|_2 \leq M_6 \sqrt{n}\epsilon_n + M_5 \sqrt{N}\epsilon_n\}$ for some $M_6 > 0$. However, $\sqrt{n}\epsilon_n \asymp \sqrt{N}\epsilon_n$ due to Assumption (A1), so the posterior is also asymptotically supported on the event $\{\|\mathbf{U}(\boldsymbol{\gamma} - \boldsymbol{\gamma}_0)\|_2 \leq M_4 \sqrt{N}\epsilon_n\}$ for some $M_4 > 0$. This completes the proof. \square

Proof of Theorem 2. First, we let $\mathbf{g}_0(\mathbf{t}) = [g_{01}(\mathbf{t}), \dots, g_{0p}(\mathbf{t})]$ and $\boldsymbol{\kappa}_0(\mathbf{t}) = [\kappa_{01}(\mathbf{t}), \dots, \kappa_{0p}(\mathbf{t})]$ be $N \times p$ matrices, where $\kappa_{0k}(\mathbf{t})$ is the approximation error for the k th basis expansion evaluated at \mathbf{t} , as in (4.3). We have

$$\begin{aligned}
\|\boldsymbol{\beta}(\mathbf{t}) - \boldsymbol{\beta}_0(\mathbf{t})\|_n^2 &= \|\boldsymbol{\beta}(\mathbf{t}) - \mathbf{g}_0(\mathbf{t}) + \mathbf{g}_0(\mathbf{t}) - \boldsymbol{\beta}_0(\mathbf{t})\|_n^2 \\
&\leq 2\|\boldsymbol{\beta}(\mathbf{t}) - \mathbf{g}_0(\mathbf{t})\|_n^2 + 2\|\boldsymbol{\kappa}_0(\mathbf{t})\|_n^2 \\
&\asymp \frac{\|\boldsymbol{\gamma} - \boldsymbol{\gamma}_0\|_2^2}{d} + \|\boldsymbol{\kappa}_0(\mathbf{t})\|_n^2 \\
&\lesssim d^{-1}\|\boldsymbol{\gamma} - \boldsymbol{\gamma}_0\|_2^2 + s_0 n^{-2\alpha/(2\alpha+1)} \\
&\lesssim \|\boldsymbol{\gamma} - \boldsymbol{\gamma}_0\|_2^2.
\end{aligned} \tag{E.28}$$

In the above display, we used Lemmas A.1 and A.2 of [36] in the third line. In the fourth line, we used Assumption (A1) that $d \asymp n^{1/(2\alpha+1)}$ and the properties of B-splines. In the final line of the display, we used the fact that $d \succ 1$ and $s_0 = o(n^{2\alpha/(2\alpha+1)})$ by Assumption (A1). Following from (E.28), we have that for sufficiently large n and large enough constant $M_2 > 0$,

$$\{\|\boldsymbol{\beta}(\mathbf{t}) - \boldsymbol{\beta}_0(\mathbf{t})\|_n \geq M_2 \epsilon_n\} \subset \{\boldsymbol{\gamma} : \|\boldsymbol{\gamma} - \boldsymbol{\gamma}_0\|_2 \geq M_2 \epsilon_n\},$$

Therefore, in order to prove posterior contraction for the smooth functionals, it suffices to prove that

$$\mathbb{E}_0 \Pi(\boldsymbol{\gamma} : \|\boldsymbol{\gamma} - \boldsymbol{\gamma}_0\|_2 \geq M_2 \epsilon_n | \mathbf{Y}) \rightarrow 0 \text{ as } n, p \rightarrow \infty. \tag{E.29}$$

By Theorem 1, the posterior is asymptotically supported on the event $\mathcal{B}_n = \{\boldsymbol{\gamma} : |\boldsymbol{\nu}(\boldsymbol{\gamma})| \leq M_1 s_0\}$. Thus, using the compatibility condition in Assumption (A3), we have $\|\mathbf{U}(\boldsymbol{\gamma} - \boldsymbol{\gamma}_0)\|_2 \geq \phi_2(M_1 s_0) \|\mathbf{U}\|_* \|\boldsymbol{\gamma} - \boldsymbol{\gamma}_0\|_2 \asymp \sqrt{N} \|\boldsymbol{\gamma} - \boldsymbol{\gamma}_0\|_2$. The result in Lemma 3 then immediately implies that (E.29) holds for $\boldsymbol{\gamma}$ under ℓ_2 error loss. Consequently, the smooth functionals also contract at the same rate ϵ_n with respect to the $\|\cdot\|_n$ norm. \square

E.3 Proof for Theorem 3

As in the proof of Theorem 2, we first prove posterior contraction w.r.t. Rényi divergence of order $1/2$, from which we can infer posterior contraction for the functionals $\boldsymbol{\beta}$. The main difference is that for the fractional posterior, it is sufficient to verify a single KL condition [5] to obtain our result. We do not need to verify technical conditions regarding the effective support of the prior or show the existence of a certain sieve and exponentially powerful tests. Throughout this section, we let $\mathbf{S} = \text{diag}(\mathbf{S}_1, \dots, \mathbf{S}_n)$.

Proof of Theorem 3. We first prove posterior contraction with respect to Rényi divergence of order 1/2 for the fractional posterior (5.1). Let \tilde{f}_i denote the marginal density for $\mathbf{y}_i \sim \mathcal{N}_{n_i}(\mathbf{U}_i \boldsymbol{\gamma}, \mathbf{S}_i)$ and let $\tilde{f} = \prod_{i=1}^n \tilde{f}_i$. Let \tilde{f}_{0i} denote the marginal density for $\mathbf{y}_{0i} \sim \mathcal{N}_{n_i}(\mathbf{U}_i \boldsymbol{\gamma}_0 + \boldsymbol{\delta}_{0i}, \boldsymbol{\Sigma}_{0i})$, where $\boldsymbol{\delta}_{0i}$ is the subvector of $\boldsymbol{\delta}_0$ with n_i entries corresponding to the i th subject, and let $\tilde{f}_0 = \prod_{i=1}^n \tilde{f}_{0i}$. We show that under the conditions of Theorem 3,

$$\Pi_{n,\xi} \left(\frac{1}{n} \rho(\tilde{f}, \tilde{f}_0) > M_7 n \epsilon_n^2 | \mathbf{Y} \right) \rightarrow 0 \text{ a.s. } \mathbb{P}_0 \text{ as } n, p \rightarrow \infty, \quad (\text{E.30})$$

for some $M_7 > 0$.

To establish (E.30), it suffices (by Theorem 3.1 of [5]) to show that

$$\Pi(\tilde{\mathcal{B}}_n) \gtrsim \exp(-\tilde{C} n \epsilon_n^2), \quad (\text{E.31})$$

for some $\tilde{C} > 0$, where

$$\tilde{\mathcal{B}}_n := \left\{ K(\tilde{f}_0, \tilde{f}) \leq n \epsilon_n^2, V(\tilde{f}_0, \tilde{f}) \leq n \epsilon_n^2 \right\}.$$

Let $\boldsymbol{\Omega}_i^* = \boldsymbol{\Sigma}_{0i}^{-1/2} \mathbf{S}_i \boldsymbol{\Sigma}_{0i}^{-1/2}$, and denote the ordered eigenvalues of $\boldsymbol{\Omega}_i^*$ as $\tilde{\lambda}_{ij}, 1 \leq j \leq n_i$. Similarly as in the proof of Lemma 1, we have that

$$\begin{aligned} K(\tilde{f}_0, \tilde{f}) &= \frac{1}{2} \left\{ \sum_{i=1}^n \sum_{j=1}^{n_i} (\tilde{\lambda}_{ij} - 1 - \log \tilde{\lambda}_{ij}) + \|\mathbf{S}^{-1/2}(\mathbf{U}(\boldsymbol{\gamma} - \boldsymbol{\gamma}_0) - \boldsymbol{\delta}_0)\|_2^2 \right\}, \\ V(\tilde{f}_0, \tilde{f}) &= \left[\sum_{i=1}^n \sum_{j=1}^{n_i} \frac{(1 - \tilde{\lambda}_{ij})^2}{2} \right] + \|\boldsymbol{\Sigma}_0^{1/2} \mathbf{S}^{-1}(\mathbf{U}(\boldsymbol{\gamma} - \boldsymbol{\gamma}_0) - \boldsymbol{\delta}_0)\|_2^2. \end{aligned}$$

Similarly as in the proof of Theorem 1, we may expand $\log \tilde{\lambda}_{ij}$ in powers of $(1 - \tilde{\lambda}_{ij})$ to obtain $\tilde{\lambda}_{ij} - 1 - \log \tilde{\lambda}_{ij} \sim (1 - \tilde{\lambda}_{ij})^2/2$, and so we have

$$\begin{aligned} 2K(\tilde{f}_0, \tilde{f}) - V(\tilde{f}_0, \tilde{f}) &\sim \|\mathbf{S}^{-1/2}(\mathbf{U}(\boldsymbol{\gamma} - \boldsymbol{\gamma}_0) - \boldsymbol{\delta}_0)\|_2^2 - \|\boldsymbol{\Sigma}_0^{1/2} \mathbf{S}^{-1}(\mathbf{U}(\boldsymbol{\gamma} - \boldsymbol{\gamma}_0) - \boldsymbol{\delta}_0)\|_2^2 \\ &\asymp \|\mathbf{U}(\boldsymbol{\gamma} - \boldsymbol{\gamma}_0) - \boldsymbol{\delta}_0\|_2^2, \end{aligned}$$

where we used Assumptions (B1)-(B2) in the last line, and the fact that for any $N \times 1$ vector \mathbf{z} and $N \times N$ matrix \mathbf{A} where $0 < \lambda_{\min}(\mathbf{A}) \leq \lambda_{\max}(\mathbf{A}) < \infty$, $\|\mathbf{A}\mathbf{z}\|_2^2 \asymp \|\mathbf{z}\|_2^2$ and $\|\mathbf{A}^{-1}\mathbf{z}\|_2^2 \asymp \|\mathbf{z}\|_2^2$. Thus, for sufficiently large n , we have for some constant $\tilde{b}_1 > 0$,

$$\tilde{\mathcal{B}}_n \supseteq \{\|\mathbf{U}(\boldsymbol{\gamma} - \boldsymbol{\gamma}_0) - \boldsymbol{\delta}_0\|_2^2 \leq \tilde{b}_1 n \epsilon_n^2\}. \quad (\text{E.32})$$

From (E.32), we thus have

$$\begin{aligned}\Pi(\tilde{\mathcal{B}}_n) &\geq \Pi\left(\|\mathbf{U}(\boldsymbol{\gamma} - \boldsymbol{\gamma}_0) - \boldsymbol{\delta}_0\|_2^2 \leq \tilde{b}_1 n \epsilon_n^2\right) \\ &\gtrsim \exp\left(-\tilde{C} n \epsilon_n^2\right),\end{aligned}$$

where we used Assumptions (A1)-(A4) and almost identical steps as those used to prove (E.3) in order to obtain the second inequality of the display. Thus, (E.31) has been proven, which then implies (E.30).

Similarly as in the proof of Lemma 3, we can show that

$$\left\{\frac{1}{n}\rho(\tilde{f}, \tilde{f}_0) > M_7 n \epsilon_n^2\right\} \supset \left\{\boldsymbol{\gamma} : \|\mathbf{U}(\boldsymbol{\gamma} - \boldsymbol{\gamma}_0)\|_2 > M_8 \sqrt{N} \epsilon_n\right\},$$

for some $M_8 > 0$, and thus, from (E.30), we have

$$\Pi_{n,\xi}\left(\boldsymbol{\gamma} : \|\mathbf{U}(\boldsymbol{\gamma} - \boldsymbol{\gamma}_0)\|_2 > M_8 \sqrt{N} \epsilon_n | \mathbf{Y}\right) \rightarrow 0 \text{ a.s. } \mathbb{P}_0 \text{ as } n, p \rightarrow \infty. \quad (\text{E.33})$$

Similarly as in the proof of Theorem 1, we can show that for some $C_6 > 0$, the fractional posterior is asymptotically supported on the event, $\tilde{\mathcal{C}}_n = \{\boldsymbol{\gamma} : |\boldsymbol{\nu}(\boldsymbol{\gamma})| \leq M_1 s_0\}$, for sufficiently large constant $M_1 > 0$. Therefore, using the same arguments as those in the proof of Theorem 2 and invoking Assumptions (A1)-(A4), we can show that for some $M_9 > 0$, $\{\|\boldsymbol{\beta}(\mathbf{t}) - \boldsymbol{\beta}_0(\mathbf{t})\|_n > M_9 \epsilon_n\} \subset \{\boldsymbol{\gamma} : \|\mathbf{U}(\boldsymbol{\gamma} - \boldsymbol{\gamma}_0)\|_2 > M_8 \sqrt{N} \epsilon_n\}$, and therefore, the statement in Theorem 3 has been proven. \square

F Additional Details for the Yeast Cell Cycle Data Analysis

Here, we provide further analysis of the yeast cell cycle data analyzed in Section 7 and place our results within the context of existing results about the cell cycle process in the literature. We also compare the performance of the NVC-SSL model against the performance of parametric linear models and demonstrate that the NVC-SSL model gives far superior performance, while also retaining interpretability.

F.1 Additional Analysis of Genes Selected by NVC-SSL

In total, the NVC-SSL model selected 37 TFs as being significantly associated with cell-cycle regulated genes that are periodically expressed. Figure

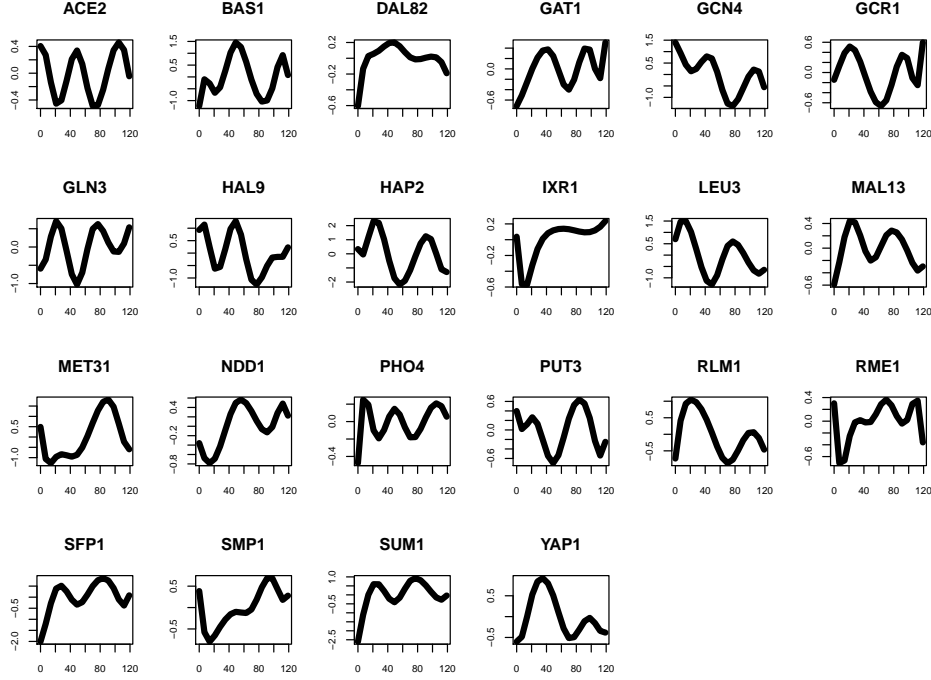


Figure F.1: Plots of the estimated transcriptional effects over time for the 22 TFs that were selected by NVC-SSL but not by NVC-gLASSO, NVC-gSCAD, or NVC-gMCP.

3 plotted the estimated transcriptional effects for the 15 TFs that were selected by the NVC-SSL method, along with NVC-gLASSO, NVC-gSCAD, and NVC-gMCP. Figure F.1 provides the names and estimated transcriptional effects over time for the remaining 22 TFs that were selected by NVC-SSL but not by NVC-gLASSO, NVC-gSCAD, or NVC-gMCP.

The cell cycle is an ordered set of events, culminating in cell growth and division into two daughter cells. Stages of the cell cycle are commonly divided into G1-S-G2-M. The G1 stage stands for “GAP 1.” The S stage stands for “Synthesis” and is the stage when DNA replication occurs. The G2 stage stands for “GAP 2.” The M stage stands for “mitosis,” when nuclear (chromosomes separate) and cytoplasmic (cytokinesis) division occur.

The NVC-SSL model selected several TFs that have also been shown to be significant at various stages of the cell cycle in the literature. In particular, the NVC-SSL method selected NDD1, SWI5, and ACE2. Simon et al. [61] found that the NDD1 protein regulates genes in late G2 and thus

	MSPE	Number of Proteins Selected
NVC-SSL	0.071	37
Lasso	0.590	0
SCAD	0.590	1
MCP	0.590	1
SSL	0.590	0

Table F.1: Predictive accuracy and number of proteins selected by the NVC-SSL model, compared with regularized linear regression models.

controls the transcription of G2/M genes. SWI5 and ACE2 regulate genes at the end of M and early G1 [61].

Moreover, the TFs selected by the NVC-SSL model also include several pairs of synergetic, or “cooperative,” pairs of TFs that have been reported in the literature [3, 65]. These pairs of TFs are thought to cooperate together to regulate transcription in the yeast cell cycle. Among the 37 TFs selected by NVC-SSL, nine of them (ACE2, DAL81, GCN4, HIR1, NDD1, PDR1, SMP1, SUM1, and SWI5) belonged to cooperative pairs of TFs identified by [3], including the complete cooperative pairs ACE2-SMP1, PDR1-SMP1, SMP1-SWI5, and GCN4-SUM1.

F.2 Comparison of Varying Coefficient Models with Parametric Linear Models

In this section, we demonstrate the benefits of using a more flexible but still interpretable nonparametric varying coefficient model over a parametric linear model for the data set we analyzed in Section 7. Specifically, we compared the NVC-SSL model to regularized linear regression models, $\mathbf{Y} = \mathbf{X}\boldsymbol{\beta} + \boldsymbol{\varepsilon}$.

For the linear model, \mathbf{Y} consists of all the observed mRNA levels at all time points for the 47 yeast genes, the columns of the design matrix \mathbf{X} consist of the binding information for the 96 TFs, and $\boldsymbol{\beta}$ is a vector of size 96, where the j th component, β_j , is the regression coefficient corresponding to the j th TF. We fit the lasso [64], SCAD [19], the MCP [78], and the spike-and-slab lasso (SSL) [59] to this data.

Our results, compared to the NVC-SSL model, are presented in Table F.1. In particular, we see that the NVC-SSL model had much lower prediction error. The lasso and SSL both selected the null model (i.e. zero TFs), while SCAD and MCP selected only one TF, PHD1. Moreover, the estimated regression value for PHD1 was very small: $\hat{\beta}_{61} = 4.16 \times 10^{-17}$ for

SCAD and $\hat{\beta}_{61} = 2.22 \times 10^{-17}$ for MCP. Consequently, their prediction error was almost the same as the prediction error for lasso and SSL. On this data set, all of the regularized linear models gave poor fits.

Our results illustrate that the NVC-SSL model often provides a much better fit for repeated measures data than the parametric linear model. Meanwhile, the NVC-SSL model *also* provides a relatively interpretable model, allowing the scientist to study which TFs are significantly associated with periodically-expressed cell-cycle regulated genes and how the transcriptional effects of these TFs vary over the cell cycle.